VŠB – Technical University of Ostrava
Faculty of Electrical Engineering and Computer Science

Non-Orthogonal Multiple Access schemes for Next Generation Cellular Networks: *System Model and Performance Consideration*

PHD THESIS

2021 Nguyen Ngoc Long

VSB TECHNICAL UNIVERSITY OF OSTRAVA | FACULTY OF ELECTRICAL ENGINEERING AND COMPUTER SCIENCE

Non-Orthogonal Multiple Access Schemes for Next Generation Cellular Networks: *System Model and Performance Consideration*

Nguyen Ngoc Long
Doctoral Study Program: 2601V018 - Communication Technology

PhD Thesis
Supervisor: Assoc. prof. Jaroslav Zdrálek, Ph.D.
Ostrava, 2021

Declaration

I declare that I have written my doctoral thesis on the theme of "Non-Orthogonal Multiple Access schemes for Next Generation Cellular Networks: System Model and Performance Consideration" independently, under the guidance of the doctoral thesis supervisor and using the technical literature and other sources of information which are all quoted in the thesis and detailed in the list of literature at the end of the thesis. As the author of the doctoral thesis, I furthermore declare that, as regards the creation of this doctoral thesis, I have not infringed any copyright. In particular, I have not unlawfully encroached on anyone's personal and/or ownership rights, and I am fully aware of the consequences in the case of breaking Regulation S 11 and the following of the Copyright Act No 121/2000Sb., and of the rights related to intellectual property right and changes in some Acts (Intellectual Property Act) and formulated in later regulations, inclusive of the possible consequences resulting from the provisions of Criminal Act No 40/2009 Sb., Section 2, Head VI, Part 4.

Acknowledgements

- First of all, I would like to express my sincere gratitude to my supervisor **Assoc. prof. Jaroslav Zdrálek, Ph.D.** for his consideration, continuous support and guidance.
- I deeply thank Dr. Do Dinh Thuan for providing extensive knowledge, his professionalism, detailed instructions for research, and offering a valuable interdisciplinary view.
- I deeply appreciate and thank the collaboration from my colleagues and friends for the assistance I received during my time at VSB.
- I would also like to thank the Ton Duc Thang University, where developed the cooperation in training and research between Vietnam and the Czech Republic and gave me the opportunity to study abroad at the prestigious VSB - Technical University of Ostrava.
- And finally, I wish to express my love and gratitude to my mother, my wife and son for their constant support, encouragement and never-ending patience.

Abstrakt

Disertační práce se zabývá buňkovými sítěmi příští generace, zejména s ohledem na integraci bezdrátových sítí, které používají neortogonální vícenásobný přístup (NOMA) a další pokročilé techniky, jako jsou víceanténové systémy, získávání energie z elektromagnetického záření (EH), zabezpečení fyzické vrstvy (PLS) a satelitní komunikace.

Disertační práce nejprve zkoumá model komunikace s více anténami s cílem dosáhnout vyšší efektivity přenosu. Nový model distribuce energie uživatelům NOMA, kteří se připojili přímým spojem anebo zprostředkovaně (přes realy uzel), je navržen tak, aby zlepšil kvalitu přenosu. Dále je v modelu navržen výkonový maják, který je schopen dodávat energii do relay uzlu, aby podpořil přenos k příjemcům.

Za druhé, disertační práce studuje výkonnost PLS v sítích kognitivního rádia (CR)-NOMA. V návrhu je uvažována architektura více vstupů s jedním výstupem (MISO) kombinující strategii výběru vysílací antény (TAS), přičemž úroveň zabezpečení je zkoumána metrikou pravděpodobnosti výpadku utajení (SOP). Dále lze pro optimalizaci výkonu SOP získat faktor optimálního přidělování energie (PA). Vzhledem k předpokládané přítomnosti nelegitimního uživatele vylepšujeme SOP pomocí výběru relay uzlu (RS) kombinující režimy dekóduj a přepošli (DF) s plně duplexním (FD) přenosem.

A konečně, jako nejsilnější přínos disertační práce, je představena aplikace techniky vícenásobného přístupu NOMA v satelitních sítích, která vylepšuje spektrální účinnost. Satelitní komunikační systémy se integrují s nově vznikajícími buňkovými sítěmi malého dosahu. Zajišťují bezproblémové připojení a vysokorychlostní širokopásmový přístup pro mobilní uživatele v budoucích bezdrátových sítích. V disertační práci studujeme hybridní satelitně-terestrický relay systém (HSTRS). K popisu sítě malých buněk s asistencí HSTRS je v případě satelitní komunikace použit útlumový model "Shadowed-Rician" a v případě terestrické pak "Nakagami-m."

Klíčová slova: NOMA, MISO, EH, HSTRS, nová generace buňkových sítí.

Abstract

THE dissertation deals with next generation cellular networks, especially in regard to the integration of wireless networks which apply non-orthogonal multiple access (NOMA) and other advanced techniques such as multi-antennae, radio frequency energy harvesting (EH), physical layer security (PLS) and satellite communication.

Firstly, the dissertation investigates a multi-antenna transmission model to enhance the performance of communications. A novel model of power distribution to NOMA users, who joined both direct link and relay link, is designed to improve transmission quality. Further, we deploy the power beacon, which is able to feed energy to power-constraint relay node to further support transmission to destinations.

Secondly, the dissertation studies the secrecy performance of a PLS in cognitive radio (CR)-NOMA networks. The multi-input single-output (MISO) architecture combining transmit antenna selection (TAS) strategy is considered to achieve secure performance analysis such as the secrecy outage probability (SOP). Further, optimal power allocation (PA) factor can be obtained to optimize SOP performance. Since the presence of an illegitimate user, we improve the SOP by adopting relay selection (RS) combining decode-and-forward (DF) with full-duplex (FD) relaying.

Finally, as the strongest contribution of the dissertation, an application of the NOMA technique, which improves the spectral efficiency, in satellite networks is introduced. Satellite communication systems integrate with emerging small-cell networks to provide seamless connectivity and high-speed broadband access for mobile users in future wireless networks. In the dissertation, we study a hybrid satellite-terrestrial relay system (HSTRS). To characterizing the HSTRS-assisted small-cell network, Shadowed-Rician fading for satellite links and Nakagami-m fading for terrestrial links are adopted.

Keywords: NOMA, MISO, EH, HSTRS, next generation cellular networks.

Contents

List of Abbreviations

5G fifth-generation

AF amplify-and-forward

AP access point

AWGN additive white Gaussian noise

BS base station

CDF cumulative distribution function

C-NOMA cooperative non-orthogonal multiple access

CR cognitive radio

CSI channel state information

D2D device-to-device

DF decode-and-forward

DoF degree-of-freedom

EH energy harvesting

FD full-duplex

GEO geosynchronous earth orbit

G-WNs green wireless networks

HARR hybrid automatic repeat request

Hetnet heterogeneous network

HSTRS hybrid satellite-terrestrial relay system

IoT Internet of Things

LoS line of sight

MIMO multi-input multi-output

MISO multi-input single-output

MRC maximum ratio combining

MUD multiple user detection

NOMA non-orthogonal multiple access

OMA orthogonal multiple access

OP outage probability

ORS optimal relay selection

PA power allocation

PD primary device

PDF probability density function

PLS physical layer security

RF radio frequency

RS relay selection

SBSs small cell base stations

SCB small-cell base station

SCR small-cell relay

SIC successive interference cancellation

SINR signal to interference plus noise ratio

SNR signal to noise ratio

SOP secrecy outage probability

SWIPT simultaneous wireless information and power transfer

TAS transmit antenna selection

TS time switching

UAV unmanned aerial vehicle

UE user equipment

WPT wireless power transfer

WSN wireless sensor network

QoS quality of service

List of Figures

Chapter 1:

Introduction

1.1 Motivations

The NOMA technique has received much attention recently for its ability to improve spectral utilization [1]. By adopting the NOMA technique in next generation cellular wireless networks, the base station (BS) may transmit signals to selected relays with a RS strategy and serve multiple mobile users [2]. To expand network coverage, various relaying schemes have been proposed. The outage probability (OP) performance has also been investigated to prove that reliable transmission can be satisfied through the use of relaying models underlay NOMA technique [3–7]. The authors in [3,4] proposed fixed PA factors for NOMA deployed in a wireless power transfer (WPT) scenario to introduce green wireless networks (G-WNs). The device-to-device (D2D) technique is another application of NOMA [7]. Greater benefits may be achieved by combining cooperative relays and NOMA in a so-called cooperative non-orthogonal multiple access (C-NOMA) [4].

It is difficult to supply power to large numbers of sensors in wireless sensor network (WSN). The EH technique is therefore adopted to address this problem by collecting the radio frequency (RF)-EH from flat-earth environments. To collect the wireless energy from RF signals, the RF-EH technique is adopted [8]. Cooperative networks are very useful through their flexibility, sustainability, and stability in serving devices in such networks [9–13]. In [10], renewable energy was found an effective source for a large number of small cell base stations (SBSs) to adapt to the growing demand of wireless communication services. The authors in [11] proposed unmanned aerial vehicle (UAV)-assisted networks as a potential solution for power resource allocation issues. In [11], multiple RF-EH-powered D2D pairs were powered by a UAV operating as a wireless energy source for WPT supply. In [12], system throughput was improved through the use of an optimal channel state information (CSI) selection method and RF-EH. The benefit of RF-EH on cognitive radio CR WSN was investigated in [13], [NNL12].

The CR-NOMA has been confirmed as a potential technique in next generation wireless cellular networks for its ability to enhance user network access efficiency [14–17]. The NOMA technique may significantly enhance spectral efficiency by serving multiple devices simultaneously with power domain multiplexing. The BS transmits superimposed signals to multiple users, simultaneously adopting superposition coding [18]. In NOMA networks, the near user first decodes the message of the far user and then decodes its own message after removing the decoded message of the far user by applying successive interference cancellation (SIC) [NNL13]. The OP and ergodic capacity of NOMA systems were studied in [19]. NOMA may also make the RF power resource allocation more flexible and improve the fairness of quality of service (QoS) by allocating appropriate PA factors [20–24].

The RF-EH operations for both primary network and secondary networks were investigated in recent studies [5,25–27]. Motivated by these major studies, I am going to examine the security performance of next generation cellular networks through the application of the CR-NOMA technique in terms of SOP.

In the past few decades, satellite communication systems have been widely adopted for their coverage benefits to terrestrial users in various broadcasting and navigation applications [28]. Satellite communication systems have received much attention from researchers [29, 30]. The transmission of the line of sight (LoS) link from source to a terrestrial destination in such satellite communication systems has been limited by obstacles related to the masking effect. In the worst cases, satellite communications systems are affected by obstacles when the satellite's angle is low or when the need to communicate with indoor terrestrial users arises. By adopting relay networks to extend networking coverage and higher reliability, the feature study [28] proposed an HSTRS to reduce the masking effect. Recently, the HSTRS has been advanced to integrate with existing communication systems. For example, the authors in [31–33] investigated the amplify-and-forward (AF) protocol [NNL04] to enhance the system performance of HSTRS [NNL01, NNL02]. HSTRS has also been examined with the DF relay [34, 35]. The authors in [36] investigated the effect of hardware imperfections on HSTRS in a scenario where a geosynchronous earth orbit (GEO) satellite sends data to terrestrial users with the cooperation of DF terrestrial relays; the authors also derived the closed-form of the OP. The authors in [37] examined the delay-limited throughput of an HSTRS in hybrid automatic repeat request (HARR) mode. In their system model, a satellite communicates with a terrestrial user through an AF terrestrial relay. Specifically, the authors provided a theoretical analysis for two cases, i.e., the AF fixed gain relay and the CSI-assisted protocols [37]. Paper [38] investigated an HSTRS where multiple DF three-dimensional (3-D) mobile UAV relays assist a satellite in transmitting data to a terrestrial user. In other work, the secure performance at the physical layer in a hybrid satellite and free-space optical (FSO) cooperative system was studied [39]. The authors derived an exact analytical equation together with an asymptotic analysis for the average secrecy capacity and SOP for both cases of AF and DF relaying. However, the studies in [33–39] only examined a hybrid terrestrial-satellite adopted in popular mobile networks. Note that the system performance of hybrid terrestrial-satellite systems is low due to a large number of connections and higher traffic requirements.

To face these challenges, the NOMA technique has been proposed and recently applied to HSTRS [5, 25, 27, 40–43]. The studies in [5, 25, 27] examined NOMA systems with multiple users to allocate resources equally, i.e., the RF, time, space, or code domains. The other benefits of the NOMA technique include massive connections, high spectral efficiency, and low delay. For example, fairness and spectral efficiency requirements may be satisfied by CR transmission and considered attractive benefits of NOMA [27]. In [40], the authors studied the security and the reliability of ambient back scatter (AmBC) NOMA systems in which the BS was able to transmit data to two NOMA users while an eavesdropper wiretapped the main signal. In [41, 42] the advantages of UAV were explored in a UAV-NOMA system. In multi-way relaying NOMA networks [42], multiple terrestrial users transmit their signals by adopting AF-aided UAV

relaying. The authors in [42] considered the real situation of residual hardware impairments (RHIs) at the transceivers. Some works have integrated NOMA with HSTRS [43–47]. The authors in [43] deployed a user with the best CSI as a relay node for forwarding the signal to other users with worse CSI to alleviate the masking effect for users with weak CSI in heavy shadowing. The authors in [45, 46] examined NOMA to CR-based HSTRS, which permits spectrum sharing. The authors in [45] examined NOMA for HSTRS adopting cooperative transmission. The studies [45, 46] explored the architecture of spectrum sharing; however, the authors only considered the priority of the primary user, while the fairness of QoS between the primary network and the secondary network was not considered. The authors in [47] investigated the system performance of a CR HSTRS system which included a primary satellite transmitter with corresponding terrestrial receiver while the secondary transmitter communicates with its paired users on the ground.

In other emerging networks, a potential network architecture is well-known, i.e., heterogeneous network (Hetnet). In a Hetnet-based cellular network, some macro cells coexist with different types of other small cells, i.e., pico cells, femto cells and micro cells [48]. In a Hetnet system, an expensive macro BS (MBS) needs the cooperation of a number of surrounding economical SBSs to extend the network's coverage and produce higher throughput capacity [49]. A small-cell approach is better for improvements in networking capacity and networking coverage than a conventional macro-centric network [50]. A small-cell solution is simpler, with lower cost deployment. Some other techniques, i.e., FD, caching and massive multi-input multi-output (MIMO), were proposed to facilitate dense implementation of SBSs [51]. Small-cell networks were also examined in the context of Hetnet adopted mobile networks for both down-link and uplink utilizing three techniques, i.e., FD, EH, and NOMA [52]. The authors derived analytical equations to evaluate the system's performance in terms of the OP and throughput.

1.2 Dissertation structure

The dissertation is structured as follows: Chapter 2 describes the background knowledge related to the dissertation directly, Chapter 3 introduces State-of-the-Art which strongly contributed for cellular network evolution. Chapter 4 specifies the aims, Chapters 5, 6 and 7 details how I achieve the aims and explains the achieved results which are how to contribute to future cellular networks. Finally, Chapter 8 concludes the achieved results in the dissertation.

Chapter 2:

Background

2.1 NOMA-assisted multi-users

In Ph.D. dissertation [53], the author sketched the differences of orthogonal multiple access (OMA) and NOMA techniques. In contrast OMA technique, the NOMA technique is designed to share spectrum among mobile devices with superposition and consequently needs to employ multiple user detection (MUD) to separate interfered devices which shares the same RF, as plotted in Figure 2.1.

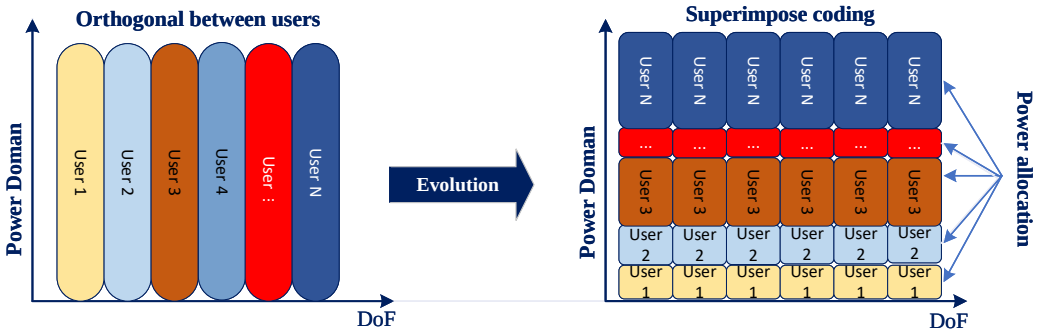

Figure 2.1: Difference 4G-OMA to 5G-NOMA for cellular networks.

The NOMA technique is advantage to density connections by allocating distinct PA factors in the same power domain. Therefore, the NOMA technique could improve network capacity and latency, whereas multiple user equipment (UE) with bit-rate requirements may be multiplexed to transmit on the same RF. A comparison of OMA and NOMA is sketched in Table 2.1.

NOMA has therefore been confirmed as a potential multi-access technique for beyond fifth-generation (5G) cellular networks because of its higher spectral efficiency, greater number of connections, lower latency, and better fairness in QoS.

Table 2.1: Comparison of the OMA and NOMA-assisted cellular network.

	Advantages	**Disadvantages**
OMA	- Easy mobile device detection	- Lower spectral efficiency - Lower number of mobile devices - Unfairness for mobile devices
NOMA	- Higher spectral efficiency - Higher number of mobile devices - Higher fairness for mobile devices - Lower latency - Providing diverse QoS for mobile devices	- Higher mobile device complexity

2.2 Multi-antennas assisted wireless communications

For the uplink multi-antenna model, Endo et al. [54] investigated a multi-NOMA network cells. however, the authors assumed that devices in the same cell were orthogonally allocated in resource blocks.

In [55], the authors proposed another uplink model underlay NOMA technique for the multi-antenna environment, where a BS with N antennas to serve up to $2N$ devices simultaneously and to enhance the sum capacity as well by sharing the space resource as shown Figure 2.2.

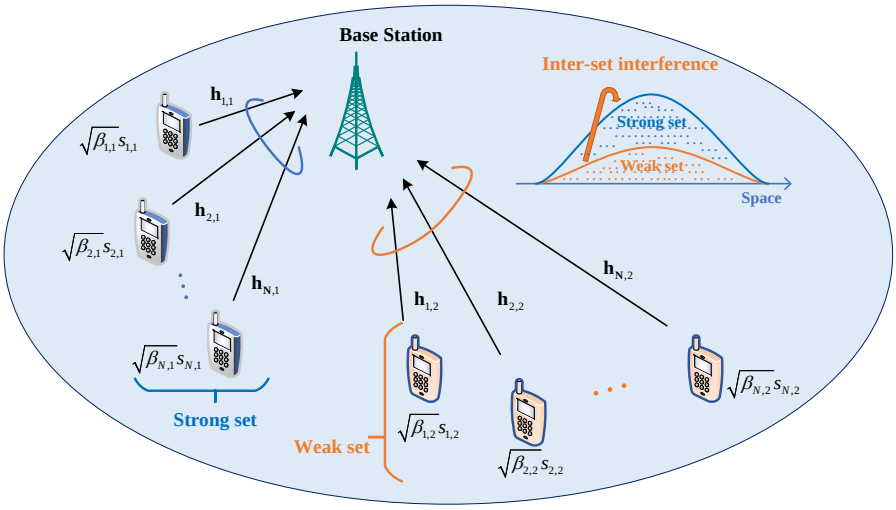

Figure 2.2: System model of MISO for NOMA networks .

From the achieved results as shown in studies [54, 55], the authors confirmed that the MISO technique with multiple antennas on BS could improve network capacity for uplink cellular network. From another point of view, my dissertation focuses on MISO technique as well, however, my dissertation deals with MISO-NOMA techniques enabling for downlink cellular networks. Further, the dissertation also proposes some novel solutions in order to improve QoS for users joined the cellular network.

2.3 Satellite-assisted future cellular networks

This section describes the characteristics of satellite communication systems assisted future cellular networks. It aims to satisfy the QoS requirements of mobile devices. Satellite communications are issued from the outcome of research in the area of communications and space technologies whose objective is to achieve ever increasing ranges and capacities with the lowest possible costs. The authors provided an overview of a satellite communication systems and illustrates its interfacing with terrestrial entities [56]. The satellite systems are consisted of a space segment, a control segment and a ground segment as Figure 2.3. These segments are detailed as follows:

- The space segment includes one or some active and spare satellites allocated into a constellation.

- The control segment contains all ground facilities for the control and monitoring of the satellites, which is named TTC (tracking, telemetry and command) stations, and for the management of the traffic and the associated resources on-board the satellite.
- The ground segment covers of all the traffic earth stations. Depending on the type of service considered, these stations can be of different size, from a few centimetres to tens of metres

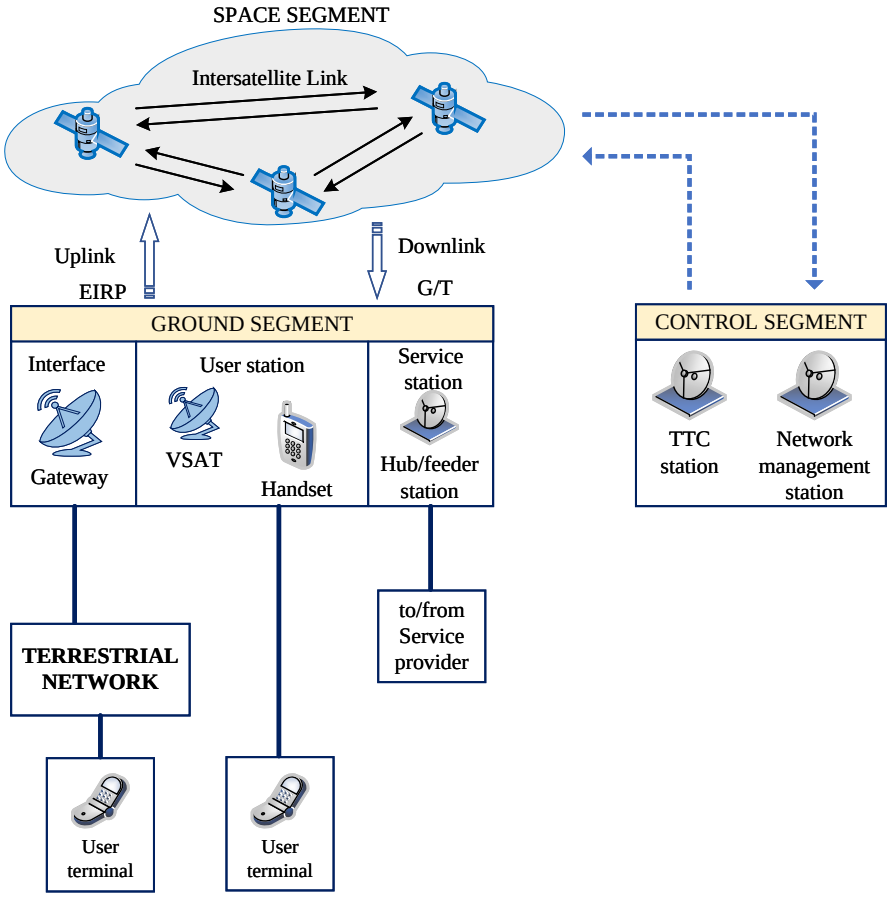

Figure 2.3: Satellite communications system.

The types of link shown in Figure 2.3 are:

- The uplinks from the earth stations to the satellites.
- The downlinks from the satellites to the earth stations.
- The intersatellite links, between the satellites.

Chapter 3:

State-of-the-Art

From investigating the other research, it is well-known that a large number of antennae may enhance the system performance of a NOMA network. In [57], the authors analyzed the system performance of MISO adopted NOMA systems based on optional down-link beamforming. In [58], MIMO-NOMA models were proposed to provide a significantly higher spectral efficiency compared to conventional MIMO-OMA systems by taking into account the benefit of the degree-of-freedom (DoF) provided in both the spatial domain and the power domain. More attention was paid to the MIMO radio system [59, 60]. This is a communication model between transceiver pairs equipped with multiple antennae. However, it is not feasible to equip multiple antennae in compact mobile devices. Therefore, this dissertation proposal aims to investigate the OP and throughput performance by adopting the NOMA technique underlay MISO scheme [NNL07, NNL11]. The wireless network consists of a pair of NOMA users, a BS equipped with two antennae, and a cooperative relay. Additionally, all end-users operate in the NOMA transmission protocol simultaneously. The following is some of the main work which will be discussed in the dissertation.

- A new MISO-enabled NOMA model will be designed. The performance gap of two NOMA users will also be subjected to QoS requirements.
- The exact OP satisfying the conditional power distribution for two NOMA users will be derived.
- The system performance of the MISO-NOMA network will be investigated.

As a feature wireless access technique for next generation wireless communication, NOMA was introduced and analyzed in [61]. To provide better spectral efficiency, NOMA communicates non-orthogonal signals with the receivers. The BS allocates different PA factors to serve multiple users with a superposed signal. In contrast with the OMA technique, NOMA can serve multiple users over the same resource block. NOMA can therefore significantly enhance network capacity [5, 25]. To decode user data, SIC is adopted at the receiver [NNL02]. Specifically, the receiver first decodes the data with the biggest PA factor for the user with the weakest CSI by treating other users' data as interference. However, the authors in [5] did not consider multiple antennae and power beacons, which can significantly enhance system performance. The advantages of Internet of Things (IoT) networks with power beacons was investigated in [62]. Motivated by the papers [5, 25, 62], I will model the issue of power beacon and antenna selection to evaluate the OP performance of two NOMA users.

The multi-antenna technique has recently been adopted in NOMA networks to enhance system performance [20–23]. The OP performance of a CR-NOMA system with a multi-antenna

EH relay was analyzed in [22], [NNL08, NNL10]. Although system performance may potentially improve with a large number of antennae, it leads to a high cost of RF chains at the terminal devices. To face the high cost of hardware while maintaining the diversity and throughput benefits of multiple antennae, the TAS protocol is considered an effective solution [22, 23]. Efficient and flexible, the OMA technique may be combined with various emerging techniques, i.e., cooperative communication [24,63], FD [64], CR-NOMA [65], millimeter wave (mmW) [66], and visible light communication [67] to enhance system performance. The PLS issue is one of the most popular topics in both information security and wireless communications for its advantages in secrecy achieved by utilizing the randomness and time-varying nature of wireless channels without an encryption algorithm [68]. The authors in [69] investigated the PLS of a CR-NOMA system in large-scale networks wherein both NOMA users and eavesdroppers were spatially deployed at random locations. New exact and asymptotic expressions for the SOP were also derived. The study [70] investigated the SOP performance of multi-antennae NOMA with artificial noise and derived the exact and asymptotic expressions.

The current multiple access techniques have been described according to two schemes, i.e., OMA and NOMA, by distinctively considering a specific resource block occupied by multiple UE [71]. Different types of the NOMA technique have also been described, i.e., code-domain NOMA and power-domain NOMA, through an examination of the multiplexing gain gathered from the different domains. The paper [72] explored a scenario of randomly roaming users to examine the performance of the NOMA down-link. In [70], NOMA systems in large-scale networks were investigated with respect to PLS for randomly arranged NOMA users and eavesdroppers. Motivated by previous works and to fill the gap related to the relaying schemes in [73, 74], my dissertation research will enhance the SOP performance of an FD relay network with a DF scheme [NNL05], and more importantly, compare both OMA and NOMA schemes.

The authors in [75] investigated a cooperative small-cell system containing M small-cell transmitters and N relays to examine the OP performance of an opportunistic relaying scheme. A renewable energy-based power resource allocation method was proposed for FD small-cell networks [76]. The authors presented a method for an outage-aware PA scheme, which was considered an optimal transmission strategy for two-way transmission between a BS and UE in a single small-cell network. The study [77] explored a sleeping scheme in next generation small-cell networks by enabling the EH function. Cooperative caching and the energy consumption minimization problem were also considered. To my best knowledge, the authors in recent works [75–77] did not analyze the performance of a small-cell HSTRS which employs NOMA. This motivates me to study small-cell HSTRS which adopt the NOMA technique. This type of configuration may boost the system performance of HSTRS, especially with extended coverage under the bottleneck link behaviour of traditional communications.

Chapter 4:

The Aims of the Dissertation

BASED on the State-of-the-Art on Chapter 3 and the motivations, I propose three main aims in the dissertation, described in the chapter as follows.

4.1 Aim 1: Study of system models with a multiple-antennae transmission technique in a cooperative relay network using NOMA to power the allocation efficiency of users

Over the last decade, the unprecedented proliferation of smart devices and internet-enabled applications has urged next generation cellular networks to accommodate massively networked devices. Contrary to preceding generations of wireless networks which primarily focused on enhancing peak achievable rates for all active users, next generation cellular networks are required to enable IoT, machine-to-machine (M2M), and cellular IoT platforms. Facilitating such technologies calls for novel EE and spectral efficiency transmission techniques which can be easily scaled to millions of devices and accommodate diverse QoS requirements. RF-EH has been especially acknowledged as a potential technology to support EE dense networks, and NOMA has emerged as a technique to improve the spectral efficiency of wireless networks [78].

Most of the studies on NOMA and RF-EH have so far been conducted on single-antenna devices. In next generation cellular systems, the devices should be equipped with multiple antennae, especially at the BS. Therefore, the first aim of the dissertation is to integrate the EH and NOMA techniques into wireless cellular networks with a multiple-antennae transmitter. Specifically, I propose two approaches as follows:

- First, I will examine a next generation cellular wireless network which uses the NOMA technique and investigate the efficiency of multiple antennae equipped at the BS to serve and enhance the OP of multiple NOMA end-users. I will introduce a power distribution model to NOMA users who use direct links and relay links to improve transmission quality. I will then determine the signal to noise ratio to discover separate signals for each user and derive the exact OP expressions of the considered system. To better view my individual method, I also compare the proposed system's performance with a similar system which uses the OMA technique.

- Second, I will extend the previous model, where the access point (AP) will be equipped with multi antennae and the relay can EH from a power beacon. System improvement can be achieved through the exact closed-form expressions of the outage probability (OP). The performance gap between two users will be evaluated using a Rayleigh fading channels model. Furthermore, I will compare NOMA with the traditional scheme, i.e., the OMA technique.

4.2 Aim 2: New proposed system models enabling MISO-NOMA and multi-relaying to improve data safety efficiency for users in the wireless network

PLS has received much attention in the community recently, and the physical characteristics of wireless channels, particularly the channel impulse response (CIR), have become an attractive source of shared secrecy between two communicating parties for many wireless applications. As with other advanced techniques such as NOMA and RF-EH, most of the results on PLS were based on the assumption of single-antenna devices or simple network topology.

The second aim of the dissertation is to provide a thorough analysis of the performance of the PLS for next generation cellular wireless networks which integrate advanced techniques such as FD communication, NOMA, multiple antennae, and relay selection. I will consider two novel PLS schemes:

- For the first model, the secrecy performance of the CR network, which applies NOMA in the down-link scenario, will be derived. The MISO architecture with TAS strategy will also be given special consideration in this model. Furthermore, an optimal PA factor will be obtained to optimize SOP. Simulations will be performed to verify the proposed analytical results.

- In the second model, a NOMA based FD-DF relay network will be designed and evaluated, with the aim to secure system performance in the presence of a passive eavesdropper. The closed-form expressions for the end-to-end signal-to-interference-plus-noise ratio (SINR) in the legitimate link and the wiretap link will be derived; the closed-form expression for the exact SOP of the proposed model will be presented over a Rayleigh fading channel. I will additionally compare two SOP cases, i.e., OMA and NOMA.

4.3 Aim 3: A new proposed system model to optimize the power spectrum allocation of small-cells in the integrated networks between the satellite and terrestrial users

Satellite networks will serve as a critical segment in next generation cellular wireless networks by providing wide-ranging coverage and massive connections for areas where ground wireless infrastructures are too difficult or expensive to deploy. However, satellite networks provide services in an inefficient manner in terms of resource utilization owing to the conventional use of traditional techniques. Under specific conditions, the NOMA technique can improve spectral efficiency, increase the number of connections for multiple access schemes, and flexibly inherit the existing OMA schemes. The NOMA technique should therefore be studied with more insight for future satellite communications.

For the third aim, I propose an integrated solution to enhance service quality in satellite networks. First, satellite communications systems must be integrated with the emerging small-cell networks to provide seamless connectivity and high-speed broadband access for mobile users in future wireless networks. I will study an HSTRS which assists small-cell transmission under interference constraints with macro-cell users. An HSTRS system will be enhanced by using the

NOMA technique to improve spectrum efficiency. To provide a performance analysis, I will derive the exact expressions for OP and throughput of the considered HSTRS system under Shadowed-Rician fading channels for satellite links and Nakagami-m fading channels for terrestrial links. The OP performances of the two users, which depend on PA factors, will also be investigated. The results of this aim will provide potential deep insight for the design of future HSTRS for small-cell communications.

Chapter 5:

Multi-Antennae Combining Power Beacon-Assisted NOMA Network Model

Part I – MISO-NOMA Assisted Future Cellular Networks

In the dissertation, I deal with MISO technique in NOMA networks to improve the fairness QoS for multiple UE [NNL06, NNL10]. The feature contributions of this chapter are:

- A new MISO-enabled NOMA model is proposed and performance gap of two NOMA users is provided to meet the requirements of the QoS in such MISO-NOMA system.
- The exact outage probability for two NOMA users is calculated while meeting certain power distribution conditions. After that, the outage performance and the corresponding throughput are identified in numerical results.
- The overall network performance is analyzed, the fixed PA problems are examined under the constrained conditions of total system capacity and MISO diagram design to give solutions to performance improvement problems.

5.1 System Models

In this chapter, we study a communication with MISO model as shown in Fig. 5.1. This model comprises a BS, a relay R and a pair of NOMA users (U_1 and U_2). All entities in the network are equipped with single antenna except for the BS equipped two antennas and the communication of two antennas operate in such model using the NOMA transmission principles. It is assumed that both the relay and two NOMA users can examine their SNR since they can recognize the CSI of all the channels completely. Moreover, all channels are assumed to be quasi-static Rayleigh fading, where the channel coefficients are constant for each transmission block but vary independently between different blocks. The first antenna and the second antenna in the BS of such model transmit x_1, x_2 respectively to both relay and far NOMA users in the same time slot.

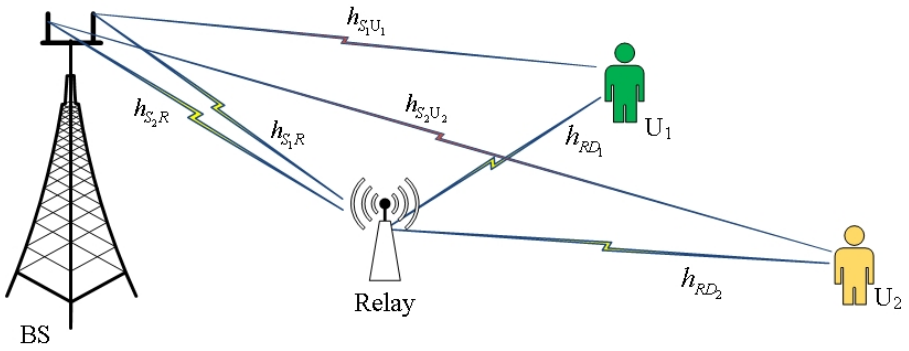

Figure 5.1: System model of MISO for NOMA networks.

Besides, a_1 and a_2, where $a_1 < a_2$, are PA factors for two NOMA users U_1 and U_2 [NNL03], respectively, and they satisfy condition $a_1 + a_2 = 1$. We denote P_{S_1} and P_{S_2} are transmit power at two antennae. We then denote $d_{a,b}$ is distance between node a and node b. h_{S_1,U_1} , h_{S_2,U_2} , $h_{S_1,R}$, $h_{S_2,R}$, h_{R,U_1} and h_{R,U_2}, are denoted as the complex channel coefficient of $BS \to \{U_1, U_2\}$, $BS \to R$ and $R \to \{U_1, U_2\}$, respectively. The channel power gains$|h_{S_1,U_1}|^2$, $|h_{S_2,U_2}|^2$, $|h_{S_1,R}|^2$, $|h_{S_2,R}|^2$, $|h_{R,U_1}|^2$ and $|h_{R,U_2}|^2$ are assumed to be exponentially distributed random variables (RVs).

The first antenna and the second antenna at the BS transmit x_1 and x_2, respectively. It is assumed that inter-symbol among these signal does not exist. In the first phase, relay R may receive the synthetic message from the BS

$$y_R = h_{S_1,R}\sqrt{a_1 P_{S_1}}x_1 + h_{S_2,R}\sqrt{a_2 P_{S_2}}x_2 + n_R, \tag{5.1}$$

where n_R is additive white Gaussian noise (AWGN) at relay and following $n_R \sim (0, \sigma^2)$ with zero mean and variance σ^2.

The received signal at destination U_1 in relay link is shown by

$$y_{R,U_1} = h_{R,U_1}\left(\sqrt{a_1 P_R}x_1 + \sqrt{a_2 P_R}x_2\right) + n_{U_1}, \tag{5.2}$$

where n_{U_1} is AWGN at user U_1 and following $n_{U_1} \sim (0, \sigma^2)$ with zero mean and variance σ^2.

Similarly, the received signal at destination U_2 in relay link is expressed as follows:

$$y_{R,U_2} = h_{R,U_2}\left(\sqrt{a_1 P_R}x_1 + \sqrt{a_2 P_R}x_2\right) + n_{U_2}. \tag{5.3}$$

where n_{U_2} is AWGN at user U_2 and following $n_{U_2} \sim (0, \sigma^2)$ with zero mean and variance σ^2.

The received signal at destination U_1 in direct link is given by

$$y_{S_1,U_1} = h_{S_1,U_1}\sqrt{P_{S_1}}x_1 + n_{U_1}. \tag{5.4}$$

The received signal at destination U_2 in direct link is given by

$$y_{S_2,U_2} = h_{S_2,U_2}\sqrt{P_{S_2}}x_2 + n_{U_2}. \tag{5.5}$$

In this case, we assume variance noise terms given by $\sigma^2 = \sigma_R^2 = \sigma_{R,U_1}^2 = \sigma_{R,U_2}^2 = \sigma_{S_1,U_1}^2 = \sigma_{S_2,U_2}^2$ and SNR $\rho = \frac{P_{S_1}}{\sigma^2} = \frac{P_{S_2}}{\sigma^2} = \frac{P_R}{\sigma^2}$.

It can be computed various signal to interference plus noise ratio (SINR) as below. SINR at relay when it detects x_2 is expressed as follows:

$$\gamma_{R,x_2} = \frac{a_2\rho|h_{S_2,R}|^2}{a_1\rho|h_{S_1,R}|^2 + 1}. \tag{5.6}$$

SINR at relay when it detects x_1 is expressed as follows:

$$\gamma_{R,x_1} = a_1\rho|h_{S_1,R}|^2. \tag{5.7}$$

Besides, SINR at U_1 when it to detect x_2 is expressed as follows:

$$\gamma_{RU_1,x_2} = \frac{a_2\rho|h_{R,U_1}|^2}{a_1\rho|h_{R,U_1}|^2 + 1}. \tag{5.8}$$

It is noted that relay adopted DF protocol. SINR at U_1 in cooperative link when U_1 detects x_1 is expressed as follows:

$$\gamma_{RU_1,x_2} = a_1\rho|h_{R,U_1}|^2. \tag{5.9}$$

SINR at U_2 in cooperative scheme when U_2 detects x_2 is expressed as follows:

$$\gamma_{RU_2,x_2} = \frac{a_2\rho|h_{R,U_2}|^2}{a_1\rho|h_{R,U_2}|^2 + 1}. \tag{5.10}$$

Particularly, SINR at U_1 and U_2 in direct link to detect their own signal are respectively expressed as follows:

$$\gamma_{S_1U_1,x_1} = \rho|h_{S_1,U_1}|^2, \tag{5.11}$$

$$\gamma_{S_2U_2,x_2} = \rho|h_{S_2,U_2}|^2. \tag{5.12}$$

5.2 System Performance Analysis

In this section, the outage behavior for the MISO-NOMA downlink cooperative network with perfect CSI is investigated [NNL07]. To this end, we first study exact expressions for the OP. In order to achieve best throughput and the behavior of the network, a numerical method is employed to detect optimal throughput, while fairness among NOMA users is satisfied as requirement of NOMA scheme. We use maximum ratio combining (MRC) to further process

signal at U_1, U_2 as representatives of direct link and relay link between the BS and NOMA end-users [78].

An outage event happens at the far NOMA user and SINR at each user can be first formulated as follows:

$$\begin{aligned}\gamma_{U_1}^{MRC} &= \gamma_{S_1U_1,x_1} + \gamma_{RU_1,x_1} \\ &= \rho|h_{S_1,U_1}|^2 + a_1\rho|h_{R,U_1}|^2,\end{aligned} \tag{5.13}$$

and

$$\begin{aligned}\gamma_{U_2}^{MRC} &= \gamma_{S_2U_2,x_2} + \gamma_{RU_2,x_2} \\ &= \rho|h_{S_2,U_2}|^2 + \frac{a_2\rho|h_{R,U_2}|^2}{a_1\rho|h_{R,U_2}|^2 + 1}.\end{aligned} \tag{5.14}$$

Then, the OP at user U_1 can be expressed as follows:

$$P_{U_1} = \underbrace{\Pr\left(\gamma_{U_1}^{MRC} < \gamma_1\right)}_{A_1}\underbrace{\Pr\left(\gamma_{R,x_1} > \gamma_1\right)}_{A_2} + \underbrace{\Pr\left(\gamma_{R,x_1} < \gamma_1, \gamma_{S_1U_1,x_1} < \gamma_1\right)}_{A_3}, \tag{5.15}$$

where $\gamma_1 = 2^{2R_1} - 1$.

Proposition 1: The closed-form expression of OP at user U_1 can be expressed as follows:

$$P_{U_1} = \varphi_{U_1}\exp\left(-\frac{\gamma_1}{d_{S_1,R}^{-m}\rho}\right) + \left(1 - \exp\left(-\frac{\gamma_1}{d_{S_1,R}^{-m}\rho}\right)\right)\left(1 - \exp\left(-\frac{\gamma_1}{d_{S_1,U_1}^{-m}\rho}\right)\right), \tag{5.16}$$

where

$$\begin{aligned}\varphi_{U_1} = 1 &- \exp\left(-\frac{\gamma_1}{d_{R,U_1}^{-m}a_1\rho}\right) - \frac{d_{S_1,U_1}^{-m}}{d_{S_1,U_1}^{-m} - d_{R,U_1}^{-m}a_1}\exp\left(-\frac{\gamma_1}{d_{S_1,U_1}^{-m}\rho}\right) \\ &\times\left(1 - \exp\left(-\frac{\gamma_1}{a_1\rho}\left(\frac{1}{d_{R,U_1}^{-m}} - \frac{a_1}{d_{S_1,U_1}^{-m}}\right)\right)\right).\end{aligned} \tag{5.17}$$

Proof: From expression (5.15), each component A_1, A_2 or A_3 is computed, respectively, as follows:

$$\begin{aligned}A_1 &= \Pr\left(\gamma_{U_1}^{MRC} < \gamma_1\right) \\ &= \int_0^{\frac{\gamma_1}{a_1\rho}} F_{|h_{S_1,U_1}|^2}\left(\frac{\gamma_1}{\rho} - a_1x\right) f_{|h_{S_1,U_1}|^2}(x)\,dx \\ &= \varphi_{U_1} = 1 - \exp\left(-\frac{\gamma_1}{d_{R,U_1}^{-m}a_1\rho}\right) - \frac{d_{S_1,U_1}^{-m}}{d_{S_1,U_1}^{-m} - d_{R,U_1}^{-m}a_1}\exp\left(-\frac{\gamma_1}{d_{S_1,U_1}^{-m}\rho}\right) \\ &\times\left(1 - \exp\left(-\frac{\gamma_1}{a_1\rho}\left(\frac{1}{d_{R,U_1}^{-m}} - \frac{a_1}{d_{S_1,U_1}^{-m}}\right)\right)\right),\end{aligned} \tag{5.18}$$

$$A_2 = \Pr\left(\gamma_{R,x_1} > \gamma_1\right) = \Pr\left(|h_{S_1,R}|^2 > \frac{\gamma_1}{\rho}\right)$$
$$= \int_{\frac{\gamma_1}{\rho}}^{\infty} f_{|h_{S_1,R}|^2}(x)\, dx = \exp\left(-\frac{\gamma_1}{d_{S_1,R}^{-m}\rho}\right), \tag{5.19}$$

$$A_3 = \Pr\left(\gamma_{R,x_1} < \gamma_1, \gamma_{S_1U_1,x_1} < \gamma_1\right)$$
$$= \Pr\left(|h_{S_1,R}|^2 < \frac{\gamma_1}{\rho}, |h_{S_1,U_1}|^2 < \frac{\gamma_1}{\rho}\right)$$
$$= \int_0^{\frac{\gamma_1}{\rho}} \int_0^{\frac{\gamma_1}{\rho}} f_{|h_{S_1,R}|^2}(x)\, f_{|h_{S_1,U_1}|^2}(y)\, dxdy$$
$$= \left(1 - \exp\left(-\frac{\gamma_1}{d_{S_1,R}^{-m}\rho}\right)\right)\left(1 - \exp\left(-\frac{\gamma_1}{d_{S_1,U_1}^{-m}\rho}\right)\right). \tag{5.20}$$

By substituting expressions (5.18), (5.19) and (5.20) into (5.15), we obtain closed form OP at user U_1. This is end of the proof.

Similarly, OP at user U_2 can be calculated by

$$P_{U_2} = \underbrace{\Pr\left(\gamma_{U_2}^{MRC} < \gamma_2\right)}_{B_1}\underbrace{\Pr\left(\gamma_{R,x_2} > \gamma_2\right)}_{B_2} + \underbrace{\Pr\left(\gamma_{R,x_2} < \gamma_2, \gamma_{S_2U_2,x_2} < \gamma_2\right)}_{B_3}, \tag{5.21}$$

where $\gamma_2 = 2^{2R_2} - 1$.

From [78], the closed-form expression of OP at user U_2 as shown (5.21) could be solved and expressed in closed-form as follows:

$$P_{U_2} = \left(1 - \exp\left(-\frac{\tau}{d_{R,U_2}^{-m}}\right) - \frac{\exp(\xi)}{\Psi_2}\sum_{n=0}^{\infty}\frac{(-1)^n}{n!\left(d_{R,U_2}^{-m}a_1\rho\right)}\Xi_2\right)$$
$$\times \frac{d_{S_2,R}^{-m}}{d_{S_2,R}^{-m} + \gamma_2 d_{S_1,R}^{-m}}\exp\left(-\frac{\gamma_2}{d_{S_2,R}^{-m}\rho}\right) + 1 - \exp\left(-\frac{\gamma_2}{d_{S_2,U_2}^{-m}\rho}\right)$$
$$- \frac{d_{S_2,R}^{-m}}{d_{S_2,R}^{-m} + \gamma_2 d_{S_1,R}^{-m}}\exp\left(-\frac{\gamma_2}{d_{S_2,R}^{-m}\rho}\right) - \exp\left(-\frac{\gamma_2}{d_{S_2,U_2}^{-m}\rho} - \frac{\gamma_2}{d_{S_2,R}^{-m}\rho}\right), \tag{5.22}$$

where

$$\Xi_2 = \frac{(-1)^{2n+1}\Psi_1^{n+1}}{(n+1)!}\left(Ei(\xi) - Ei(\Psi_1)\right)$$
$$+ \sum_{k=0}^{n}\frac{\exp(\xi)(1 + a_1\rho\tau)^{n+1} - \exp(\Psi_1)\Psi_1^k}{(n+1)\, n \ldots (n+1-k)}, \tag{5.23}$$

and $\xi = \frac{1}{a_1 \rho d_{R,U_2}^{-m}} - \frac{\gamma_2}{\rho d_{S_2,U_2}^{-m}} - \Psi_1$, $\Psi_1 = -\frac{a_2}{a_1 \rho d_{S_2,U_2}^{-m}}$ and $\Psi_2 = a_1 \rho d_{S_2,U_2}^{-m}$.

we further investigate optimal throughput in case of fixed data rates are known. Such system throughput can be expressed as follows:

$$\tau = (1 - P_{U_1}) R_1 + (1 - P_{U_2}) R_2. \tag{5.24}$$

5.3 Numerical Results and Discussions

In this section, a model of two-user MISO NOMA system is investigated in term of OP and throughput performance. Computer simulations are performed to confirm the correctness of the analytical results. We set $a_1 = 0.2$ and $a_2 = 0.8$. We present analytical result in many figures where the parameters are set as wherein. $R_1 = 3$, $R_2 = 0.5$, $m = 2$, $d_{S_1,R} = d_{S_2,R} = 0.3$, $d_{R,U_1} = d_{R,U_2} = 0.7$ and $d_{S_1,U_1} = d_{S_2,U_2} = 1$

OP performance can be seen in 5.2. For these target rate setups, it can be seen OP decreases as increasing SNR and performance gap between two NOMA users exist in range of SNR. By observing such figure, it can be confirmed that lower target rate exhibits better performance. This confirmation can be explained as such target rate make varying outage levels. Analytical and simulation result are matched well. In addition, our study provide improvement compared results from [78].

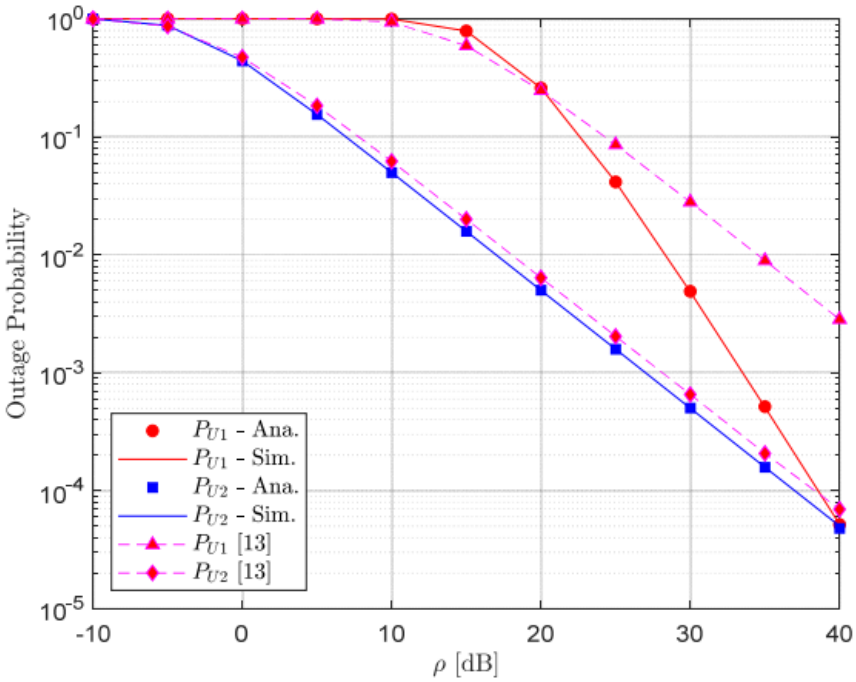

Figure 5.2: OP of two NOMA users versus transmit SNR at the BS.

Figure 5.3 indicates that OP increases at higher target rates. Other observation is that higher SNR at the BS contributes to improved outage performance of considered system. Performance gap of two NOMA users still remains in range of target rate regime.

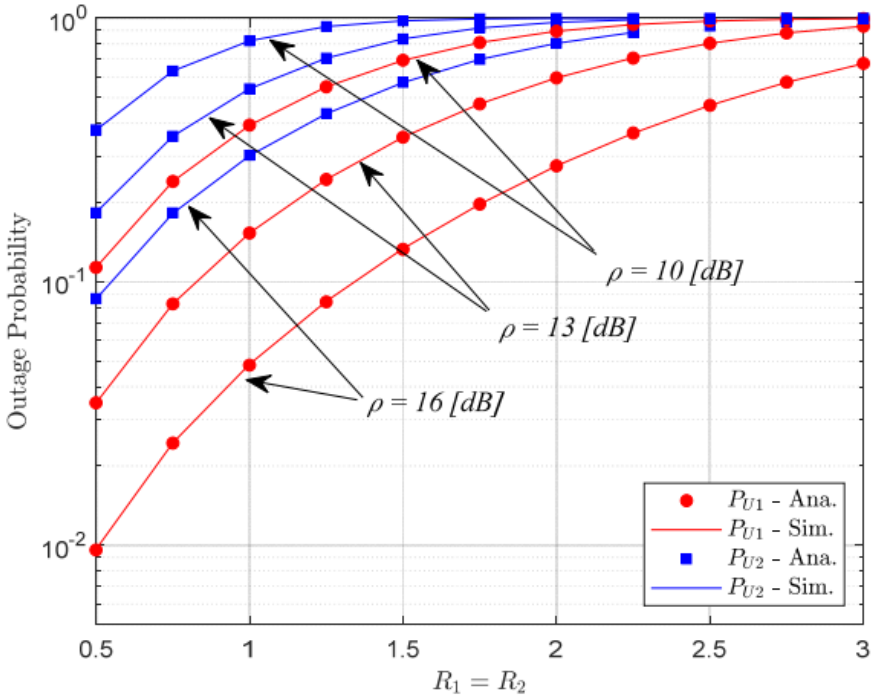

Figure 5.3: Outage probability versus target rates at each user.

It can be observed throughput performance in Figure 5.4 where optimal throughput happens as we change target rates and transmit SNR at the BS. In this situation, optimal throughout can be achieved at $\rho = 40\,(dB)$, $R_1 = R_2 = 7\,(bps/Hz)$.

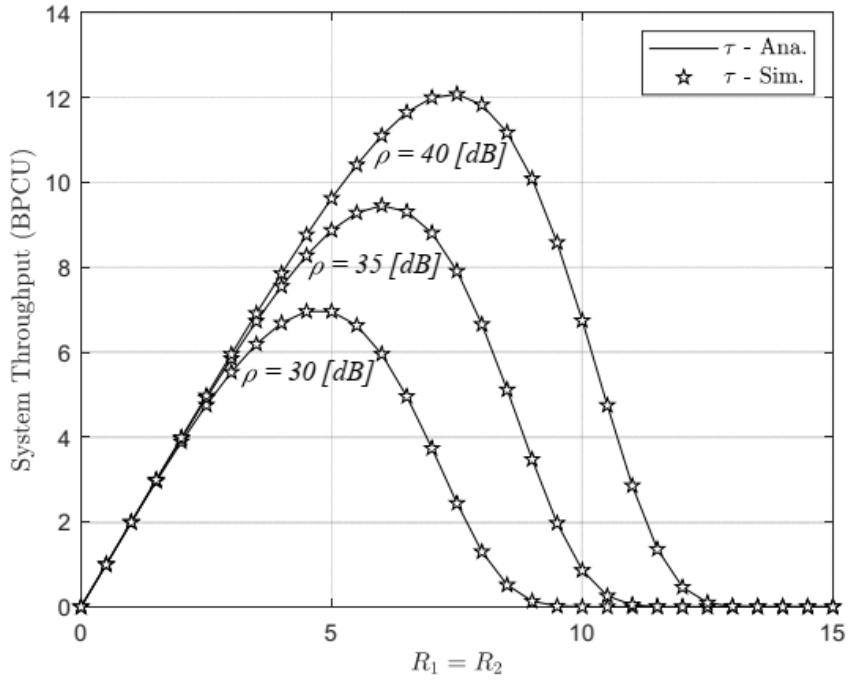

Figure 5.4: Throughput versus target rates.

5.4 Conclusion

In this chapter, we examined outage and throughput performance in MISO based NOMA systems. A BS equipped two antennas can provide signal transmitting to relay and then the superimposed signal can be obtained at the NOMA end users. This scheme was applied for supplying multiple access in downlink. Simulation results proved that the proposed MISO NOMA system using the suggested fixed power distribution scheme can ensure fairness in NOMA considerably. For specific data rate, the highest throughput can be achieved. In addition, our results proved that the outage performance gap among two NOMA users of the proposed scheme was small in regard to varying transmit SNR and validated the effect of various system parameters on performance. Full MIMO NOMA with higher diversity order is goal in our future work.

Part II – Power Beacon Combining MISO Technique-Assisted NOMA Networks

THE WPT is a significant technique for future cellular networks. Recently, more interest has been focused on multiple access technique without orthogonal signals for wireless communication. NOMA scheme is proposed to allow users to be served simultaneously. In this chapter, we propose the power beacon which is able to feed energy to power-constraint relay node to further support transmission from the source to destinations in future cellular networks. NOMA system is benefited by with WPT and antenna selection technique [NNL06]. The system improvement can be achieved through the exact closed-form expressions of OP. The performance gap among two users is evaluated using model of the Rayleigh fading channels. Furthermore, we compare NOMA with traditional scheme to highlight advantage of such IoT system.

5.5 System Models

In this model, Figure 5.5 shows the cellular network containing the access point (AP), the relay R, two users D_1 and D_2, and power beacon (B). Wireless channels denoted as in Figure 5.5 in such cellular network relying NOMA are subjected to Rayleigh flat fading plus AWGN. The complex channel coefficients for the links $AP \rightarrow R$, $B \rightarrow R$, $R \rightarrow D_1$ and $R \rightarrow D_2$ are presented by $|h_{S_kR}|^2 \sim CN(0, \lambda_{SR})$, $|h_{BR}|^2 \sim CN(0, \lambda_{BR})$, $|h_{RD_1}|^2 \sim CN(0, \lambda_{RD_1})$, and $|h_{RD_2}|^2 \sim CN(0, \lambda_{RD_2})$, respectively. The are K antennae equipped at the AP.

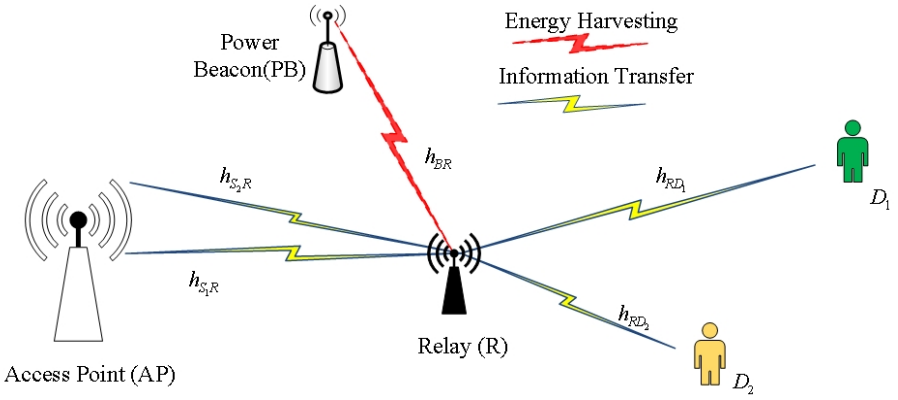

Figure 5.5: System Model of multiple antennae in a NOMA assisted by a power beacon.

There are two links from the AP to NOMA users. In the first phase, the received signal at the relay R is expressed as follows:

$$y_{AP-R} = h_{AP_k}\left(\sqrt{a_1 P_{AP}}x_1 + \sqrt{a_2 P_{AP}}x_2\right) + \omega_R, \tag{5.25}$$

where P_{AP} is the transmit power of AP, x_i for $i \in \{1, 2\}$ is the information symbol for device D_i, and ω_R is AWGN at the relay. Optimization of such PA is out of concern in this chapter.

It can be achieved by the SINR at the receivers. In order to decode x_1 at R, the corresponding

SINR is expressed by

$$\gamma_{AP_kR-x_1} = \frac{a_1 P_{AP} |h_{AP_kR}|^2}{a_2 P_{AP} |h_{AP_kR}|^2 + N_0}. \tag{5.26}$$

In NOMA, SIC is employed to eliminate interference, the SINR to decode x_2 is expressed as follows:

$$\gamma_{AP_kR-x_2} = \frac{a_2 P_{AP} |h_{AP_kR}|^2}{N_0}. \tag{5.27}$$

During time for signal processing in the second phase, R transmits the signal consisting of the decoded and re-encoded symbols to the destinations. The received signal at two users D_i is expressed as follows:

$$y_{RD_i} = h_{RD_i} \left(\sqrt{a_1 P_R} x_1 + \sqrt{a_2 P_R} x_2 \right) + \omega_{D_i}, \tag{5.28}$$

where P_R is the transmit power of R, ω_{D_i} is the AWGN at device D_i

The SINR at each receiver needs to be calculated. In this case, the destination is required to decode x_1 at D_1 as below

$$\gamma_{RD_1-x_1} = \frac{a_1 P_R |h_{RD_1}|^2}{a_2 P_R |h_{RD_1}|^2 + N_0}. \tag{5.29}$$

The SINR to decode x_1 at D_2 is expressed as follows:

$$\gamma_{RD_2-x_1} = \frac{a_1 P_R |h_{RD_2}|^2}{a_2 P_R |h_{RD_2}|^2 + N_0}. \tag{5.30}$$

After SIC, the SINR to decode x_2 is expressed as follows:

$$\gamma_{RD_2-x_2} = \frac{a_2 P_R |h_{RD_2}|^2}{N_0}. \tag{5.31}$$

The best channel is selected with the index of antennae equipped at the AP as follows:

$$k^* = \arg \max_{k=\{1,\ldots,K\}} \left(|h_{AP_kR}|^2 \right). \tag{5.32}$$

Together with (5.32), the cumulative distribution function (CDF) and probability density function (PDF) related to selected channels are given as follows:

$$F_{|h_{AP_{k^*}R}|^2}(x) = 1 - \sum_{k=1}^{K} \binom{K}{k} (-1)^{k-1} \exp\left(-\frac{kx}{\lambda_{APR}} \right) \tag{5.33}$$

and

$$f_{|h_{AP_{k^*}R}|^2}(x) = \sum_{k=1}^{K} \binom{K}{k} (-1)^{k-1} \frac{k}{\lambda_{APR}} \exp\left(-\frac{kx}{\lambda_{APR}}\right) \tag{5.34}$$

In the considered system, the relay harvests energy from beacons. The operation of the second stage of signal processing is supported by harvesting energy at relay.

At EH phase, the time switching (TS) based EH technique is applied. In a transmission block time T (in which a block of information is sent from the power beacon to the relay), the relay takes αT to harvest energy from the power beacon, in which α is the EH time fraction that depends on the schedule of B. We allocate the time slot of $(1-\alpha)T$ into two equal sub-time slots for the link from the AP to relay and the link from relay to destinations. Then, we can compute harvested energy at the relay [9] as follows:

$$E_R = \tau P_B \alpha T |h_{BR}|^2, \tag{5.35}$$

where $0 < \tau < 1$ stands for the efficiency coefficient of the energy conversion process, P_B is the transmit power of the power beacon, assuming that these power beacons have the same power level, respectively (optimizing TS factor α is out of the scope of this dissertation). Under the assumption that the processing energy at R is negligible, the transmit power of the relay is expressed as follows:

$$P_R = \frac{2\tau P_B \alpha |h_{BR}|^2}{(1-\alpha)} = \xi |h_{BR}|^2, \tag{5.36}$$

where $\xi = \frac{2\tau P_B \alpha}{(1-\alpha)}$.

5.6 System Performance Analysis

In this section, we consider the OP analyses for the cellular network to look for impact of harvested energy and the number of transmit antennae at the AP. In particular, we derive the closed-form expressions to show the OP, and performance difference happens as comparing two users' performance. To provide insights, asymptotic outage performance analyses for the considered system are determined in the high transmit signal to noise ratio (SNR) region.

A. Outage Performance Analysis for NOMA

5.6.1 Outage Analysis at D_1

With respect to the system performance evaluation, the OP can be achieved related to ability to detect signal at relay and destinations as well. The expression of OP for the first user can be

defined as follows:

$$\begin{aligned} OP_1 &= \Pr\left(\min\left(\gamma_{AP_{k^*}R-x_1}, \gamma_{RD_1-x_1}\right) < \gamma_1\right) \\ &= 1 - \Pr\left(\gamma_{AP_{k^*}R-x_1} > \gamma_1, \gamma_{RD_1-x_1} > \gamma_1\right) \\ &= 1 - \underbrace{\Pr\left(\gamma_{AP_{k^*}R-x_1} > \gamma_1\right)}_{\partial_1} \underbrace{\Pr\left(\gamma_{RD_1-x_1} > \gamma_1\right)}_{\partial_2}, \end{aligned} \tag{5.37}$$

Proposition 1: The close-form expression is computed to provide outage analysis at D_1 as follow:

$$\begin{aligned} OP_1 = 1 - \sum_{k=1}^{K} \binom{K}{k} (-1)^{k-1} \exp\left(-\frac{k\gamma_1 N_0}{P_{AP}\left(a_1 - \gamma_1 a_2\right)\lambda_{APR}}\right) \\ \times \sqrt{\frac{4\gamma_1 N_0}{\xi\left(a_1 - \gamma_1 a_2\right)\lambda_{APR}\lambda_{RD_1}}} K_1\left(\sqrt{\frac{4\gamma_1 N_0}{\xi\left(a_1 - \gamma_1 a_2\right)\lambda_{APR}\lambda_{RD_1}}}\right), \end{aligned} \tag{5.38}$$

where $K_1(.)$ is the second kind of modified Bessel functions.

Proof: Refer to Appendix 5.9.1 (pp. 31).

5.6.2 Outage Analysis at D_2 with Perfect SIC

At the second user, it can be seen outage performance evaluated by

$$\begin{aligned} OP_2 &= \Pr\left(\min\left(\gamma_{AP_{k^*}R-x_2}, \gamma_{RD_2-x_1}, \gamma_{RD_2-x_2}\right) < \gamma_2\right) \\ &= 1 - \Pr\left(\gamma_{AP_{k^*}R-x_2} > \gamma_2, \gamma_{RD_2-x_1} > \gamma_2, \gamma_{RD_2-x_2} > \gamma_2\right) \\ &= 1 - \underbrace{\Pr\left(\gamma_{AP_{k^*}R-x_2} > \gamma_2\right)}_{V_1} \underbrace{\Pr\left(\gamma_{RD_2-x_1} > \gamma_2, \gamma_{RD_2-x_2} > \gamma_2\right)}_{V_2}. \end{aligned} \tag{5.39}$$

Proposition 2: It can be achieved the close-form expression to provide outage analysis perfect SIC at D_2 in perfect SIC case as

$$\begin{aligned} OP_2 = 1 - \sum_{k=1}^{K} \binom{K}{k} (-1)^{k-1} \exp\left(-\frac{k\gamma_2 N_0}{\alpha_2 P_{AP}\lambda_{APR}}\right) \\ \times \sqrt{\frac{4\theta\gamma_2 N_0}{\xi\lambda_{BR}\lambda_{RD_2}}} K_1\left(\sqrt{\frac{4\theta\gamma_2 N_0}{\xi\lambda_{BR}\lambda_{RD_2}}}\right). \end{aligned} \tag{5.40}$$

Proof: Refer to Appendix 5.9.2 (pp. 31).

5.6.3 Scenario of Imperfect SIC

The SINR to decode x_2 at the first link AP-relay is given by

$$\gamma_{AP_kRip} = \frac{a_2 P_{AP}|h_{AP_kR}|^2}{a_1 P_{AP}|g_{AP_kR}|^2 + N_0}, \tag{5.41}$$

where $g_{AP_kR} \sim CN\left(0, \mu\lambda_{APRip}\right)$ and μ is denoted as the level of residual interference caused by imperfect SIC as $0 < \mu < 1$.

The second link is evaluated via SINR as below. It is used to decode x_2 D_2 and such SINR is formulated by

$$\gamma_{RD_2ip-x_2} = \frac{a_2 P_R |h_{RD_2}|^2}{a_1 P_R |g_{RD_2}|^2 + N_0}, \tag{5.42}$$

where $g_{RD_2ip} \sim CN\left(0, \mu\lambda_{RD_2ip}\right)$.

The outage performance of user D_2 in imperfect SIC case can be written as follows:

$$\begin{aligned} OP_{2ip} &= \Pr\left(\min\left(\gamma_{AP_{k^*}Rip-x_2}, \gamma_{RD_2ip-x_2}\right) < \gamma_2\right) \\ &= 1 - \Pr\left(\gamma_{AP_{k^*}Rip-x_2} > \gamma_2, \gamma_{RD_2ip-x_2} > \gamma_2\right) \\ &= 1 - \underbrace{\Pr\left(\gamma_{AP_{k^*}Rip-x_2} > \gamma_2\right)}_{\psi_1} \underbrace{\Pr\left(\gamma_{RD_2ip-x_2} > \gamma_2\right)}_{\psi_2}. \end{aligned} \tag{5.43}$$

Proposition 3: The closed-form in outage analysis at D_2 is formulated (imperfect SIC case) by

$$\begin{aligned} OP_{2ip} = 1 &- \sum_{k=1}^{K}\sum_{m=1}^{K} \binom{K}{k}\binom{K}{m} (-1)^{k+m-2} \\ &\times \frac{m a_2 \lambda_{APR}}{k\gamma_2 a_1 \lambda_{APRip} + m a_2 \lambda_{APR}} \exp\left(-\frac{k\gamma_2 N_0}{a_2 P_{AP} \lambda_{APR}}\right) \\ &\times \frac{a_2 \xi \lambda_{RD_2}}{\gamma_2 a_1 \xi \lambda_{RD_2ip} + a_2 \xi \lambda_{RD_2ip}} \sqrt{\frac{4\gamma_2 N_0}{a_2 \xi \lambda_{RD_2} \lambda_{BR}}} K_1\left(\sqrt{\frac{4\gamma_2 N_0}{a_2 \xi \lambda_{RD_2} \lambda_{BR}}}\right). \end{aligned} \tag{5.44}$$

Proof: Refer to Appendix 5.9.3 (pp. 32).

5.6.4 Asymptotic OP Analysis

When $P_{AP} \to \infty$, asymptotic performance of D_1 and D_2 can be obtained. We first look on the asymptotic performance of the first user in terms of as follows::

$$OP_1^{asym} = 1 - \sqrt{\frac{4\gamma_1 N_0}{\xi\left(a_1 - \gamma_1 a_2\right)\lambda_{RD_1}\lambda_{BR}}} K_1\left(\sqrt{\frac{4\gamma_1 N_0}{\xi\left(a_1 - \gamma_1 a_2\right)\lambda_{RD_1}\lambda_{BR}}}\right), \tag{5.45}$$

$$OP_1^{asym} = 1 - \sqrt{\frac{4\theta\gamma_2 N_0}{\xi\lambda_{RD_2}\lambda_{BR}}} K_1\left(\sqrt{\frac{4\theta\gamma_2 N_0}{\xi\lambda_{RD_2}\lambda_{BR}}}\right). \tag{5.46}$$

It is worth noting that perfect SIC and imperfect SIC cases are considered for user D_2,

respectively, as follows:

$$OP_{2ip}^{asym} = 1 - \sum_{k=1}^{K}\sum_{m=1}^{K}\binom{K}{k}\binom{K}{m}(-1)^{k+m-2} \times \frac{ma_2\lambda_{APR}}{k\gamma_2 a_1\lambda_{APRip} + ma_2\lambda_{APR}} \frac{a_2\xi\lambda_{RD_2}}{\gamma_2 a_1\xi\lambda_{RD_2ip} + a_2\xi\lambda_{RD_2ip}} \times \sqrt{\frac{4\gamma_2 N_0}{a_2\xi\lambda_{RD_2}\lambda_{BR}}} K_1\left(\sqrt{\frac{4\gamma_2 N_0}{a_2\xi\lambda_{RD_2}\lambda_{BR}}}\right). \quad (5.47)$$

B. Outage Performance of OMA

In the first phase, the received signal at the first link AP - relay is expressed as follows:

$$y_{APR}^{OMA} = \sqrt{P_{AP}} h_{AP_kR} x_i + \omega_R. \quad (5.48)$$

The SINR computed to decode x_i at R is expressed as follows:

$$\gamma_{AP_kR-x_i}^{OMA} = \frac{P_{AP}|h_{AP_kR}|^2}{N_0}. \quad (5.49)$$

After that, R transmits the mixture signal (the decoded and re-encoded symbols) to the destinations. The received signal at D_i is expressed as follows:

$$y_{RD_i}^{OMA} = \sqrt{P_R} h_{RD_i} x_i + \omega_{D_i}. \quad (5.50)$$

The SINR to decode x_i at D_i is expressed as follows:

$$\gamma_{RD_i-x_i}^{OMA} = \frac{P_R|h_{RD_i}|^2}{N_0}. \quad (5.51)$$

The OP at D_i can be expressed as

$$\begin{aligned}
OP_i^{OMA} &= \Pr\left(\min\left(\gamma_{AP_kR-x_i}^{OMA}, \gamma_{RD_i-x_i}^{OMA}\right) < \gamma_i^{OMA}\right) \\
&= 1 - \Pr\left(\gamma_{AP_kR-x_i}^{OMA} > \gamma_i^{OMA}\right) \Pr\left(\gamma_{RD_i-x_i}^{OMA} > \gamma_i^{OMA}\right) \\
&= 1 - \Pr\left(|h_{AP_kR}|^2 > \frac{\gamma_i^{OMA} N_0}{P_{AP}}\right) \Pr\left(|h_{BR}|^2 > \frac{\gamma_i^{OMA} N_0}{\xi |h_{RD_i}|^2}\right) \\
&= 1 - \sum_{k=1}^{K} \binom{K}{k} (-1)^{k-1} \frac{1}{\lambda_{RD_i}} \exp\left(-\frac{\gamma_i^{OMA} N_0}{P_{AP} \lambda_{APR}}\right) \\
&\times \int_0^{\infty} \exp\left(-\frac{\gamma_i^{OMA} N_0}{\xi x} - \frac{x}{\lambda_{RD_i}}\right) dx \\
&= 1 - \sum_{k=1}^{K} \binom{K}{k} (-1)^{k-1} \frac{1}{\lambda_{RD_i}} \exp\left(-\frac{\gamma_i^{OMA} N_0}{P_{AP} \lambda_{APR}}\right) \\
&\times \sqrt{\frac{4\gamma_i^{OMA} N_0}{\xi \lambda_{RD_i}}} K_1\left(\sqrt{\frac{4\gamma_i^{OMA} N_0}{\xi \lambda_{RD_i}}}\right),
\end{aligned} \tag{5.52}$$

where $\gamma_i^{OMA} = 2^{4R_i} - 1$.

5.7 Numerical Results and Discussion

In this section, we show the comparisons of cellular network related outage performance of two users using NOMA and OMA. These users are grouped in downlink of the AP using Rayleigh fading channels under different simulated parameters.

The OP versus the transmit SNR at the AP is illustrated in Figure 5.6, where we consider two main scenarios, i.e., NOMA and OMA. The different PA coefficients are assigned to two users, and hence outage performance of the first user is better than that of the second user. It can be easily seen that more antennas result in lowest outage. When the SNR is greater than 30 (dB), outage probabilities for these cases go to straight line. It means that they meet saturation situation.

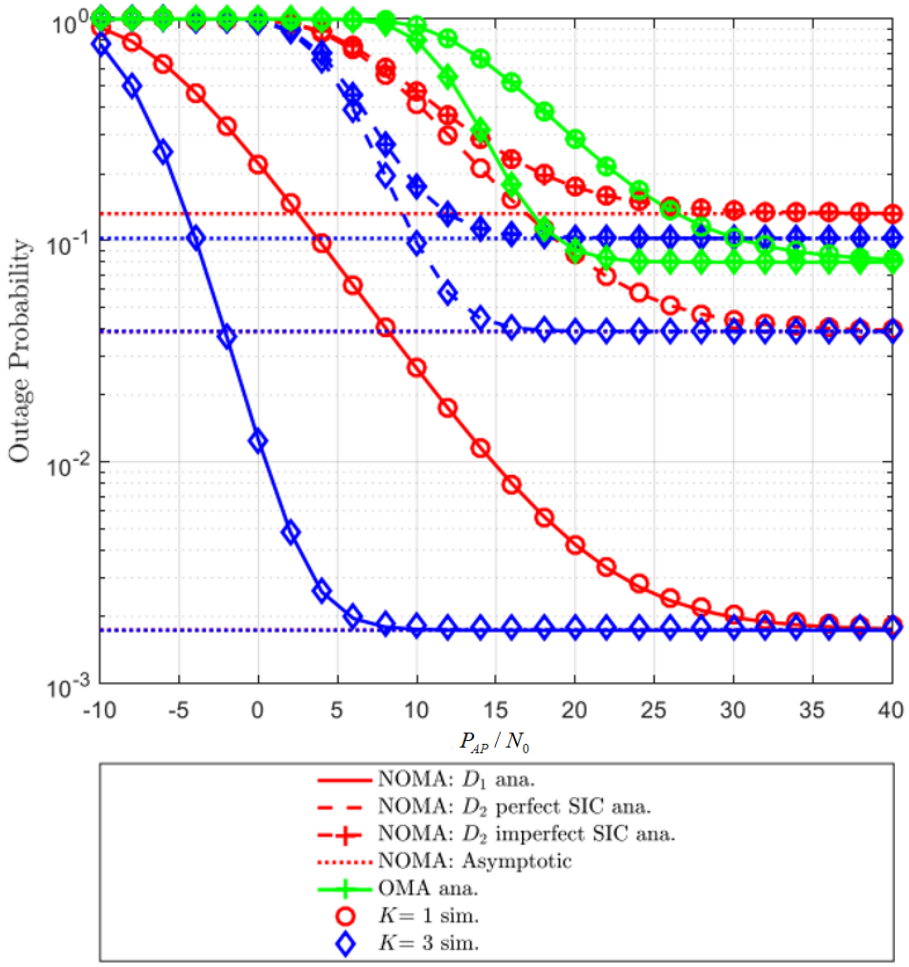

Figure 5.6: Outage performance comparison of D_1, D_2 of NOMA and OMA versus P_{AP}/N_0 by varying K ($a_1 = 0.7$, $\tau = 0.6$, $\alpha = 0.5$, $R_1 = 0.5$, $R_2 = 2$, $\lambda_{AP} = \lambda_{BR} = 1$, $\lambda_{APR} = \lambda_{RD_1} = 10$, $\lambda_{RD_2} = 5$, $\lambda_{APRip} = \lambda_{RD_2} = 0.01$, $P_B/N_0 = 30$ (dB))

In addition, imperfect SIC at the second user has worse outage performance compared with perfect case. It is further confirmed that NOMA in IoT is better than in OMA case. The exactness of the asymptotic lines corresponding with derived expressions for all the considered cases is confirmed at high SNR. Similar trend can be seen in Figure 5.7 as considering impact of transmit SNR at the power beacon on the OP.

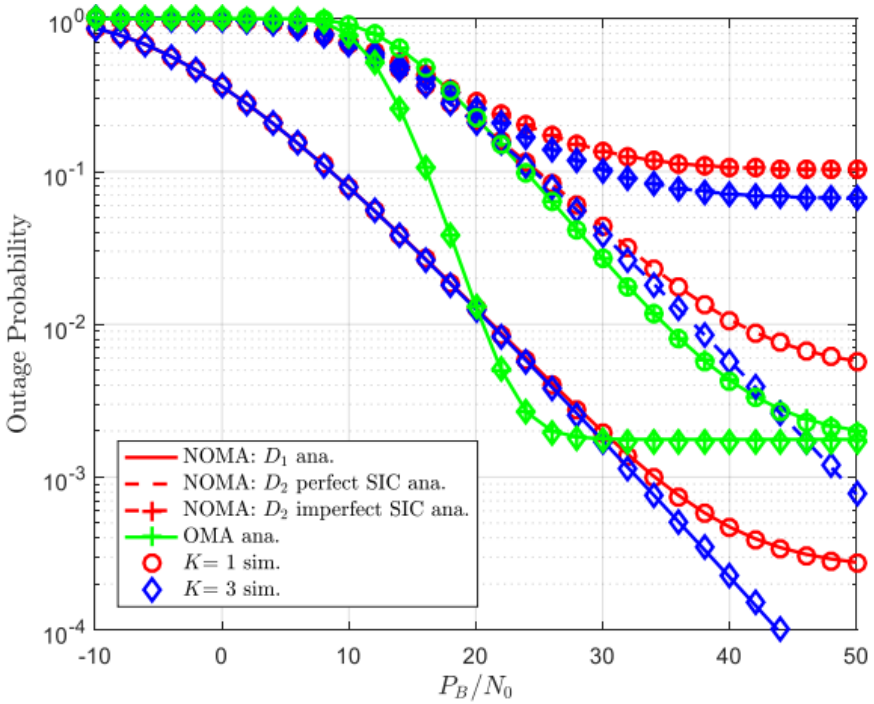

Figure 5.7: Outage performance comparison of D_1, D_2 of NOMA and OMA versus P_{AP}/N_0 by varying K ($a_1 = 0.7$, $\tau = 0.6$, $\alpha = 0.5$, $R_1 = 0.5$, $R_2 = 2$, $\lambda_{AP} = \lambda_{BR} = 1$, $\lambda_{APR} = \lambda_{RD_1} = 10$, $\lambda_{RD_2} = 5$, $\lambda_{APRip} = \lambda_{RD_2} = 0.01$, $P_B/N_0 = 30$ (dB))

Considering outage performance of two users versus transmit SNR at the AP with different PA factors as in Figure 5.8, the users' performance change based on the amount of power allocated. Higher a_1 leads to better outage performance at the first user. These trends of curves related outage behavior are similar as in Figures 5.6 and 5.7. While considering how transmit SNR at beacon makes impact on outage probability, it can be seen similar performance as in Figure 5.9.

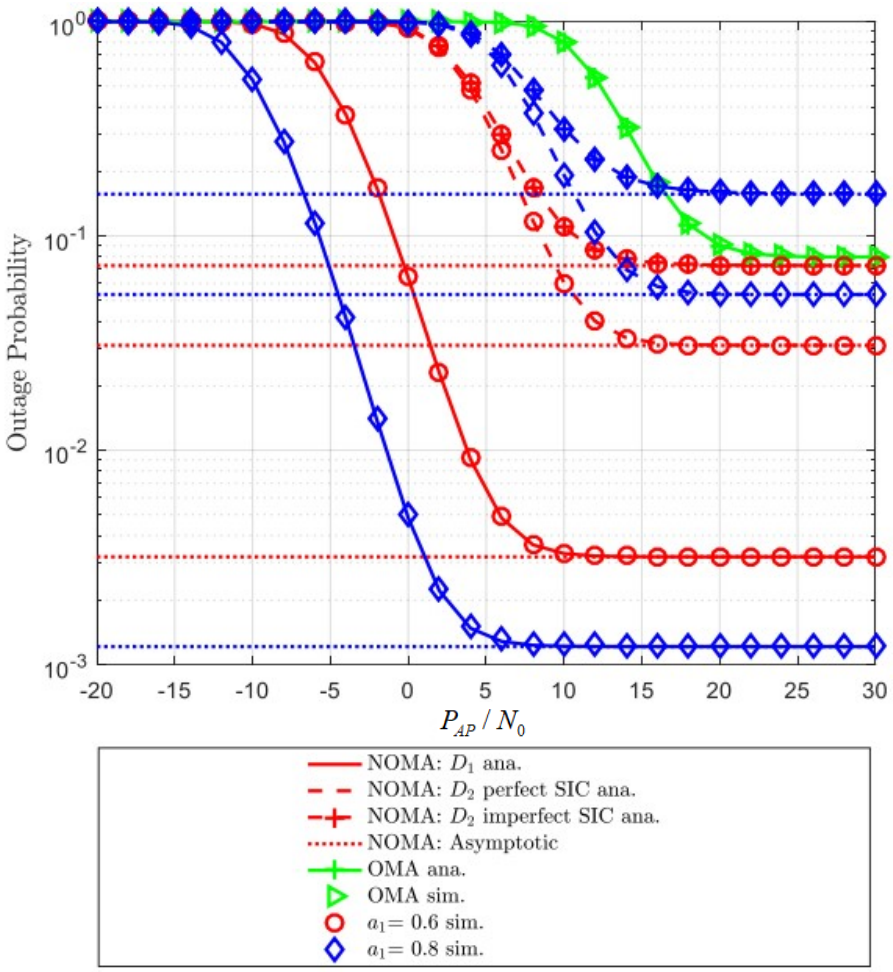

Figure 5.8: Outage performance comparison of D_1, D_2 of NOMA and OMA versus P_{AP}/N_0 by varying a_1 ($\tau = 0.6$, $\alpha = 0.5$, $R_1 = 0.5$, $R_2 = 2$, $\lambda_{AP} = \lambda_{BR} = 1$, $\lambda_{APR} = \lambda_{RD_1} = 10$, $\lambda_{RD_2} = 5$, $\lambda_{APRip} = \lambda_{RD_2} = 0.01$, $P_B/N_0 = 30$ (dB), $K = 3$).

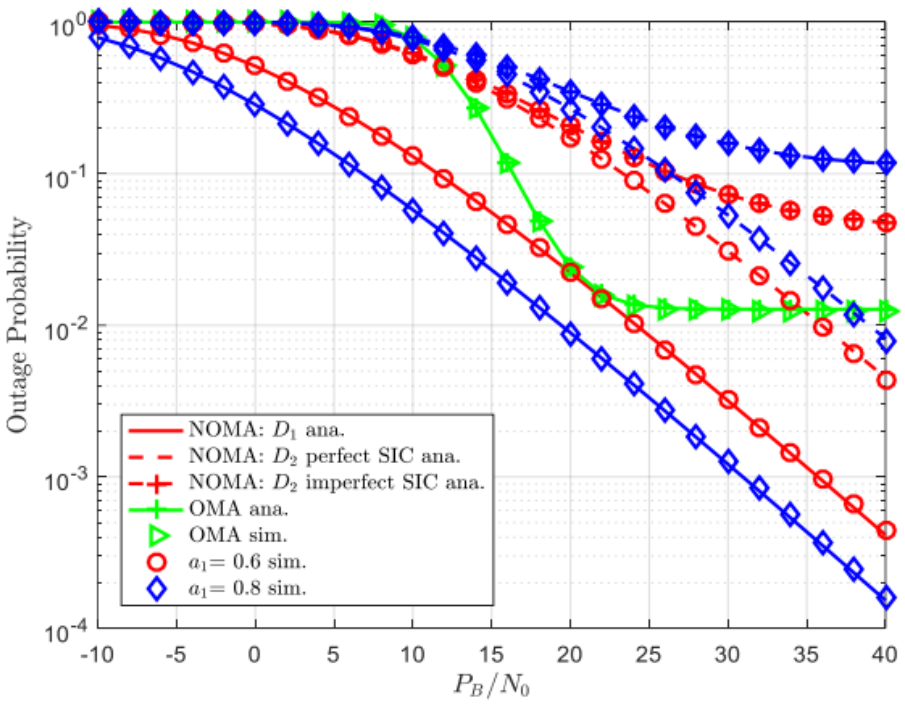

Figure 5.9: Outage performance comparison of D_1, D_2 of NOMA and OMA versus P_{AP}/N_0 by varying a_1 ($\tau = 0.6$, $\alpha = 0.5$, $R_1 = 0.5$, $R_2 = 2$, $\lambda_{AP} = \lambda_{BR} = 1$, $\lambda_{APR} = \lambda_{RD_1} = 10$, $\lambda_{RD_2} = 5$, $\lambda_{APRip} = \lambda_{RD_2} = 0.01$, $P_B/N_0 = 30$ (dB), $K = 3$).

5.8 Conclusion

In this chapter, we have investigated the cellular network by enabling EH and TAS schemes. The main result of NOMA scheme provide acceptable outage performance. Such performance is improved significantly at high SNR regime. The relaying scheme with WPT technique benefits to such cellular network with performance improvement for two far users who need assistance of WPT-assisted relay. Depending on PA factors, different performance of two users can be observed. When SIC can be operated perfectly, it is able to exhibit better performance for the second user. For the antenna selection scheme, it is unnecessary design of multiple antennas system with complex signal processing technique, it can be reduced by exploiting antenna selection as presented in this chapter. We derived in closed-form for the OP for two distant users in the considered IoT system. More importantly, the asymptotic expressions for the outage probabilities are provided. The superior outage performance achieved by the proposed cellular network is confirmed in numerical results.

5.9 Appendix

5.9.1 Proof of Proposition 1

By using (5.33) and (5.37), can be formulated by

$$\begin{aligned}\partial_1 &= \Pr\left(\gamma_{AP_{k^*}R-x_1} > \gamma_1\right)\\ &= \Pr\left(\left|h_{AP_{k^*}R}\right|^2 > \frac{\gamma_1 N_0}{P_{AP}\left(a_1-\gamma_1 a_2\right)}\right)\\ &= \sum_{k=1}^{K}\binom{K}{k}(-1)^{k-1}\exp\left(-\frac{k\gamma_1 N_0}{P_{AP}\left(a_1-\gamma_1 a_2\right)\lambda_{APR}}\right).\end{aligned} \tag{5.53}$$

In similar way, from (5.34) and (5.37), it can be obtained ∂_2 as follows:

$$\begin{aligned}\partial_2 &= \Pr\left(\gamma_{RD_1-x_1} > \gamma_1\right)\\ &= \Pr\left(\left|h_{RD_1}\right|^2 > \frac{\gamma_1 N_0}{\left|h_{BR}\right|^2\xi\left(a_1-\gamma_1 a_2\right)}\right)\\ &= \int_0^{\infty}\exp\left(-\frac{\gamma_1 N_0}{\xi\left(a_1-\gamma_1 a_2\right)\lambda_{RD_1}x}\right)\frac{1}{\lambda_{BR}}\exp\left(-\frac{x}{\lambda_{BR}}\right)dx\\ &= \frac{1}{\lambda_{BR}}\int_0^{\infty}\exp\left(-\frac{\gamma_1 N_0}{\xi\left(a_1-\gamma_1 a_2\right)\lambda_{RD_1}x}-\frac{x}{\lambda_{BR}}\right)dx\\ &= \sqrt{\frac{4\gamma_1 N_0}{\xi\left(a_1-\gamma_1 a_2\right)\lambda_{RD_1}\lambda_{BR}}}K_1\left(\sqrt{\frac{4\gamma_1 N_0}{\xi\left(a_1-\gamma_1 a_2\right)\lambda_{RD_1}\lambda_{BR}}}\right).\end{aligned} \tag{5.54}$$

It is worth noting that the last equation follows from the fact that $\int_0^{\infty}\exp\left(-\frac{\delta}{4x}-\varphi x\right)dx = \sqrt{\frac{\delta}{\varphi}}K_1\left(\sqrt{\delta\varphi}\right)$ in [79, Eq. 3.324].

If we substitute (5.53) and 5.54 into (5.37), OP_1 as the proposition can be achieved.

5.9.2 Proof of the Proposition 2

By applying (5.33) and (5.39), ∇_1 can be computed as follows:

$$\begin{aligned}\nabla_1 &= \Pr\left(\gamma_{AP_{k^*}R-x_2} > \gamma_2\right)\\ &= \Pr\left(\left|h_{AP_{k^*}R}\right|^2 > \frac{\gamma_2 N_0}{P_{AP}a_2}\right)\\ &= \sum_{k=1}^{K}\binom{K}{k}(-1)^{k-1}\exp\left(-\frac{k\gamma_2 N_0}{P_{AP}a_2\lambda_{APR}}\right).\end{aligned} \tag{5.55}$$

Next, (5.39) is used to calculate ∇_2 as follows:

$$\begin{aligned}\nabla_2 &= \Pr\left(\gamma_{RD_2-x_1} > \gamma_2, \gamma_{RD_2-x_2} > \gamma_2\right) \\ &= \Pr\left(|h_{RD_2}|^2 > \frac{\gamma_2 N_0}{|h_{BR}|^2 \xi\left(a_1 - \gamma_1 a_2\right)}, |h_{RD_1}|^2 > \frac{\gamma_2 N_0}{|h_{BR}|^2 \xi a_2}\right) \\ &= \Pr\left(|h_{RD_2}|^2 > \frac{\gamma_2 N_0}{|h_{BR}|^2 \xi} max\left(\frac{1}{\left(a_1 - \gamma_1 a_2\right)}, \frac{1}{a_2}\right)\right). \end{aligned} \tag{5.56}$$

To make our computation simpler, we denote $\theta = max\left(\frac{1}{(a_1-\gamma_1 a_2)}, \frac{1}{a_2}\right)$, ∇_2 can be rewritten as follows:

$$\begin{aligned}\nabla_2 &= \Pr\left(|h_{RD_2}|^2 > \frac{\theta\gamma_2 N_0}{|h_{BR}|^2 \xi}\right) \\ &= \int_0^\infty \left(1 - F_{|h_{RD_2}|^2}\left(\frac{\theta\gamma_2 N_0}{|h_{BR}|^2 \xi}\right)\right) f_{|h_{RD_2}|^2}(x)\, dx \\ &= \int_0^\infty \exp\left(-\frac{\theta\gamma_2 N_0}{\lambda_{RD_2}\xi x}\right) \frac{1}{\lambda_{BR}} \exp\left(-\frac{x}{\lambda_{BR}}\right) dx \\ &= \frac{1}{\lambda_{BR}} \int_0^\infty \exp\left(-\frac{\theta\gamma_2 N_0}{\lambda_{RD_2}\xi x} - \frac{x}{\lambda_{BR}}\right) dx \\ &= \sqrt{\frac{4\theta\gamma_2 N_0}{\lambda_{BR}\lambda_{RD_2}\xi}} K_1\left(\sqrt{\frac{4\theta\gamma_2 N_0}{\lambda_{BR}\lambda_{RD_2}\xi}}\right). \end{aligned} \tag{5.57}$$

By substituting (5.55) and (5.57) into (5.39), OP_2 can be obtained.

5.9.3 Proof of the Proposition 3

Plugging (5.33) and (5.43) to corresponding result, ψ_1 can be written by

$$\begin{aligned}\psi_1 &= \Pr\left(\gamma_{AP_{k^*}Rip-x_2} > \gamma_2\right) \\ &= \Pr\left(|h_{AP_{k^*}R}|^2 > \frac{\gamma_2\left(a_1 P_{AP}|g_{AP_{k^*}R}|^2 + N_0\right)}{a_2 P_{AP}}\right) \\ &= \int_0^\infty \left(1 - F_{|h_{AP_{k^*}R}|^2}\frac{\gamma_2\left(a_1 P_{AP} x + N_0\right)}{a_2 P_{AP}}\right) f_{|h_{AP_{k^*}R}|^2}(x)\, dx. \end{aligned} \tag{5.58}$$

By applying (5.33) and (5.34), then further employs corresponding CDF and PDF, ψ_1 can

be computed by

$$\begin{aligned}\psi_1 &= \sum_{k=1}^{K}\sum_{m=1}^{K}\binom{K}{k}\binom{K}{m}(-1)^{k+m-2}\frac{m}{\lambda_{APRip}} \\ &\times \exp\left(-\frac{k\gamma_2 N_0}{a_2 P_{AP}\lambda_{APR}}\right)\int_0^{\infty}\exp\left(-\left(\frac{k\gamma_2 a_1}{a_2\lambda_{APR}}+\frac{m}{\lambda_{APRip}}\right)x\right)dx \\ &= \sum_{k=1}^{K}\sum_{m=1}^{K}\binom{K}{k}\binom{K}{m}(-1)^{k+m-2}\frac{ma_2\lambda_{APR}}{k\gamma_2 a_1\lambda_{APRip}+ma_2\lambda_{APR}}\exp\left(-\frac{k\gamma_2 N_0}{a_2 P_{AP}\lambda_{APR}}\right).\end{aligned} \tag{5.59}$$

Based on (5.43), we compute ψ_2 as follows:

$$\begin{aligned}\psi_2 &= \Pr\left(\gamma_{RD_2ip-x_2} > \gamma_2\right) \\ &= \Pr\left(|h_{RD_2}|^2 > \frac{\gamma_2\left(a_1\xi|h_{BR}|^2|g_{RD_2}|^2+N_0\right)}{a_2\xi|h_{BR}|^2}\right) \\ &= \int_0^{\infty}\int_0^{\infty}\left(1-F_{|h_{RD_2}|^2}\left(\frac{\gamma_2\left(a_1\xi xy+N_0\right)}{a_2\xi x}\right)\right)f_{|h_{BR}|^2}(x)\,dx f_{|g_{RD_2}|^2}(y)\,dy.\end{aligned} \tag{5.60}$$

In next step, using results of CDF and PDF, ψ_2 is formulated as follows:

$$\begin{aligned}\psi_2 &= \frac{1}{\lambda_{BR}}\frac{1}{\lambda_{RD_2ip}}\int_0^{\infty}\exp\left(-\left(\frac{\gamma_2 N_0}{a_2\xi\lambda_{RD_2}}+\frac{1}{\lambda_{RD_2ip}}\right)y\right)dy \\ &\times\int_0^{\infty}\exp\left(-\frac{\gamma_2 N_0}{a_2\xi\lambda_{RD_2}x}-\frac{x}{\lambda_{BR}}\right)dx \\ &= \frac{a_2\xi\lambda_{RD_2}}{\gamma_2 a_1\xi\lambda_{RD_2ip}+a_2\xi\lambda_{RD_2}}\sqrt{\frac{4\gamma_2 N_0}{a_2\xi\lambda_{RD_2}\lambda_{BR}}}K_1\left(\sqrt{\frac{4\gamma_2 N_0}{a_2\xi\lambda_{RD_2}\lambda_{BR}}}\right).\end{aligned} \tag{5.61}$$

Plugging (5.59), (5.61) into (5.43), OP_{2ip} can be achieved.

Chapter 6:

MISO-NOMA Combining Multi-Relays Enabling Future Cellular Networks

Part I – MISO Combining Cognitive Radio

This section presents the secrecy performance of CR [NNL02, NNL09] networks by enabling downlink NOMA. The MISO architecture with TAS strategy is considered. In particular, PLS of CR-NOMA is studied to achieve secure performance analysis, i.e., SOP. Furthermore, optimal PA factor can be obtained to show optimal value of SOP. Monte-Carlo simulations are performed to verify the proposed analytical results

6.1 System model

We consider the BS is equipped with N antenna, two legitimate including user D_i for $i = \{1, 2\}$ and a primary device (PD) as Figure 6.1. It is noted that TAS is adopted to indicate the best antenna required to serve in downlink of the secondary network. In CR-NOMA, the BS make interference to PD. It is noted that BS requires AF mode to forward signal to far users [NNL03]. It is assumed that BS is placed very far from the transmit primary source PD and hence it cannot interfere with the primary network as shown in Figure 6.1.

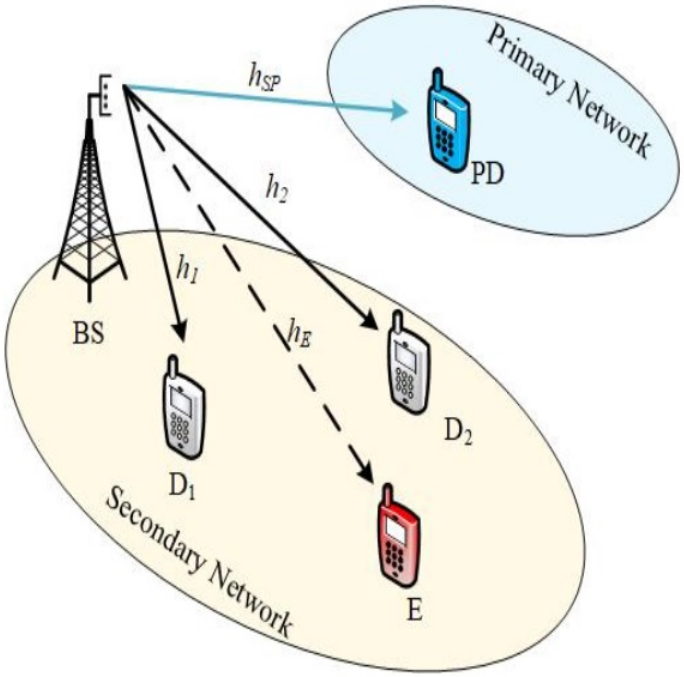

Figure 6.1: System model of secure CR-NOMA.

However, in secure viewpoint, the existence of an eavesdropper (E) is main reason related to unsecured transmission. We also assume that all receiving nodes are followed by AWGN with mean zero and variance N_0. Without loss of generality, all the wireless channels in Figure 6.1 are modeled to be independent quasi-static block Rayleigh fading channels. Furthermore, the channel power gains $|h_k|^2$ ($k \in \{1, 2, SP, E\}$) have channel coefficients as λ_z. The interference power at the PD should not exceed the maximum tolerable level I_P , and therefore the cognitive transmitter power at the BS should satisfy [14].

$$P_S = \min\left\{Q, \frac{I}{|h_{SP}|^2}\right\}, \tag{6.1}$$

where P_S is the transmit power at BS and Q denotes the maximum power at BS. Following principle of NOMA transmission, BS send the superimposed signal $\sqrt{a_1}x_1 + \sqrt{a_2}x_2$ to the user D_i. In which x_1, x_2 are denoted as the messages from BS to NOMA user. Then, the signal received at D_i is expressed as follows:

$$y_{D_i} = h_{D_i}\sqrt{P_S}\,(\sqrt{a_1}x_1 + \sqrt{a_2}x_2) + n_i, \tag{6.2}$$

where n_i is the AWGN. Moreover, the SINR at D_1 when decode the own signal x_1. Such SINR is expressed as follows:

$$\gamma_{1,1} = \frac{P_S|h_{D_1}|^2 a_1}{P_S|h_{D_1}|^2 a_2 + N_0}. \tag{6.3}$$

Similarly, the SINR at D_2 when decode x_1 is expressed as follows:

$$\gamma_{2,1} = \frac{P_S|h_{D_2}|^2 a_1}{P_S|h_{D_2}|^2 a_2 + N_0}. \tag{6.4}$$

Apply SIC, the SINR at D_2 to decode the own signal x_2 is expressed as follows:

$$\gamma_{2,2} = \frac{P_S|h_{D_2}|^2 a_2}{N_0}. \tag{6.5}$$

The received signal at the eavesdropper can be expressed as follows:

$$y_E = h_E\sqrt{P_S}\,(\sqrt{a_1}x_1 + \sqrt{a_2}x_2) + n_E, \tag{6.6}$$

where n_E is the AWGN. The SINR at the eavesdropper when detected signal x_1 is expressed as follows:

$$\gamma_{E,1} = \frac{P_S|h_E|^2 a_1}{P_S|h_E|^2 a_2 + N_0}. \tag{6.7}$$

Similarly, the SINR at the E when it detects signal x_2 is expressed as follows:

$$\gamma_{E,2} = \frac{P_S |h_E|^2 a_2}{N_0}. \tag{6.8}$$

The secrecy capacity of D_1 can be obtained as follows:

$$C_{E,1} = \left[\log_2 \left(\frac{1+\gamma_{1,1}}{1+\gamma_{E,1}} \right) \right]^+, \tag{6.9}$$

where $[a]^+ = \max\{0, a\}$, $C_i = 2^{R_{x,i}} - 1$ and $R_{x,i}$ is the target rate of D_i. Then, the secrecy capacity of D_2 can be obtained as follows:

$$C_{x,2} = \begin{cases} \left[\log_2 \left(\frac{1+\gamma_{1,1}}{1+\gamma_{E,1}} \right) \right]^+, \text{ where } \gamma_{2,1} > C_1 \\ 0, \text{ where } \gamma_{2,1} < C_1 \end{cases} \tag{6.10}$$

6.2 Secrecy Outage Probability

6.2.1 Channel gain

Based on [79] the PDF and CDF of h_z, where $z \in \{D_1, D_2, SP, E\}$, are respectively expressed as follows:

$$f_{|h_z|^2}(x) = \sum_{n=1}^{N} \binom{N}{n} \frac{(-1)^{n-1} n}{\lambda_z} \exp\left(-\frac{nx}{\lambda_z} \right), \tag{6.11}$$

and

$$F_{|h_z|^2}(x) = 1 - \sum_{n=1}^{N} \binom{N}{n} (-1)^{n-1} \exp\left(-\frac{nx}{\lambda_z} \right). \tag{6.12}$$

6.2.2 SOP of D_1

We investigate SOP performance of D_1 as follows:

$$SOP_{D_1} = \Pr\left(C_{x,1} \leq R_{x,1} \right). \tag{6.13}$$

In particular, the closed-form expression of D1 in term of SOP is obtained as follows:

$$SOP_{D_1} = 1 - I_1 \times I_2. \tag{6.14}$$

Proof: See in Appendix 6.5 (pp. 43).

6.2.3 SOP of D_2

Different from SOP of D_1, user D_2 exhibits its SOP performance as follows:

$$\begin{aligned} SOP_{D_2} &= \Pr\left(C_{x,2} \le R_{x,2} | \gamma_{2,1} \ge C_2\right) \Pr\left(\gamma_{2,1} \ge C_1\right) \\ &\quad + \Pr\left(\gamma_{2,1} < C_1\right) \Pr\left(C_{x,2} \le R_{x,2} | \gamma_{2,1} < C_2\right), \end{aligned} \tag{6.15}$$

where $\Pr\left(C_{x,2} \le R_{x,2} | \gamma_{2,1} < C_2\right) = 1$.

First, $\Pr\left(C_{x,2} \le R_{x,2}\right) \triangleq \Xi_1$ is expressed as follows:

$$\begin{aligned} \Xi_1 &= 1 - \Pr\left(C_{x,2} > R_{x,2}\right) \\ &= 1 - \Pr\left(\frac{P_S |h_{D_2}|^2 a_2}{N_0} > \frac{\gamma_{x,2} P_E |h_E|^2 a_2}{N_0} + C_2\right) \\ &= 1 - \underbrace{\Pr\left(|h_{D_2}|^2 > \frac{Q_4 |h_E|^2 + Q_5}{\rho}, |h_{SP}|^2 < \frac{\rho_I}{\rho}\right)}_{H_1} \\ &\quad - \underbrace{\Pr\left(|h_{D_2}|^2 > \left(\frac{Q_4 |h_E|^2 + Q_5}{\rho}\right) |h_{SP}|^2, |h_{SP}|^2 < \frac{\rho_I}{\rho}\right)}_{H_2}, \end{aligned} \tag{6.16}$$

where $Q_4 = \gamma_{x,2} \rho_E$, $Q_5 = \frac{C_2}{a_2}$.

Moreover, H_1 can be rewritten as follows:

$$H_1 = \underbrace{\Pr\left(|h_{D_2}|^2 > \frac{Q_4 |h_E|^2 + Q_5}{\rho}\right)}_{H_{1,1}} \Pr\left(|h_{SP}|^2 < \frac{\rho_I}{\rho}\right). \tag{6.17}$$

It is noted that $H_{1,1}$ is expressed as follows:

$$\begin{aligned} H_{1,1} &= \Pr\left(|h_{D_2}|^2 > \frac{Q_4 |h_E|^2 + Q_5}{\rho}\right) \\ &= \int_0^\infty \bar{F}_{|h_{D_2}|^2}\left(\frac{Q_4 z + Q_5}{\rho}\right) f_{|h_E|^2}(z)\, dz \\ &= \sum \sum \binom{N}{i} \binom{N}{m} \frac{m \rho \lambda_{D_2} (-1)^{i+m-2}}{i Q_4 \lambda_E + \rho \lambda_{D_2} m} \exp\left(-\frac{i Q_5}{\rho \lambda_{D_2}}\right). \end{aligned} \tag{6.18}$$

Then, after some mathematical manipulations, H_2 can be expressed as following formula

$$\begin{aligned}
H_2 &= \Pr\left(|h_{D_2}|^2 > \frac{Q_4|h_E|^2 + Q_5}{\rho_I}|h_{SP}|^2, |h_{SP}|^2 > \frac{\rho_I}{\rho}\right) \\
&= \int_0^{\infty}\int_{\frac{\rho_I}{\rho}}^{\infty} \bar{F}_{|h_{D_2}|^2}\left(\left(\frac{Q_4 z + Q_5}{\rho_I}\right)t\right) f_{|h_{SP}|^2}(t)\, f_{|h_E|^2}(z)\, dtdz \\
&= \sum_{i=1}^{N}\sum_{s=1}^{N}\sum_{m=1}^{N}\binom{N}{i}\binom{N}{s}\binom{N}{m}\frac{(-1)^{i+s+m-2}\lambda_{D_2}\rho_I sm}{i\lambda_{SP}Q_4\lambda_E} \\
&\times \exp\left(-\frac{s\lambda_{D_2}\rho_I + iQ_5\lambda_{SP}}{\rho\lambda_{SP}\lambda_{D_2}}\right)\int_0^{\infty}\frac{z}{z+Q_6}\exp\left(-\frac{iQ_4}{\lambda_{D_2}\rho} - \frac{m}{\lambda_E}\right)dz, \qquad (6.19)
\end{aligned}$$

where $Q_6 = \frac{Q_5}{Q_4} + \frac{s\lambda_{D_2}\rho_I}{iQ_4\lambda_{SP}}$. By applying [79, Eq. (3.352.4)], we obtain

$$\begin{aligned}
H_2 = &-\sum_{i=1}^{N}\sum_{s=1}^{N}\sum_{m=1}^{N}\binom{N}{i}\binom{N}{s}\binom{N}{m}\frac{(-1)^{i+s+m-3}\lambda_{D_2}\rho_I sm}{i\lambda_{SP}Q_4\lambda_E} \\
&\times \exp\left(\frac{iQ_4Q_6}{\rho\lambda_{D_2}} + \frac{mQ_6}{\lambda_E} - \frac{s\lambda_{D_2}\rho_I + iQ_5\lambda_{SP}}{\rho\lambda_{SP}\lambda_{D_2}}\right)Ei\left(-\frac{iQ_4Q_6}{\rho\lambda_{D_2}} - \frac{mQ_6}{\lambda_E}\right). \qquad (6.20)
\end{aligned}$$

By substituting (6.18), (6.20) and (6.29) into (6.16), Ξ_1 can be obtained as follows:

$$\begin{aligned}
\Xi_1 = 1 &- \sum_{i=1}^{N}\sum_{m=1}^{N}\binom{N}{i}\binom{N}{m}\frac{(-1)^{i+m-2}\lambda_{D_2}\rho sm}{iQ_4\lambda_E + m\rho\lambda_{D_2}} \\
&\times \exp\left(-\frac{iQ_5}{\rho\lambda_{D_2}}\right)\left(1 - \sum_{s=1}^{N}\binom{N}{s}(-1)^{i-1}\exp\left(-\frac{s\rho_I}{\rho\lambda_{SP}}\right)\right) \\
&+ \sum_{i=1}^{N}\sum_{s=1}^{N}\sum_{m=1}^{N}\binom{N}{i}\binom{N}{s}\binom{N}{m}\frac{(-1)^{i+s+m-3}\lambda_{D_2}\rho_I sm}{i\lambda_{SP}Q_4\lambda_E} \\
&\times \exp\left(\frac{iQ_4Q_6}{\rho\lambda_{D_2}} + \frac{mQ_6}{\lambda_E} - \frac{s\lambda_{D_2}\rho_I + iQ_5\lambda_{SP}}{\rho\lambda_{SP}\lambda_{D_2}}\right)Ei\left(-\frac{iQ_4Q_6}{\rho\lambda_{D_2}} - \frac{mQ_6}{\lambda_E}\right) \qquad (6.21)
\end{aligned}$$

Next, $\Xi_2 \triangleq \Pr(\lambda_{2,1} \geq C_1)$ is formulated as follows:

$$\begin{aligned}
\Xi_2 = &\underbrace{\Pr\left(\frac{\rho|h_{D_2}|^2 a_1}{\rho|h_{D_2}|^2 a_2 + 1} \geq C_2, |h_{SP}|^2 < \frac{\rho_I}{\rho}\right)}_{K_1} \\
&+ \underbrace{\left(\frac{\rho_I|h_{D_2}|^2 a_1}{\rho_I|h_{D_2}|^2 a_2 + |h_{SP}|^2} \geq C_2\frac{\rho_I}{|h_{SP}|^2\rho} > Q\right)}_{K_2}. \qquad (6.22)
\end{aligned}$$

Next, K_1 and K_2 is calculated respectively by

$$\begin{aligned} K_1 &= \Pr\left(|h_{D_2}|^2 \geq \frac{C_1}{\rho Q_2}\right) \Pr\left(|h_{SP}|^2 < \frac{\rho_I}{\rho}\right) \\ &= \sum_{i=1}^{N} \binom{N}{i} (-1)^{i-1} \exp\left(-\frac{iC_1}{\rho \lambda_{D_2} Q_2}\right) \\ &\times \left(1 - \sum_{s=1}^{N} \binom{N}{i} (-1)^{s-1} \exp\left(-\frac{s\rho_I}{\rho \lambda_E}\right)\right), \end{aligned} \tag{6.23}$$

and

$$\begin{aligned} K_2 &= \Pr\left(|h_{D_2}|^2 \geq \frac{C_1 |h_{SP}|^2}{\rho_I Q_2}, |h_{SP}|^2 > \frac{\rho_I}{\rho}\right) \\ &= 1 - \sum_{i=1}^{N} \sum_{s=1}^{N} \binom{N}{i} \binom{N}{s} \frac{(-1)^{i+s-1} s\rho_I \lambda_{D_2} Q_2}{iC_1 \lambda_{SP} + s\rho_I \lambda_{D_2} Q_2} \\ &\times \exp\left(-\frac{iC_1 \lambda_{SP} + s\rho_I \lambda_{D_2} Q_2}{\rho \lambda_{D_2} \lambda_{SP} Q_2}\right). \end{aligned} \tag{6.24}$$

Similarly, $\Pr(\gamma_{2,1} < C_1)$ is calculated by

$$\begin{aligned} \Pr(\gamma_{2,1} < C_1) &= 1 - \Pr(\gamma_{2,1} \geq C_2) \\ &= 1 - \sum_{i=1}^{N} \binom{N}{i} (-1)^{i-1} \exp\left(-\frac{s\rho_I}{\rho \lambda_E}\right) \\ &\times \left(1 - \sum_{s=1}^{N} \binom{N}{s} (-1)^{s-1} \exp\left(-\frac{iC_2}{\rho \lambda_{D_2} Q_2}\right)\right) \\ &- \sum_{i=1}^{N} \sum_{s=1}^{N} \binom{N}{i} \binom{N}{s} \frac{(-1)^{i+s-2} s\rho_I \lambda_{D_2} Q_2}{iC_1 \lambda_{SP} + s\rho_I \lambda_{D_2} Q_2} \\ &\times \exp\left(-\frac{iC_1 \lambda_{SP} + s\rho_I \lambda_{D_2} Q_2}{\rho \lambda_{D_2} \lambda_{SP} Q_2}\right). \end{aligned} \tag{6.25}$$

With the help of (6.21), (6.23), (6.24) and (6.25), the SOP of D_2 can be obtained.

6.3 Numerical Results

In this section, some insightful numerical results are provided to exhibit the secrecy performance of CR-NOMA systems. Also, we perform Monte-Carlo simulation results to confirm our analytical results. We set power allocation factors $a_1 = 0.7$, $a_2 = 0.3$, channel gains are $\lambda_{D_1} = \lambda_{D_2} = \lambda_{SP} = \lambda_E = 1$, the target rates $R_{x,1} = 0.5$, $R_{x,2} = 1$ and the number of antenna $N = 1$ except for specific cases.

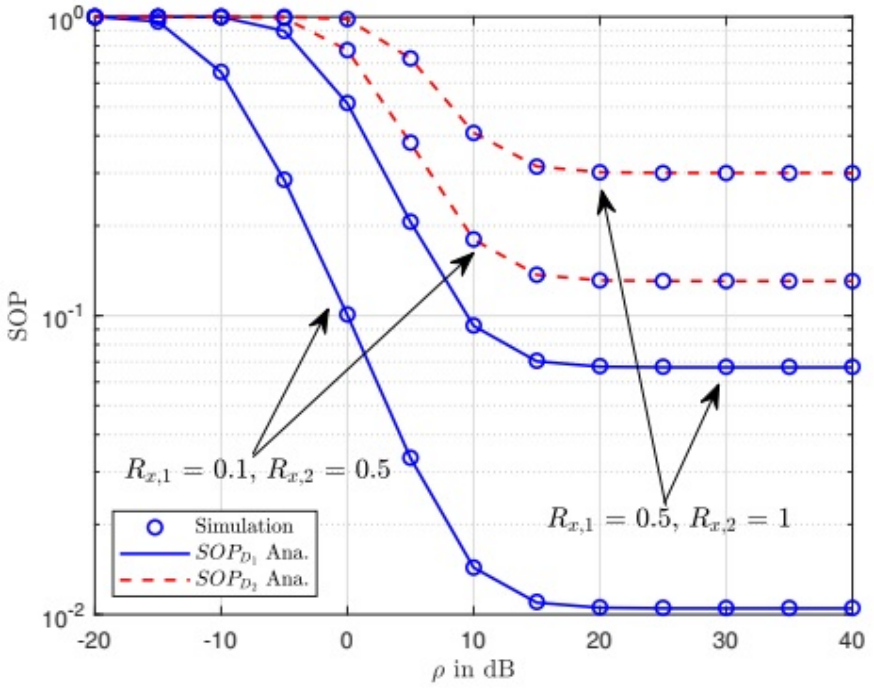

Figure 6.2: SOP of D_1 and D_2 versus ρ with varying $R_{x,1}$, $R_{x,2}$.

In Figure 6.2, we plot the SOP curves for two cases of target rates. From Figure 6.2, we can observe that the SOP of CR-NOMA tends to be a unchanged lines when SNR ρ at the source is large enough. For such a case, the SOP performance of user D_1 is better than that of user D_2. At high region of SNR, SOP performance can be enhanced significantly. Similarly, trends of SOP versus ρ_I can be seen in Figure 6.3. The main reason is that ρ leads to varying of SNR and then SOP can similar trend as Figure 6.2.

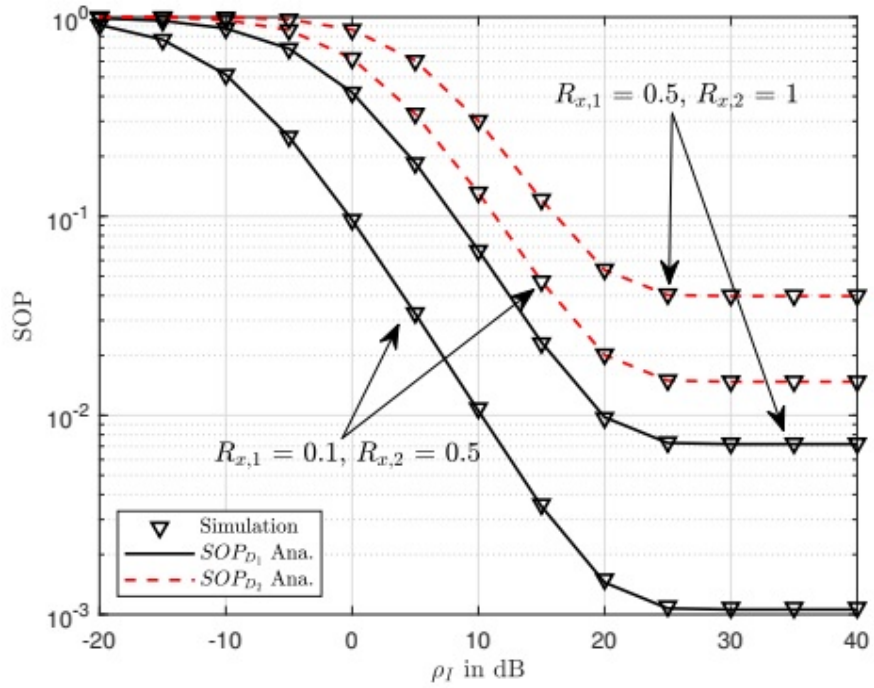

Figure 6.3: SOP of D_1 and D_2 versus ρ_I with varying $R_{x,1}$, $R_{x,2}$.

In Figure 6.4, it can be seen more antenna at the source contribute to improve SOP performance. We can see $N = 3$ shows the lowest SOP for both users D_1 and D_2. The reason is that more antenna selected leads to higher SNR, then SOP can be improved. Performance gap still exists among two users due to different PA factor assigned.

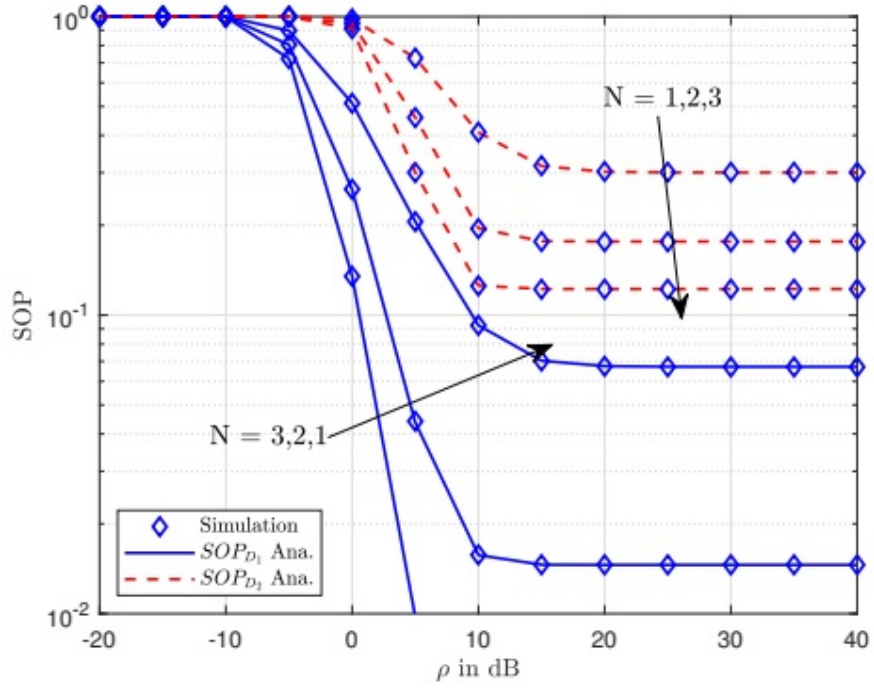

Figure 6.4: SOP of D_1 and D_2 versus ρ with varying N.

As observation in Figure 6.5, we can conclude that existence of optimal SOP for user D_2 when we change a_1. It can be explained that SNR is computed based on a_1.

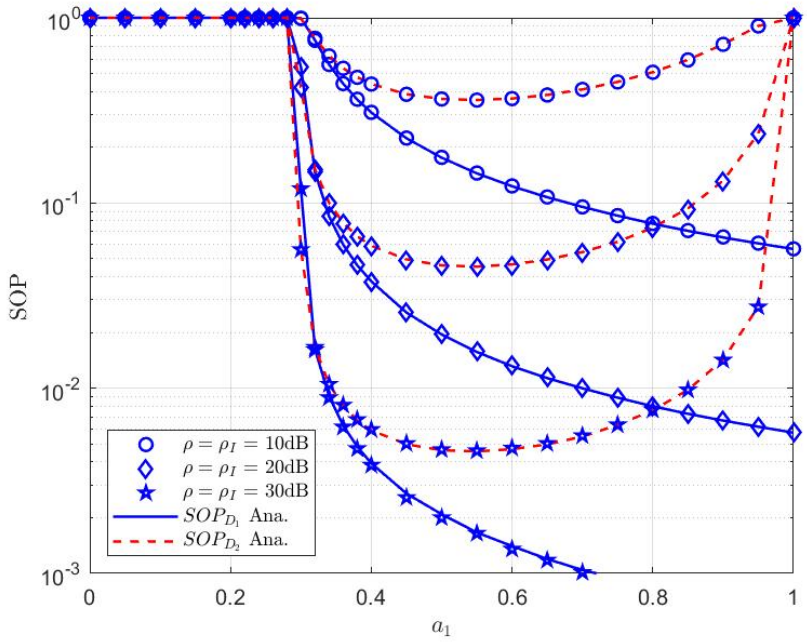

Figure 6.5: SOP of D_1 and D_2 versus a_1 with varying $\rho = \rho_I$.

6.4 Conclusion

In this section, the SOP performance of two-user in CR-NOMA system under benefit from TAS scheme is investigated. The exact and approximated closed-form expressions of the SOP for two NOMA users were derived and compared with some parameters such as the number of transmit antenna or PA factors. The proposed analytical results were verified via Monte-Carlo simulations. The results demonstrate that the secure performance can be improved at high SNR. Subsequently, an effective PA strategy has been proposed to achieve optimal secure performance of the second user D_2.

6.5 Appendix

By substituting (6.3) and (6.7) into (6.13), we can rewrite SOP_{D_1} as

$$\begin{aligned} SOP_{D_1} &= 1 - \Pr\left(\frac{P_S|h_{D_1}|^2 a_1}{P_S|h_{D_1}|^2 a_2 + N_0} > \frac{\gamma_{x,1} P_E |h_E|^2 a_1}{P_E|h_E|^2 a_2 + N_0} + C_1\right) \\ &= 1 - \underbrace{\Pr\left(\frac{\rho|h_{D_1}|^2 a_1}{\rho_S|h_{D_1}|^2 a_2 + 1} > \frac{\gamma_{x,1}\rho_E|h_E|^2 a_1}{\rho_E|h_E|^2 a_2 + 1} + C_1, \frac{\rho_I}{|h_{SP}|^2} > \rho\right)}_{I_1} \\ &\times \underbrace{\Pr\left(\frac{\rho_I|h_{D_1}|^2 a_1}{\rho_I|h_{D_1}|^2 a_2 + |h_{SP}|^2} > \frac{\gamma_{x,1}\rho_E|h_E|^2 a_1}{\rho_E|h_E|^2 a_2 + 1} + C_1, \frac{\rho_I}{|h_{SP}|^2} < \rho\right)}_{I_2}, \end{aligned} \tag{6.26}$$

where $\gamma_{x,i} = 2^{R_{x,i}}$, $\rho = \frac{Q}{N_0}$, $\rho_E = \frac{P_S}{N_E}$, $\rho_I = \frac{I_P}{N_0}$. Then, I_1 is rewritten as

$$\begin{aligned} I_1 &= \underbrace{\Pr\left(\frac{\rho|h_{D_1}|^2 a_1}{\rho_S|h_{D_1}|^2 a_2 + 1} > \frac{\gamma_{x,1}\rho_E|h_E|^2 a_1}{\rho_E|h_E|^2 a_2 + 1} + C_1\right)}_{I_{1,1}} \\ &\times \underbrace{\Pr\left(|h_{SP}|^2 < \frac{\rho_I}{\rho}\right)}_{I_{1,2}}. \end{aligned} \tag{6.27}$$

Moreover, we can obtain $I_{1,1}$ as

$$\begin{aligned} I_{1,1} &= \Pr\left(|h_{D_1}|^2 > \frac{Q_3|h_E|^2 + C_1}{Q_1\rho|h_E|^2 + Q_2\rho}\right) \\ &= \int_0^\infty \bar{F}_{|h_{D_1}|^2}\left(\frac{Q_3 x + C_1}{Q_1\rho x + Q_2\rho}\right) f_{|h_E|^2}(x)\, dx \\ &= \sum_{n=1}^{N}\sum_{m=1}^{N} \binom{N}{n}\binom{N}{m} \frac{m(-1)^{m+n-2}}{\lambda_E} \\ &\times \int_0^\infty \exp\left(-\frac{n\left(Q_3 x + C_1\right)}{\lambda_{D_1}\rho\left(Q_1 x + Q_2\right)} - \frac{mx}{\lambda_E}\right) dx, \end{aligned} \tag{6.28}$$

where $\bar{F}_{h_z}(x) = 1 - F_{h_z}(x)$, $Q_1 = \left(1 - \gamma_{x,1} - \frac{a_2 C_1}{a_1}\right) \rho_E a_1 a_2$, $Q_2 = (a_1 - a_2 C_1)$, $Q_3 = (\gamma_{x,1} a_1 + a_2 C_1) \rho_E$. Next, with the help of (6.12), $I_{1,2}$ is obtained as

$$\begin{aligned} I_{1,2} &= \Pr\left(|h_{SP}|^2 < \frac{\rho_I}{\rho}\right) = F_{|h_{SP}|^2}\left(\frac{\rho_I}{\rho}\right) \\ &= 1 - \sum_{s=1}^{N} \binom{N}{s} (-1)^{s-1} \exp\left(-\frac{s\rho_I}{\rho \lambda_{SP}}\right). \end{aligned} \tag{6.29}$$

Then, I_2 can be calculated

$$\begin{aligned} I_2 &= \Pr\left(|h_{D_1}|^2 > \frac{\left(Q_3 |h_E|^2 + C_1\right) |h_{SP}|^2}{\left(Q_1 |h_E|^2 + Q_2\right) \rho_I}, |h_{SP}|^2 > \frac{\rho_I}{\rho}\right) \\ &= \int_0^{\infty} f_{|h_E|^2}(t) \int_{\frac{\rho}{\rho_I}}^{\infty} f_{|h_{SP}|^2}(z) \bar{F}_{|h_{D_1}|^2}\left(\frac{(Q_3 t + C_1) z}{(Q_1 t + Q_2) \rho_I}\right) dz dt. \end{aligned} \tag{6.30}$$

Thus, It can be computed by

$$\begin{aligned} I_2 = &\sum_{n=1}^{N} \sum_{s=1}^{N} \sum_{m=1}^{N} \binom{N}{n} \binom{N}{s} \binom{N}{m} \frac{(-1)^{i+s+m-3} \lambda_{D_1} \rho_I s m}{\lambda_E} \\ &\times \int_0^{\infty} \frac{Q_1 t + Q_2}{n \lambda_{SP} (Q_3 t + C_1) + s \lambda_{D_1} \rho_I (Q_1 t + Q_2)} \\ &\times \exp\left(-\frac{n \lambda_{SP} (Q_3 t + C_1) + s \lambda_{D_1} \rho_I (Q_1 t + Q_2)}{\lambda_{D_1} \lambda_{SP} (Q_1 t + Q_2)} - \frac{m t}{\lambda_E}\right) dt. \end{aligned} \tag{6.31}$$

Putting (6.28) and (6.29) into (6.27) and substituting the result (6.31) into (6.26), the final result can be achieved.

It completes the proof.

Part II – Multiple Relay-Assisted Future Cellular Networks

In the presence of an illegitimate user, we investigate the SOP of the optimal relay selection (ORS) networks by applying DF based FD relaying mode. The closed-form expressions for the allocations of the end-to-end SINR in each wireless network are derived as well as the closed-form expression for the exact SOP of the proposed ORS system is presented under Rayleigh fading schemes. As an important achievement, SOP is also compared between OMA and NOMA schemes. Our results reveal that the SOP of the suggested scheme can be considerably influenced by several parameters involved, including the number of relays, the average SNR of eavesdropper links, transmit power and the average residual self-interference (SI) enforced on the FD relays.

6.6 System Model

As shown in Figure 6.6, consider a system composed of one source S, one destination D, N full- duplex DF relays R_k with $k = \{1, ..., N\}$, and an eavesdropper E. The source, destination, and the eavesdropper are assumed to have a single antenna while the relays have two antennas, one for reception and the other for transmission [NNL05]. The direct links between the source and the destination or the eavesdropper are unavailable due to severe fading and path-loss, and thus communication can be established only via relays. Also, we concentrate on the situation that the eavesdropper may only overhear the confidential message from the source through the relays' transmission.

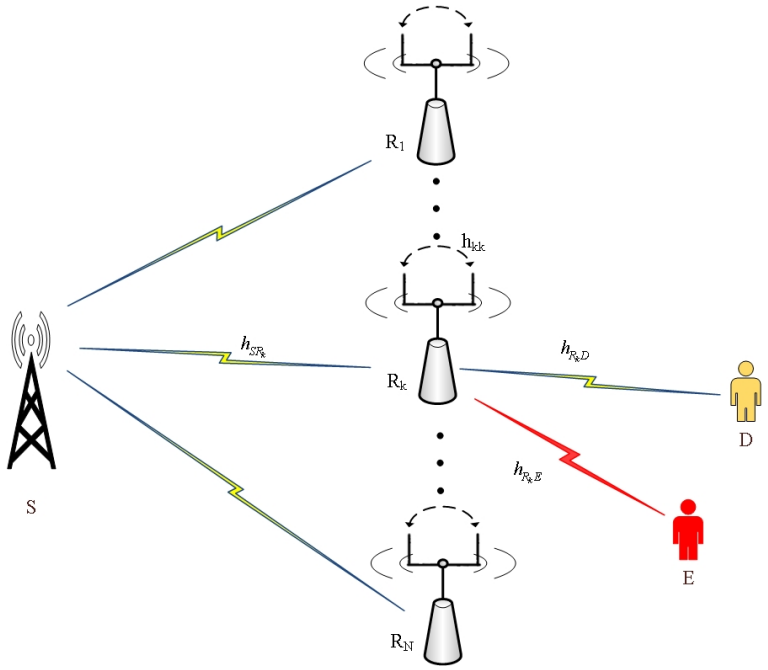

Figure 6.6: System model of OMA and NOMA.

The channel coefficients for $S \to R_k$, $R_k \to D$, $R_k \to E$ and $R_k \to R_k$ are denoted as h_{SR_k}, h_{R_kD}, h_{R_kE} and h_{kk}, respectively. It is considered that a quasi-static block-fading Rayleigh channel between two nodes with h_{SR_k}, h_{R_kD}, h_{R_kE} and h_{kk} which are modelled as zero mean

complex Gaussian random variables with variances $\delta^2_{SR_k}$, $\delta^2_{R_kD}$, $\delta^2_{R_kE}$ and $\delta^2_{R_k}$, respectively. The noise associated with each channel is modelled as mutually independent AWGN with zero mean and variance N_0. We assume that the source and the relays transmit signal with fixed powers P_S and P_R, respectively.

6.7 Secrecy Outage Probability in OMA Scheme

6.7.1 Secrecy Outage Probability for the system with FD-DF relays

Secrecy outage probability is defined as the probability that the instantaneous secrecy rate of the system is less than a predefined target rate R_o (in bits/s/Hz). We denote γ_{mn} is SNR of link $m \to n$. Mathematically, the concerned SOP, i.e. $SOP_o = \Pr\left(C_{R_o} < R_o\right)$ can be expressed as [73, 74]

$$\begin{aligned} SOP_0 &= \prod_{k=1}^{N} \Pr\left[\frac{1+\min\left(\frac{\gamma_{SR_k}}{\gamma_{kk}+1}, \gamma_{R_kD}\right)}{1+\gamma_E} < 2^{R_0}\right] \\ &= \prod_{k=1}^{N} \int_0^{\infty} F_{Z_k}(a+by) f_{\gamma_E}(y) dy \end{aligned} \tag{6.32}$$

where $Z_k = \min\left(\frac{\gamma_{SR_k}}{\gamma_{kk}+1}, \gamma_{R_kD}\right)$, $a = 2^{R_0} - 1$, and $b = 2^{R_0}$.

After some analysis, we have the following result [79]

$$SOP_0 = \prod_{k=1}^{N} \left(1 - \mathrm{A} e^{\mu\beta} Ei(\mu\beta)\right), \tag{6.33}$$

where $A = \frac{\lambda_{SR_k}}{b\lambda_{R_kE}\lambda_{R_k}} \exp\left(-u\left(\frac{1}{\lambda_{SR_k}} + \frac{1}{\lambda_{R_kD}}\right)\right)$, $\beta = \frac{\lambda_{SR_k}+\lambda_{R_k}}{b\lambda_{R_k}}$, $\mu = \frac{b}{\lambda_{SR_k}} + \frac{b}{\lambda_{R_kD}} + \frac{b}{\lambda_{R_kE}}$.

6.7.2 Secrecy outage probability for the system with HD-DF relays

In this section, we consider the SOP of the system using HD-DF relays. Similarly, secrecy outage probability for the system with HD-DF relays can be expressed as

$$\begin{aligned} SOP_0^H &= \prod_{k=1}^{N} \Pr\left[\frac{1+\min(\gamma_{SR_k}, \gamma_{R_kD})}{1+\gamma_E} < 2^{2R_0}\right] \\ &= \prod_{k=1}^{N} \int_0^{\infty} F_{Z_k^H}(a_1+b_1y) f_{\gamma_E}(y) dy, \end{aligned} \tag{6.34}$$

where $Z_k^H = \min(\gamma_{SR_k}, \gamma_{R_kD})$, $a_1 = 2^{2R_0} - 1$, and $b_1 = 2^{2R_0}$.

After some analysis we have the following result [73, 74]

$$SOP_0^H = \prod_{k=1}^{N} \left(1 - \frac{e^{-a_1 \left(\frac{1}{\lambda_{SR_k}} + \frac{1}{\lambda_{R_k D}} \right)}}{\frac{b_1 \lambda_{R_k E}}{\lambda_{SR_k}} + \frac{b_1 \lambda_{R_k E}}{\lambda_{R_k D}} + 1} \right). \tag{6.35}$$

6.8 Secrecy Outage Probability in FD-NOMA Scheme

In this scenario, the transmit signal at source X_S is composed signal intended to two different services, i.e. the first component for IoT data transfer, another for video streaming transmission. Following principle of NOMA with PA factors are a_1 and a_2 satisfying $a_1 + a_2 = 1$ and hence it can be obtained the received signals at R_k

$$y_{R_k} = h_{SR_k} \left(\sqrt{a_1 P_S} X_{S_1} + \sqrt{a_2 P_S} X_{S_2} \right) + \sqrt{P_R} h_{kk} X_{R_k} + n_{R_k}, \tag{6.36}$$

where n_{R_k} is AWGN at R_k, P_S and P_R are transmit power at S and relay, respectively.

At relay, the composited signal is decoded to obtain data X_{S_1} while considering X_{S_2} as interference. After using SIC to detect X_{S_1}. The received SNRs for detecting X_{S_1} and X_{S_2} are respectively expressed as follows:

$$\begin{cases} \gamma_{R_k}^1 = \dfrac{\frac{a_1 P_S}{N_0} |h_{SR_k}|^2}{\frac{a_2 P_S}{N_0} |h_{SR_k}|^2 + \frac{P_R}{N_0} |h_{kk}|^2 + 1} = \dfrac{a_1 \gamma_{SR_k}}{a_2 \gamma_{SR_k} + \gamma_{kk} + 1} \\ \gamma_{R_k}^2 = \dfrac{\frac{a_2 P_S}{N_0} |h_{SR_k}|^2}{\frac{P_R}{N_0} |h_{kk}|^2 + 1} = \dfrac{a_2 \gamma_{SR_k}}{\gamma_{kk} + 1} \end{cases}. \tag{6.37}$$

Then, SOP for signal X_{S_1} can be expressed by

$$\begin{aligned} SOP_0^1 &= \Pr(C_{R_0} < R_0) \\ &= \prod_{k=1}^{N} \Pr \left[\frac{1 + \min \left(\dfrac{a_1 \gamma_{SR_k}}{a_2 \gamma_{SR_k} + \gamma_{kk} + 1}, \gamma_{R_k D} \right)}{1 + \gamma_E} < 2^{R_0} \right] \\ &= \prod_{k=1}^{N} \int_0^{\infty} F_{Z_{k_1}}(a + by) f_{\gamma_E}(y) dy, \end{aligned} \tag{6.38}$$

where $Z_{k_1} = \min \left(\dfrac{a_1 \gamma_{SR_k}}{a_2 \gamma_{SR_k} + \gamma_{kk} + 1}, \gamma_{R_k D} \right)$.

After some analysis, we obtain the following result

$$SOP_0^1 = \prod_{k=1}^{N} \left(1 - \frac{1}{\lambda_{R_kE}} \int_0^{\omega} A\Big(a+by\Big) e^{-\frac{y}{\lambda_{R_kE}}} dy\right), \tag{6.39}$$

where $A(z) = \dfrac{\lambda_{SR_k}(a_1 - a_2 z)}{z\lambda_{R_k} + \lambda_{SR_k}(a_1 - a_2 z)} \exp\left\{-z\left(\dfrac{1}{\lambda_{SR_k}(a_1 - a_2 z)} + \dfrac{1}{\lambda_{R_kD}}\right)\right\}$, $\omega = \dfrac{1}{a_2 b} - 1$, $\omega < \dfrac{a_1}{a_2}$.

Proof: See Appendix 6.11 (pp. 51).

In special case as $\lambda_{SR_k} \to \infty$, $A(z)|_{\lambda_{SR_k}\to\infty} = \exp\left(-z\dfrac{1}{\lambda_{R_kD}}\right)$

$$\begin{aligned} SOP_0^1|_{\lambda_{SR_k}\to\infty} &= \prod_{k=1}^{N} \left(1 - \frac{1}{\lambda_{RE}} \int_0^{\omega} \exp\left((-a-by)\frac{1}{\lambda_{R_kD}}\right)\right) \exp\left(\frac{-y}{e^{\lambda_{RE}}}\right) dy \\ &= 1 + \left(\frac{1}{\frac{b\lambda_{RE}}{\lambda_{R_kD}} + 1}\right)\left(\exp\left(-\omega\left(\frac{b}{\lambda_{R_kD}} + \frac{1}{\lambda_{RE}}\right) - \frac{a}{\lambda_{R_kD}}\right) - \exp\left(\frac{-a}{\lambda_{R_kD}}\right)\right), \end{aligned} \tag{6.40}$$

When $\lambda_{R_kD} \to \infty$, we have $A_1(z) = A(z)|_{\lambda_{R_kD}\to\infty} = \frac{\lambda_{SR_k}(a_1 - a_2 z)}{z\lambda_{R_k} + \lambda_{SR_k}(a_1 - a_2 z)} \exp\left(\frac{-z}{\lambda_{SR_k}(a_1 - a_2 z)}\right)$, and we hence obtain

$$SOP_0^1|_{\lambda_{R_kD}\to\infty} = \prod_{k=1}^{N} \left(1 - \frac{1}{\lambda_{RE}} \int_0^{\omega} A_1\,(a+by) \exp\left(\frac{-y}{\lambda_{RE}}\right) dy\right). \tag{6.41}$$

Finally, in case of $\lambda_{RE} \to \infty$, we obtain $SOP_0^1|_{\lambda_{R_kD}\to\infty} = 1$.

Similarly, in OMA case, SOP for signal X_{S2} can be computed by

$$SOP_0^2 = \prod_{k=1}^{N} \left(1 - A_n \exp\left(\mu_n \beta_n\right) E_1\left(\mu_n \beta_n\right)\right), \tag{6.42}$$

where $A_n = \dfrac{a_2 \lambda_{SR_k}}{b\lambda_{R_kE}\lambda_{R_k}} \exp\left(-a\left(\dfrac{1}{a_2\lambda_{SR_k}} + \dfrac{1}{\lambda_{R_kD}}\right)\right)$, $\mu_n = \dfrac{b}{a_2\lambda_{SR_k}} + \dfrac{b}{\lambda_{R_kD}} + \dfrac{1}{\lambda_{R_kE}}$, $\beta_n = \dfrac{a_2\lambda_{SR_k} + \lambda_{R_k}}{b\lambda_{R_k}}$.

When $\lambda_{SR_k} \to \infty$

$$SOP_0\Big|_{\lambda_{SR_k}\to\infty} = \prod_{k=1}^{N} \left(1 - \frac{\exp\left(-a/\lambda_{R_kD}\right))}{1 + b\dfrac{\lambda_{R_kE}}{\lambda_{R_kD}}}\right). \tag{6.43}$$

When $\lambda_{R_kD} \to \infty$

$$SOP_0^2\Big|_{\lambda_{R_kD}\to\infty} = \prod_{k=1}^{N} \left(1 - A_{n1} \exp\left(\mu_{n1}\beta_{n1}\right) E_1\left(\mu_{n1}\beta_{n1}\right)\right), \tag{6.44}$$

where $A_{n1} = \dfrac{a_2\lambda_{SR_k}}{b\lambda_{R_kE}\lambda_{R_k}} \exp\left(-\dfrac{a}{a_2\lambda_{SR_k}}\right)$, $\mu_{n1} = \dfrac{b}{a_2\lambda_{SR_k}} + \dfrac{1}{\lambda_{R_kE}}$, $\beta_1 = \dfrac{a_2\lambda_{SR_k} + \lambda_{R_k}}{b\lambda_{R_k}}$.

Finally, when $\lambda_{R_kE} \to \infty$, we have $A \to 0$ and $SOP_0\Big|_{\lambda_{R_kE}\to\infty} = 1$.

Remark 1: It difficult of evaluate how the related parameter, i.e., the number of relay, P_S and P_R, which affect on system performance by analytical expressions. Fortunately, they can be determined through following simulation results for find optimal SOP.

6.9 Simulation Results

In this section, several Monte Carlo simulation results of the proposed relay section network and existing HD/FD schemes are presented. In the simulations, the transmit power of source and relay are changed to find optimal outage performance. In this chapter, we assume that the self-interference is the residual self-interference exists small amount after the imperfect self-interference suppression. For outage probability evaluation, we assume that the interference is at noise level and channel gain of each channel as $R_0 = 0.5$, $|\lambda_{SR_1}|^2 = 1.1$, $|\lambda_{SR_2}|^2 = 1.3$, $|\lambda_{R_1D}|^2 = 1.1$, $|\lambda_{R_2D}|^2 = 1.2$, $|\lambda_{R_1E}|^2 = 0.2$, and $|\lambda_{R_2E}|^2 = 0.5$, which can be achieved through numerical simulation.

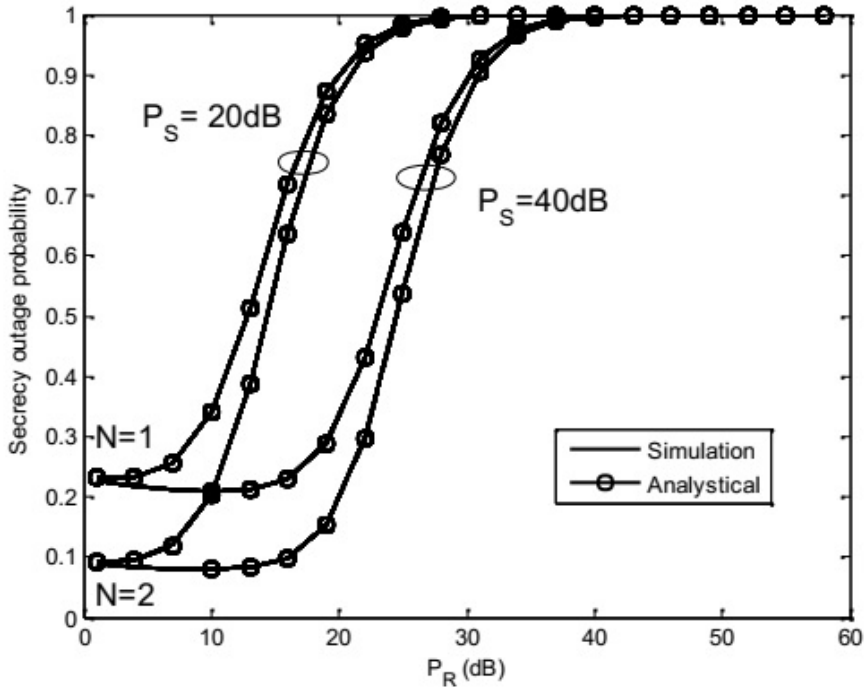

Figure 6.7: Secrecy outage probability in OMA versus PR of FD-DF relays with the number of relays $N = \{1, 2\}$ and $P_S = \{20, 40\}$ dB.

Figure 6.7 plots the SOP of the scenario in which we change the transmit power at the source and the transmit power at the relay. We can observe that as expected, the SOP decreases to an optimal point as approximately with mathematical programs such as Matlab, i.e, $P_S = 40\ dB$, $P_R = 9.2\ dB$ with $N = 2$ or $N = 1$. Another option for enhancing the PLS is to choose PA between the source and the relay properly since it reduces the total OP. It is also worth noting that having the best outage performance if we choose P_S and P_R in right manner.

In Figures 6.8 and 6.9, we compare SOP of OMA and NOMA.

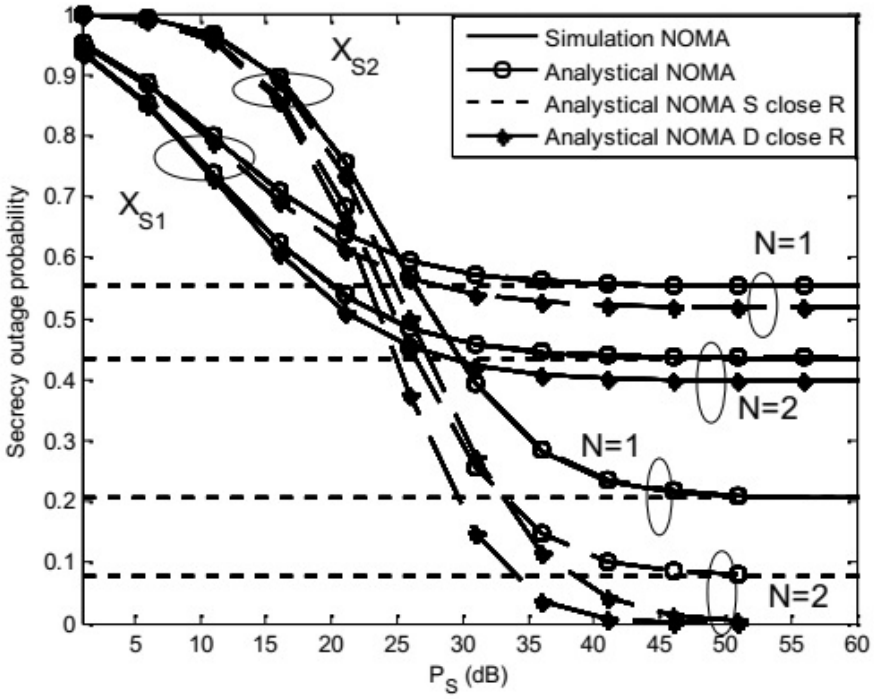

Figure 6.8: SOP of the ORS scheme versus PS of FD-DF relays in NOMA with the number of relays $N = \{1, 2\}$ and $P_R = 10\ dB$ of two signals X_{S1} and X_{S2}.

The results confirmed that SOP performance of X_{S1} and X_{S2} lower than SOP performance of OMA due to lower power allocated for each signal. In this case the transmit power at relay P_R contribute to change SOP performance at high region PS and the cross point is approximately 25 dB– 30 dB

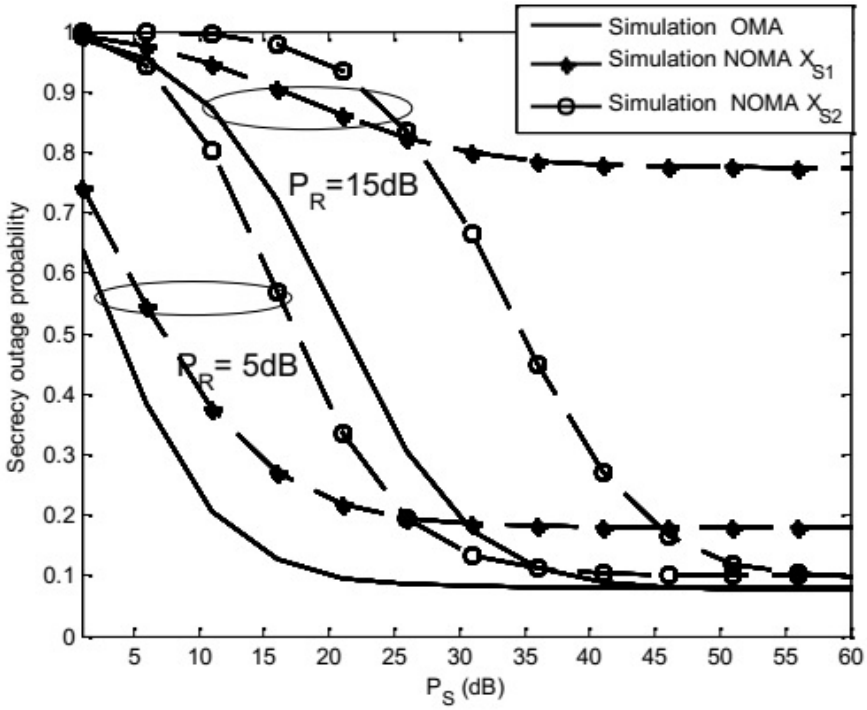

Figure 6.9: SOP of the ORS scheme versus P_S of FD-DF relays OMA and NOMA with $N = 2$, $a_1 = 0.95$, $a_2 = 0.05$ and $P_R = \{5, 15\}$ dB.

6.10 Conclusions

In this chapter, we studied the SOP of the FD relay by comparing performance of OMA and NOMA scenarios with RS scheme. We suggested a novel FD operation, where each FD receives the information signal from the previous node as well as transmits the jamming signal to the eavesdropper at the same time. The transmit PAs for FD relay are calculated by a numerical approach to minimize the lower bound of the secrecy outage performance. Numerical results have revealed that the mentioned FD relay operation with the high number of the relay significantly enhanced the outage performance compared with the conventional FD relay operation with the single relay.

6.11 Appendix

It is noted that

$$Z_{k1} = \min\left(\frac{a_1\gamma_{SR_k}}{a_2\gamma_{SR_k} + \gamma_{kk} + 1}, \gamma_{R_kD}\right) = \min\left(X_{k1}, Y_k\right). \tag{6.45}$$

We consider outage event as follows:

$$F_{Z_{k1}}(z) = 1 - \left(1 - F_{X_{k1}}(z)\right)\left(1 - F_{Y_k}(z)\right). \tag{6.46}$$

We first derive F_{X_k} with $x > 0$ as follows:

$$F_{X_{k1}}(x) = \Pr\left(\frac{a_1\gamma_{SR_k}}{a_2\gamma_{SR_k} + \gamma_{kk} + 1} < x\right)$$
$$= \Pr\left(\left(a_1 - a_2x\right)\gamma_{SR_k} < x\left(\gamma_{kk} + 1\right)\right). \tag{6.47}$$

We derive two cases as follows:

$$F_{X_{k1}} = \begin{cases} \Pr\left(\gamma_{SR_k} > \dfrac{x(\gamma_{kk}+1)}{(a_1 - a_2x)}\right) = 1 & \text{if } x \geq \dfrac{a_1}{a_2} \\ \Pr\left(\gamma_{SR_k} < \dfrac{x(\gamma_{kk}+1)}{(a_1 - a_2x)}\right) & \text{if } x < \dfrac{a_1}{a_2} \end{cases}. \tag{6.48}$$

By substituting $F_{\gamma_{SR_k}}(x) = 1 - \exp\left(\frac{-x}{\lambda_{SR_k}}\right)$ and $f_{\gamma_{SR_k}}(y) = \frac{1}{\lambda_{SR_k}}\exp\left(\frac{-y}{\lambda_{SR_k}}\right)$ into (6.47), we obtain

$$F_{X_{k1}} = \begin{cases} 1, \text{ where } x \geq \frac{a_1}{a_2} \\ \int\limits_0^{\infty}\left(1 - \exp\left(\frac{-z(y+1)}{\lambda_{SR_k}(a_1 - a_2z)}\right)\right)\frac{1}{\lambda_{R_k}}\exp\left(\frac{-y}{\lambda_{R_k}}\right), \text{ where } x < \frac{a_1}{a_2} \end{cases}. \tag{6.49}$$

$$F_{X_{k1}} = \begin{cases} 1, \text{ where } x \geq \frac{a_1}{a_2} \\ 1 - \frac{\lambda_{SR_k}(a_1 - a_2z)exp\left(\frac{-z}{\lambda_{SR_k}(a_1 - a_2z)}\right)}{z\lambda_{R_k} + \lambda_{SR_k}(a_1 - a_2z)}, \text{ where } x < \frac{a_1}{a_2} \end{cases}. \tag{6.50}$$

By combining (6.46) and (6.48), we obtain

$$F_{Z_{k1}} = \begin{cases} 1 & \text{if } z \geq \dfrac{a_1}{a_2} \\ 1 - A(z) & \text{if } x < \dfrac{a_1}{a_2} \end{cases}. \tag{6.51}$$

As a result, it can be shown that

$$SOP_0^1 = \prod_{k=1}^{N}\int\limits_0^{\infty} F_{Z_{k1}}(a + by)\, f_{\gamma_E}(y)\, dy$$
$$= \prod_{k=1}^{N}\left(1 - \frac{1}{\lambda_{R_kE}}\int\limits_0^{\omega} A\left(a + by\right)\exp\left(\frac{-y}{\lambda_{R_kE}}\right)dy\right), \tag{6.52}$$

where $A(z) = \frac{\lambda_{SR_k}(a_1 - a_2z)}{z\lambda_{R_k} + \lambda_{SR_k}(a_1 - a_2z)}\exp\left(-z\left(\frac{1}{\lambda_{SR_k}(a_1 - a_2z)} + \frac{1}{\lambda_{R_kD}}\right)\right)$ and $\left(\omega = \dfrac{1}{a_2b} - 1\right) < \dfrac{a_1}{a_2}$.

Chapter 7:

NOMA-Aided Hybrid Satellite Terrestrial Relay for Small-Cell network

Part I – A Novel Design for a SWIPT Framework with a PS protocol

SATELLITE communication systems need to be integrated with emerging small-cell network to provide seamless connectivity and high-speed broadband access for mobile users in future wireless networks. In this chapter, we study a HSTRS employing small cell transmission under interference constraint with macro-cell users. To characterize such HSTRS-assisted small-cell network, Shadowed-Rician fading for satellite links and Nakagami-m fading for terrestrial links are adopted. We further deploy NOMA to improve spectrum efficiency. To provide performance analysis, we derive exact formulas for outage probability and throughput of the considered HSTRS, and further examine its achievable diversity order. More importantly, we conduct the performance analysis by indicating performance gaps among two users, and such a gap depends on power allocation factors. We evaluate key performance metrics through the derived analytical expressions to provide useful framework of HSTRS and to characterize the impact of interference in different cells, and integer values of the per-hop fading severity parameters. The useful guidelines are introduced in the design of futuristic HSTRS for small-cell communications.

Note that the outcomes in the Chapter 7 have been published in the paper [NNL01] entitled *"On Performance Analysis of NOMA-Aided Hybrid Satellite Terrestrial Relay With Application in Small-Cell Network"* (2020) *IEEE Access*, Article ID: Access-2020-9229415. DOI: 10.1109/ACCESS.2020.3032139. **IF 3.367**.

7.1 System Models

In this section, a small-cell base station (SCB), a small-cell relay (SCR) and two small-cell user SU_i ($i = \{1, 2\}$ are considered to implement the advantage of NOMA, i.e. higher spectral efficiency. Besides, the small-cell network can be operated together with a macro-cell satellite (MCS) serving macro-cell users (MUs) [NNL01].

The transmit power at the SCB and the SCR in the context of small-cell is limited by many factors [80]. These factors partly depend on channels. In particular, we denote $\psi = \frac{1}{|h_{QM}|^2}$, then we have the transmit power at the SCB and the SCR are expressed as follows:

$$P_{SCQ} = \min\left(\bar{P}_{SCQ}, P_M\psi\right), \quad Q \in \{B, R\}. \tag{7.1}$$

In the first phase, the received signal at the SCR is formulated by

$$y_{SCR} = h_{BR}\sqrt{P_{SCB}}\left(\sqrt{a_1}x_1 + \sqrt{a_2}x_2\right) + \sqrt{P_{MCS}}h_{MR}x_M + n_{SCR}. \tag{7.2}$$

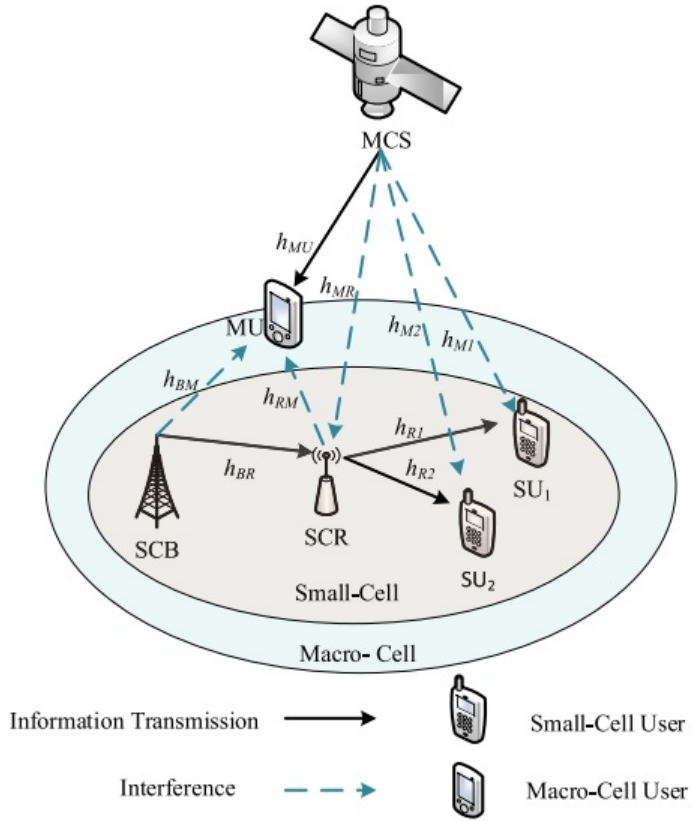

Figure 7.1: System model of small-cell HSTRS relying on NOMA.

To evaluate system performance, it need be computed the SINR at the SCR to detect signal x_1 . In particular, SINR is expressed as follows:

$$\Gamma_{SCR\to x_1} = \frac{P_{SCB}\left|h_{BR}\right|^2 a_1}{P_{SCB}\left|h_{BR}\right|^2 a_2 + P_{MCS}\left|h_{MR}\right|^2 + N_0}. \tag{7.3}$$

By employing SIC, the SINR to detect x_2 at the SCR is expressed as follows:

$$\Gamma_{SCR\to x_2} = \frac{P_{SCB}\left|h_{BR}\right|^2 a_2}{P_{MCS}\left|h_{MR}\right|^2 + N_0}. \tag{7.4}$$

In the second phase, the relay in SCR transmits signal to the cell-edge users SU_i . The

received signal at SU_i is expressed as follows:

$$y_{SU_i} = h_{Ri}\sqrt{P_{SCR}}\left(\sqrt{a_1}x_1 + \sqrt{a_2}x_2\right) + \sqrt{P_{MCS}}h_{Mi}x_M + n_{SU_i}. \tag{7.5}$$

The SINR measured at the SU_1 to detect signal x_1 is expressed as follows:

$$\Gamma_{SU_1 \to x_1} = \frac{P_{SCR}\left|h_{R1}\right|^2 a_1}{P_{SCR}\left|h_{R1}\right|^2 a_2 + P_{MCS}\left|h_{M1}\right|^2 + N_0}. \tag{7.6}$$

Then, the SINR at SU_2 for detecting of signal x_1 is expressed by

$$\Gamma_{SU_2 \to x_1} = \frac{P_{SCR}\left|h_{R2}\right|^2 a_1}{P_{SCR}\left|h_{R2}\right|^2 a_2 + P_{MCS}\left|h_{M2}\right|^2 + N_0}. \tag{7.7}$$

The user SU_2 benefits by SIC, then SINR to detect signal x_2 at SU_2 is expressed as follows:

$$\Gamma_{SU_2 \to x_2} = \frac{P_{SCR}\left|h_{R2}\right|^2 a_2}{P_{MCS}\left|h_{M2}\right|^2 + N_0}. \tag{7.8}$$

7.2 Performance Analysis

In this section, we focus on main metric, OP and throughput performance by considering delay-limited transmission mode. These metrics play important role in design relevant equipment for the HSTRS.

7.2.1 Channel models

We adopt Shadowed-Rician fading model for the satellite links. In particular, the probability density function of $|h_{Mj}|^2$ with $j \in (R, 1, 2)$ is formulated by [31]

$$f_{\left|h_{Mj}\right|^2}(x) = \alpha_{Mj} e^{-\beta_{Mj}x}\, {}_1F_1\left(m_{Mj}; 1; \delta_{Mj}x\right), \quad x > 0, \tag{7.9}$$

where $\alpha_{Mj} = \left(\frac{2b_{Mj}m_{Mj}}{2b_{Mj}m_{Mj}+\Omega_{Mj}}\right)^{m_{Mj}} / 2b_{Mj}$ and $\delta_{Mj} = \Omega_{Mj} / \left(2b_{Mj}\right)\left(2b_{Mj}m_{Mj} + \Omega_{Mj}\right)$, with Ω_{Mj} and $2b_{Mj}$ represents the respective average power of the LOS and multi-path components, m_{Mj} is the fading severity parameter and ${}_1F_1(.)$ is the first kind of confluent Hypergeometric function [79, Eq. (9.210.1)].

In the dissertation, we consider arbitrary integer-valued fading severity parameter [81]. Then, we can simplify (7.9) as follows:

$$f_{\left|h_{Mj}\right|^2}(x) = \alpha_{Mj} \sum_{n_{Mj}=0}^{m_{Mj}-1} \zeta_{Mj}\left(n_{Mj}\right) x^{n_{Mj}} e^{-\Psi_{Mj}x}, \tag{7.10}$$

where $\zeta_{Mi}(n_{Mj}) = (-1)^{n_{Mj}}(1-m_{Mj})_{n_{Mj}}\delta_{Mj}^{n_{Mj}}/(n_{Mj}!)^2$, $(.)_a$ is the Pochhammer symbol [79, p. xliii] and $\Psi_{Mi} = \beta_{Mi} - \delta_{Mi}$. Thus, the CDF of $|h_{Mj}|^2$ is expressed by

$$F_{|h_{Mj}|^2}(x) = 1 - \alpha_{Mj}\sum_{n_{Mj}=0}^{m_{Mj}-1}\zeta_{Mj}(n_{Mj}) \times \sum_{q=0}^{n_{Mj}}\frac{n_{Mj}!}{q!\left(\Psi_{Mj}\right)^{n_{Mj}-q+1}}x^q e^{-\Psi_{Mi}x}. \tag{7.11}$$

The PDF and CDF of $|h_k|^2$ for $k \in \{BR, BM, RM, R1, R2\}$ are respectively given as follows:

$$f_{|h_k|^2}(x) = \frac{x^{m_k-1}}{\Gamma(m_k)\,\omega_k^{m_k}}e^{-\frac{x}{\omega_k}}, \tag{7.12}$$

and

$$\begin{aligned} F_{|h_k|^2}(x) =& \frac{\gamma(m_k, x/\omega_k)}{\Gamma(m_k)} \\ =& 1 - e^{-\frac{x}{\omega_k}}\sum_{n_k=0}^{m_k-1}\frac{x^{n_k}}{\omega_k^{n_k}n_k!}. \end{aligned} \tag{7.13}$$

where $\omega_k = \frac{\lambda_k}{m_k}$, m_k and λ_k denoted the fading severity and average power, respectively.

7.2.2 Outage performance

7.2.2.1 Outage performance of SU_1 To evaluate how the two edge-users work in the context of small-cell, we continue to look at the OP performance. The user SU_1 need to detect its signal x_1 . Based on conditions related to such outage event, the OP of user SU_1 is formulated by

$$\begin{aligned} \mathcal{P}_{x_1} =& 1 - \Pr\left(\min\left(\Gamma_{SCR\to x_1}, \Gamma_{SU_1\to x_1}, \Gamma_{SU_2\to x_1}\right) > \gamma_1\right) \\ =& 1 - \underbrace{\Pr\left(\Gamma_{SCR\to x_1} > \gamma_1\right)}_{A_1} \\ & \times \underbrace{\Pr\left(\Gamma_{SU_1\to x_1} > \gamma_1\right)}_{A_2}\underbrace{\Pr\left(\Gamma_{SU_2\to x_1} > \gamma_1\right)}_{A_3}, \end{aligned} \tag{7.14}$$

Proposition 1: As a part of such OP, term A_1 can be expressed as follows:

$$\begin{aligned}A_1 = &\sum_{n_{MR}=0}^{m_{MR}-1}\sum_{n_{BR}=0}^{m_{BR}-1}\sum_{a=0}^{n_{BR}}\binom{n_{BR}}{a}\frac{\xi_{MR}n_{MR}\left(n_{MR}+a\right)!\rho_S^a\alpha_{MR}\theta_1^{n_{BR}}}{n_{BR}!\Gamma\left(m_{BM}\right)}\\
&\times\left(\frac{\left(\omega_{BR}\bar{\rho}_B\right)^{n_{MR}-n_{BR}+a+1}\gamma\left(m_{BM},\frac{\rho_M}{\omega_{BM}\bar{\rho}_B}\right)\exp\left(-\frac{\theta_1}{\omega_{BR}\bar{\rho}_B}\right)}{\left(\theta_1\rho_S+\Psi_{MR}\omega_{BR}\bar{\rho}_B\right)^{n_{MR}+a+1}}\right.\\
&\left.+\frac{\omega_{BM}^{n_{BR}}\Psi_{MR}^{-n_{MR}-a-1}\left(\rho_M\omega_{BR}\right)^{m_{BM}}}{\Gamma\left(n_{MR}+a+1\right)\left(\theta_1\omega_{BM}+\rho_M\omega_{BR}\right)^{m_{BM}+n_{BR}}}\right.\\
&\left.\times G_{1,[1:1],0,[1:1]}^{1,1,1,1,0}\left[\begin{array}{c|c}\frac{\theta_1\rho_S\omega_{BM}}{\Psi_{MR}(\theta_1\omega_{BM}+\rho_M\omega_{BR})} & 1+m_{BM}+n_{BR}\\ \frac{\omega_{BR}\omega_{BM}\bar{\rho}_B}{\theta_1\omega_{BM}+\rho_M\omega_{BR}} & -n_{MR}-a;1\\ & --\\ & 0;0\end{array}\right]\right).\end{aligned}\tag{7.15}$$

See appendix 7.5.1 (pp. 69) for proof.
In term of computing of A_2, by substituting (7.6) into (7.14), we obtain

$$\begin{aligned}A_2 = &\Pr\left(|h_{R1}|^2>\frac{\theta_1\left(\rho_S|h_{M1}|^2+1\right)}{\bar{\rho}_R},\bar{\rho}_R<\frac{\rho_M}{|h_{RM}|^2}\right)\\
&+\Pr\left(|h_{R1}|^2>\frac{\theta_1|h_{RM}|^2\left(\rho_S|h_{M1}|^2+1\right)}{\rho_M},\bar{\rho}_R>\frac{\rho_M}{|h_{RM}|^2}\right).\end{aligned}\tag{7.16}$$

Similarly, A_2 can be calculated by

$$\begin{aligned}A_2 = &\sum_{n_{M1}=0}^{m_{M1}-1}\sum_{n_{R1}=0}^{m_{R1}-1}\sum_{b=0}^{n_{R1}}\binom{n_{R1}}{b}\frac{\zeta_{M1}\left(n_{M1}\right)\left(n_{M1}+b\right)!\alpha_{M1}}{n_{R1}!\Gamma\left(m_{RM}\right)}\\
&\times\left(\frac{\left(\omega_{R1}\bar{\rho}_R\right)^{n_{MR}-n_{R1}+b+1}\gamma\left(m_{RM},\rho_M/\omega_{RM}\bar{\rho}_R\right)e^{-\frac{\theta_1}{\bar{\rho}_B\omega_{R1}}}}{\rho_S^{-b}\theta_1^{-n_{R1}}\left(\theta_1\rho_S+\Psi_{M1}\bar{\rho}_R\omega_{R1}\right)^{n_{MR}+b+1}}\right.\\
&\left.+\frac{\rho_S^b\theta_1^{n_{R1}}\omega_{RM}^{n_{R1}}\Psi_{M1}^{-n_{M1}-b-1}\left(\rho_M\omega_{R1}\right)^{m_{RM}}}{\Gamma\left(n_{M1}+b+1\right)\left(\theta_1\omega_{RM}+\omega_{R1}\rho_M\right)^{m_{RM}+n_{R1}}}\right.\\
&\left.\times G_{1,[1:1],0,[1:1]}^{1,1,1,1,0}\right.\\
&\left.\times\left[\begin{array}{c|c}\frac{\theta_1\rho_S\omega_{RM}}{\Psi_{M1}\left(\theta_1\omega_{RM}+\omega_{R1}\rho_M\right)} & 1+m_{RM}+n_{R1}\\ \frac{\omega_{R1}\omega_{RM}\bar{\rho}_R}{\theta_1\omega_{RM}+\omega_{R1}\rho_M} & -n_{M1}-b;1\\ & --\\ & 0;0\end{array}\right]\right).\end{aligned}\tag{7.17}$$

Moreover, we can write A_3 as follows:

$$\begin{aligned}A_3 = &\sum_{n_{M2}=0}^{m_{M2}-1}\sum_{n_{R2}=0}^{m_{R2}-1}\sum_{c=0}^{n_{R2}}\binom{n_{R2}}{c}\frac{\zeta_{M2}\left(n_{M2}\right)\left(n_{M2}+c\right)!\alpha_{M2}}{n_{R2}!\Gamma\left(m_{RM}\right)}\\ &\times\left(\frac{\left(\omega_{R2}\bar{\rho}_R\right)^{n_{MR}-n_{R2}+c+1}\gamma\left(m_{RM},\rho_M/\omega_{RM}\bar{\rho}_R\right)e^{-\frac{\theta_1}{\bar{\rho}_B\omega_{R2}}}}{\rho_S^{-C}\theta_1^{-n_{R2}}\left(\theta_1\rho_S+\Psi_{M2}\bar{\rho}_R\omega_{R2}\right)^{n_{MR}+c+1}}\right.\\ &+\left.\frac{\rho_S^b\theta_1^{n_{R2}}\omega_{RM}^{n_{R2}}\Psi_{M2}^{-n_{M2}-c-1}\left(\rho_M\omega_{R2}\right)^{m_{RM}}}{\Gamma\left(n_{M2}+c+1\right)\left(\theta_1\omega_{RM}+\omega_{R2}\rho_M\right)^{m_{RM}+n_{R2}}}\right.\\ &\times G_{1,[1:1],0,[1:1]}^{1,1,1,1,0}\\ &\times\left[\begin{array}{c|c}\frac{\theta_1\rho_S\omega_{RM}}{\Psi_{M2}\left(\theta_1\omega_{RM}+\omega_{R2}\rho_M\right)} & 1+m_{RM}+n_{R1}\\ \frac{\omega_{R2}\omega_{RM}\bar{\rho}_R}{\theta_1\omega_{RM}+\omega_{R2}\rho_M} & -n_{M2}-c;1\\ & --\\ & 0;0\end{array}\right]\Bigg).\end{aligned}\tag{7.18}$$

Finally, the closed-form expression of OP for user SU_1 can be obtained as follows:

$$\mathcal{P}_{x_1}=\begin{cases}1-A_1\times A_2\times A_3, & \text{if}:\gamma_1<\frac{a_1}{a_2}\\ 1 & ,\text{otherwise.}\end{cases}\tag{7.19}$$

7.2.2.2 Outage performance of SU_2 Different from performance of SU_1 , user SU_2 is able to detect its signal for the first hop and the second hop based on achieved SINR, i.e. $\Gamma_{SCR\to x_2}$, $\Gamma_{SU_2\to x_2}$. In particular, the OP of user SU_2 is formulated by

$$\begin{aligned}\mathcal{P}_{x_2}=&1-\Pr\left(\min\left(\Gamma_{SCR\to x_2},\Gamma_{SU_2\to x_2}\right)>\gamma_2\right)\\ =&1-\underbrace{\Pr\left(\Gamma_{SCR\to x_2}>\gamma_2\right)}_{\bar{\mathrm{A}}_1}\underbrace{\Pr\left(\Gamma_{SU_2\to x_2}>\gamma_2\right)}_{\bar{\mathrm{A}}_2}.\end{aligned}\tag{7.20}$$

Proposition 2: The first term in (7.20) can be expressed as follows:

$$\begin{aligned}\bar{\mathrm{A}}_1=&\sum_{n_{MR}=0}^{m_{MR}-1}\sum_{n_{BR}=0}^{m_{BR}-1}\sum_{a=0}^{n_{BR}}\binom{n_{BR}}{a}\frac{\zeta_{MR}\left(n_{MR}\right)\left(n_{MR}+a\right)!\alpha_{MR}}{n_{BR}!\Gamma\left(m_{BM}\right)}\\ &\times\left(\frac{\left(\omega_{BR}\bar{\rho}_B\right)^{n_{MR}-n_{BR}+a+1}\gamma\left(m_{BM},\rho_M/\omega_{BM}\bar{\rho}_B\right)e^{-\frac{\theta_2}{\bar{\rho}_B\omega_{BR}}}}{\rho_S^{-a}\theta_2^{-n_{BR}}\left(\theta_2\rho_S+\Psi_{MR}\bar{\rho}_B\omega_{BR}\right)^{n_{MR}+a+1}}\right.\\ &+\left.\frac{\rho_S^a\theta_2^{n_{BR}}\omega_{BM}^{n_{BR}}\Psi_{MR}^{-n_{MR}-a-1}\left(\rho_M\omega_{BR}\right)^{m_{BM}}}{\Gamma\left(n_{MR}+a+1\right)\left(\theta_2\omega_{BM}+\omega_{BR}\rho_M\right)^{m_{BM}+n_{BR}}}\right.G_{1,[1:1],0,[1:1]}^{1,1,1,1,0}\\ &\times\left[\begin{array}{c|c}\frac{\theta_2\rho_S\omega_{BM}}{\Psi_{MR}(\theta_2\omega_{BM}+\omega_{BR}\rho_M)} & 1+m_{BM}+n_{BR}\\ \frac{\omega_{BR}\omega_{BM}\bar{\rho}_B}{\theta_2\omega_{BM}+\omega_{BR}\rho_M} & -n_{MR}-a;1\\ & --\\ & 0;0\end{array}\right]\Bigg).\end{aligned}\tag{7.21}$$

Proof: With the help of (7.1) and (7.4), we can write $\bar{A}_1$ as follows:

$$\begin{aligned}\bar{\mathrm{A}}_1 =& \Pr\left(\frac{P_{SCB}\left|h_{BR}\right|^2 a_2}{P_{MCS}\left|h_{MR}\right|^2+N_0} > \gamma_2\right)\\ =& \Pr\left(\left|h_{BR}\right|^2 > \frac{\theta_2\left(\rho_S\left|h_{MR}\right|^2+1\right)}{\bar{\rho}_B}, \bar{\rho}_B < \frac{\rho_M}{\left|h_{BM}\right|^2}\right)\\ &+ \Pr\left(\left|h_{BR}\right|^2 > \frac{\theta_2\left|h_{BM}\right|^2\left(\rho_S\left|h_{MR}\right|^2+1\right)}{\rho_M}, \bar{\rho}_B > \frac{\rho_M}{\left|h_{BM}\right|^2}\right),\end{aligned} \tag{7.22}$$

where $\theta_2 = \frac{\gamma_2}{a_2}$. Similarly Appendix 7.5.2 (pp. 71), the closed-form expression of $\bar{A}_1$ can be obtained.

The proof is completed.

Similarly, $\bar{A}_2$ is given as follows:

$$\begin{aligned}\bar{\mathrm{A}}_2 =& \sum_{n_{M2}=0}^{m_{M2}-1}\sum_{n_{R2}=0}^{m_{R2}-1}\sum_{c=0}^{n_{R2}}\binom{n_{R2}}{c}\frac{\zeta_{M2}\left(n_{M2}\right)\left(n_{M2}+c\right)!\alpha_{M2}}{n_{R2}!\Gamma\left(m_{RM}\right)}\\ &\times\left(\frac{\left(\omega_{R2}\bar{\rho}_R\right)^{n_{MR}-n_{R2}+c+1}\gamma\left(m_{RM},\rho_M/\omega_{RM}\bar{\rho}_R\right)e^{-\frac{\theta_2}{\bar{\rho}_B\omega_{R2}}}}{\rho_S^{-C}\theta_2^{-n_{R2}}\left(\theta_2\rho_S+\Psi_{M2}\bar{\rho}_R\omega_{R2}\right)^{n_{MR}+c+1}}\right.\\ &+\frac{\rho_S^b\theta_2^{n_{R2}}\omega_{RM}^{n_{R2}}\Psi_{M2}^{-n_{M2}-c-1}\left(\rho_M\omega_{R2}\right)^{m_{RM}}}{\Gamma\left(n_{M2}+c+1\right)\left(\theta_2\omega_{RM}+\omega_{R2}\rho_M\right)^{m_{RM}+n_{R2}}}\,G_{1,[1:1],0,[1:1]}^{1,1,1,1,0}\\ &\left.\times\left[\begin{array}{c|c}\dfrac{\theta_2\rho_S\omega_{RM}}{\Psi_{M2}\left(\theta_2\omega_{RM}+\omega_{R2}\rho_M\right)} & 1+m_{RM}+n_{R1}\\ & -n_{M2}-c;1\\ \dfrac{\omega_{R2}\omega_{RM}\bar{\rho}_R}{\theta_2\omega_{RM}+\omega_{R2}\rho_M} & --\\ & 0;0\end{array}\right]\right).\end{aligned} \tag{7.23}$$

Thus, the closed-form expression of OP for user SU_2 is expressed as follows:

$$\mathcal{P}_{x_2} = 1-\bar{A}_1\times\bar{A}_2. \tag{7.24}$$

Remark 1: In this section, we provide our analytical result on OP. Although, these expressions of OP are complicated, but main impacts rely on the transmit SNR at he small-cell base station and various fading scenarios. For the considered Shadowed-Rician fading for satellite links and Nakagami-m fading for terrestrial links, we further examine these related parameters in numerical simulations. It is predicted that power allocation factors lead to different performance of two small-cell users. To obtain more insight in term of the desired OP expressions, one can derive the expression for asymptotic OP for two users. We also obtain the achievable diversity order. Such findings are extra benefits to design of such network in practice.

7.2.3 Asymptotic and diversity outage behavior analysis

In this section, we examine the peak interference constraint. In particular, P_M is fixed value and only $\bar{P}_{SCQ}$ becomes large in the high SNR region. The asymptotic behaviors of OP for user SU_1 in this case is presented as Proposition 3 below.

Proposition 3: The asymptotic OP of SU_1 can be expressed as follows:

$$\begin{aligned} P_{x_1}^{\infty} = 1 - & \left(1 - \sum_{n_{MR}=0}^{m_{MR}-1} \sum_{n_{BR}=0}^{m_{BR}} \binom{m_{BR}}{n_{BR}} \frac{\xi_{MR} n_{MR} \rho_S^{n_{BR}} \alpha_{MR} \left(n_{MR}+n_{BR}\right)!}{\Gamma\left(m_{BR}+1\right)\Gamma\left(m_{BM}\right)\Psi_{MR}^{n_{MR}+n_{BR}+1}} \left(\frac{\theta_1}{\omega_{BR}}\right)\right. \\ & \left. \times \left(\frac{\gamma\left(m_{BM}, \frac{\rho_N}{\bar{\rho}_B \omega_{BM}}\right)}{\bar{\rho}_B^{m_{BR}}} + \Gamma\left(m_{SP}+m_R, \frac{\rho_M}{\bar{\rho}_B \omega_{BM}}\right)\left(\frac{\omega_{BM}}{\rho_M}\right)^{m_{BR}}\right)\right) \\ & \times \prod_{i=1}^{2} \left(1 - \sum_{n_{Mi}=0}^{m_{Mi}-1} \sum_{n_{Ri}=0}^{m_{Ri}} \binom{m_{Ri}}{n_{Ri}} \frac{\xi_{Mi} n_{Mi} \rho_S^{n_{Ri}} \alpha_{Mi} \left(n_{Mi}+n_{Ri}\right)!}{\Gamma\left(m_{Ri}+1\right)\Gamma\left(m_{RM}\right)\Psi_{Mi}^{n_{Mi}+n_{Ri}+1}} \left(\frac{\theta_1}{\omega_{Ri}}\right)^{m_{Ri}}\right. \\ & \left. \times \left(\frac{\gamma\left(m_{RM}, \frac{\rho_M}{\bar{\rho}_R \omega_{RM}}\right)}{\bar{\rho}_R^{m_R}} + \Gamma\left(m_{RM}+m_{Ri}, \frac{\rho_M}{\bar{\rho}_R \omega_{RM}}\right)\left(\frac{\omega_{RM}}{\rho_M}\right)^{m_{Ri}}\right)\right). \end{aligned} \tag{7.25}$$

See appendix 7.5.2 (pp. 71) for proof.

Similar to the derivation reported in appendix 7.5.2, the asymptotic of OP for user SU_2 can be obtained as follows:

$$\begin{aligned} P_{x_2}^{\infty} = 1 - & \left(1 - \sum_{n_{MR}=0}^{m_{MR}-1} \sum_{n_{BR}=0}^{m_{BR}} \binom{m_{BR}}{n_{BR}} \frac{\xi_{MR} n_{MR} \rho_S^{n_{BR}} \alpha_{MR} \left(n_{MR}+n_{BR}\right)!}{\Gamma\left(m_{BR}+1\right)\Gamma\left(m_{BM}\right)\Psi_{MR}^{n_{MR}+n_{BR}+1}} \left(\frac{\theta_2}{\omega_{BR}}\right)^{m_{BR}}\right. \\ & \left. \times \left(\frac{\gamma\left(m_{BM}, \frac{\rho_N}{\bar{\rho}_B \omega_{BM}}\right)}{\bar{\rho}_B^{m_{BR}}} + \Gamma\left(m_{SP}+m_R, \frac{\rho_M}{\bar{\rho}_B \omega_{BM}}\right)\left(\frac{\omega_{BM}}{\rho_M}\right)^{m_{BR}}\right)\right) \\ & \times \prod_{i=1}^{2} \left(1 - \sum_{n_{M2}=0}^{m_{M2}-1} \sum_{n_{R2}=0}^{m_{R2}} \binom{m_{R2}}{n_{R2}} \frac{\xi_{M2} n_{M2} \rho_S^{n_{R2}} \alpha_{M2} \left(n_{M2}+n_{R2}\right)!}{\Gamma\left(m_{R2}+1\right)\Gamma\left(m_{RM}\right)\Psi_{M2}^{n_{M2}+n_{R2}+1}} \left(\frac{\theta_2}{\omega_{R2}}\right)^{m_{Ri}}\right. \\ & \left. \times \left(\frac{\gamma\left(m_{RM}, \frac{\rho_M}{\bar{\rho}_R \omega_{RM}}\right)}{\bar{\rho}_R^{m_R}} + \Gamma\left(m_{RM}+m_{R2}, \frac{\rho_M}{\bar{\rho}_R \omega_{RM}}\right)\left(\frac{\omega_{RM}}{\rho_M}\right)^{m_{R2}}\right)\right). \end{aligned} \tag{7.26}$$

Regarding the diversity order, we have such formula

$$\mathcal{D} = -\lim_{\bar{\rho}\to\infty} \frac{\log_{10}\left(\mathcal{P}_{\S\rangle}\left(\bar{\rho}\right)\right)}{\log_{10}\left(\bar{\rho}\right).}, \tag{7.27}$$

It can be concluded that when SNR is larger, the diversity order is zero. We further check this result in numerical simulation section. It is useful insights in design of practical system. newpage

7.2.4 Throughput performance

It is necessary to consider other metric of such system. In particular, the overall throughput can be achieved based on obtained OP derived for performance evaluation of two users. In delay-limited mode, at fixed target rates R_1, R_2 the throughput can be obtained.

According to obtained OPs, we can calculate the overall throughput as

$$\mathcal{T}_{total} = (1 - \mathcal{P}_{x_1})\, R_1 + (1 - \mathcal{P}_{x_2})\, R_2. \tag{7.28}$$

7.3 Numerical Results

To provide mathematical analysis, it is necessary to simulate and illustrate for the proposed small-cell HSTRS relying on NOMA scheme. According main configuration, we set the shadowing scenarios of the satellite links h_{Pj} , including the heavy shadowing (HS) and average shadowing (AS) in Table 7.1 like [82]. We further set $\bar{\rho} = \bar{\rho}_B = \bar{\rho}_R$ and the parameters in Table 7.2. Moreover, we vary $m = 1$ for the Nakagami-m fading related to terrestrial links. In these following figures, Monte-Carlo simulations are performed to validate the analytical results.

Table 7.1: Channel parameters related to the satellite

Shadowing	b	m	Ω
The heavy shadowing (HS)	0.063	1	0.0007
The average shadowing (AS)	0.251	5	0.279

Table 7.2: Table of main parameters in simulations

Monte Carlo simulations	10^6 iterations
PA factors	$a_1 = 0.8$ and $a_2 = 0.2$
The target rates	R_1, $R_2 = 0.5$ bit per channel user (BPCU)
Average power	$\lambda_{BM} = \lambda_{RM} = 0.01$, $\lambda = BR = \lambda_{R1} = \lambda_{R2} = 1$
The fading severity	$m = m_{BR} = m_{BM} = m_{RM} = m_{R1} = m_{R2}$

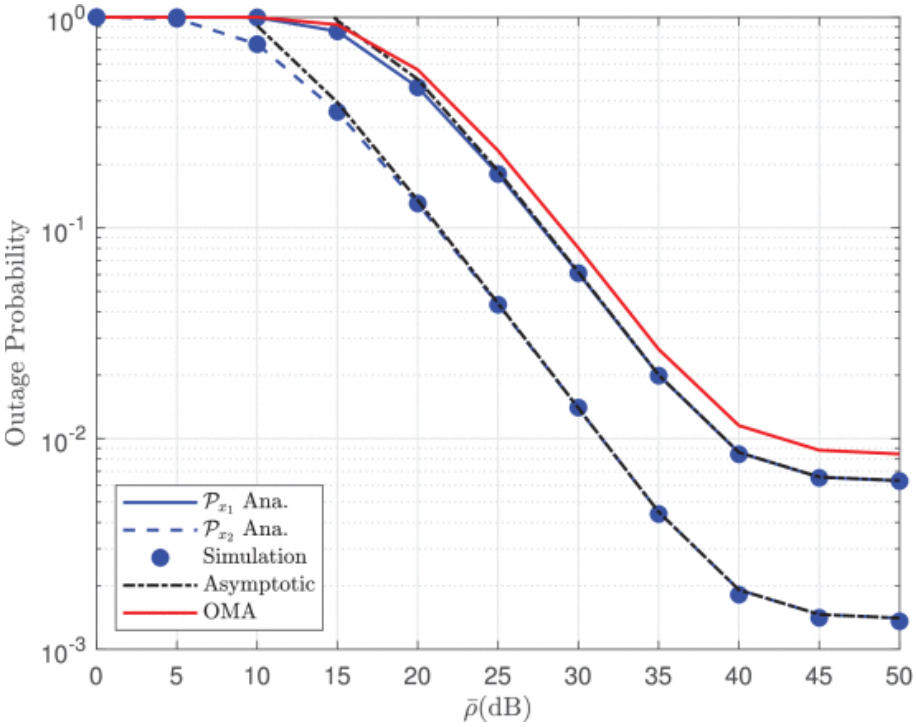

Figure 7.2: The outage probability versus $\bar{\rho}$, where $m = 1$, $\rho_m = 20dB$, $\rho_S = 5dB$ and the satellite link is set HS case.

Figures 7.2 and 7.3 plot the OPs of two users in the considered HSTRS versus the transmit SNR at the MCB $\bar{\rho}$ and the transmit SNR at the SCB ρ_M, respectively. It is valuable result as analytical and Monte-Carlo curves are matched very tightly and it confirms the exactness of derived OP in this chapter. It is clearly seen that the OP performance would be improved at high SNR region. The performance gap among two users is resulted by different power allocation factors. More specifically, the OP performance of SU_2 is better than that of SU_1 and two OPs of two users are still better than that of the OMA-based HSTRS. The reason is that the OMA-based HSTRS needs more time slots to transmit two consecutive signals x_1 and x_2 while only one time slot is served for NOMA-based HSTRS counterpart. Moreover, the asymptotic curves of OP is matched with the exact OP curves at high SNR regime. It is further confirmed that OP will be unchanged at high SNR. Such situation is consistent with diversity order found in previous section. In Figure 7.3, similar trends of OP can be seen.

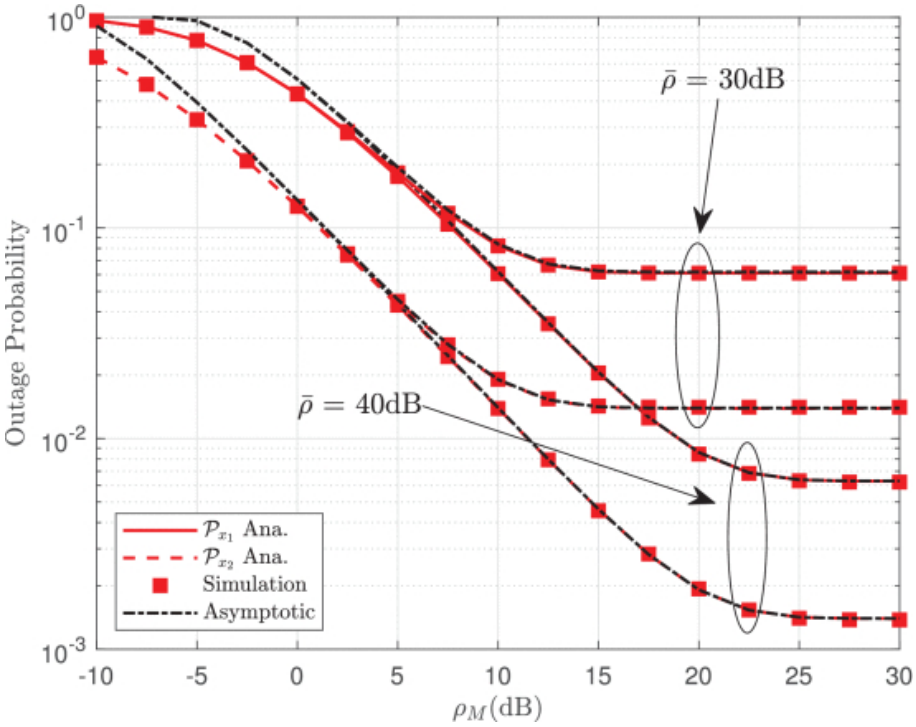

Figure 7.3: The outage probability versus ρ_M, with different values of $\bar{\rho}$, where $m = 1$, $\rho_S = 5dB$ and the satellite link is set HS case.

In Figure 7.4, we can see the impact of ρ_S on the OP performance of small-cell network. It can be explained that higher transmit power at MCB leads to limit the transmit power at SCB, then OP will reduce. The other trend of these OPs can be seen similarly with Figures 7.2 and 7.3. In this experiment, $\rho_S = 5$ exhibits the best performance of small-cell network in term of OP.

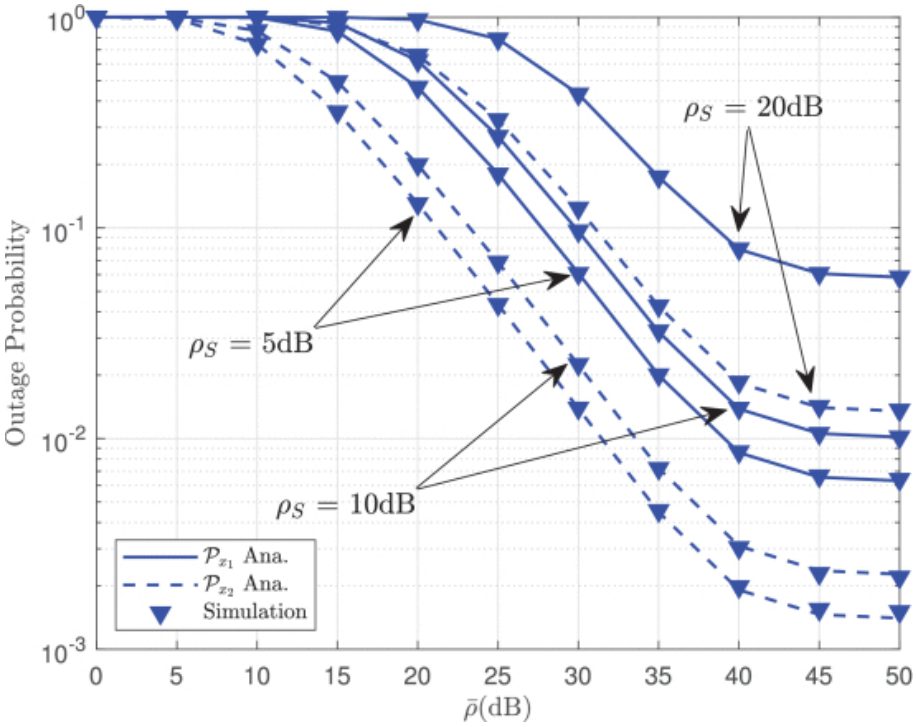

Figure 7.4: The outage probability versus $\bar{\rho}$, with different values of ρ_S, where $m = 1$, $\rho_M = 20dB$ and the satellite link is set HS case.

Figure 7.5 illustrates the OPs of the two users as varying average SNR at SCB from 0 to 50, where the satellite link undergoes HS case. Three cases of channel coefficients are $m = \{1, 2, 3\}$. The performance gap is still seen for these curves related OPs of two users. It is reported that the OPs of two users are best case as $m = 3$. It is obvious to conclude that the improved channels result in better OP performance.

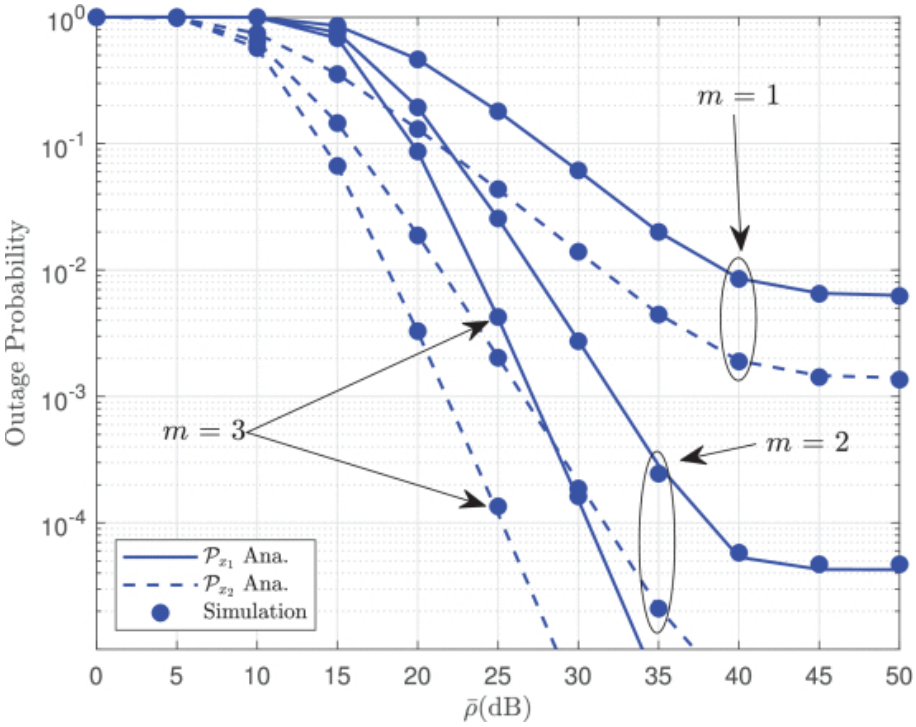

Figure 7.5: The outage probability versus $\bar{\rho}$, with different values of m, where $\rho_M = 20dB$, $\rho_S = 5\ dB$ and the satellite link is set HS case.

Figure 7.6 depicts the OPs of the two users against two crucial parameters, i.e., status of satellite links (HS or AF cases) and the transmit SNR at the SCB $\bar{\rho}$. From the figure, the OPs of two users in the case of HS are better that of AS. At the considered range of the transmit SNR at the SCB $\bar{\rho}$, performance gaps of two users in cases of HS and AS are similar. It is concluded that such OP depends on $\bar{\rho}$ and PA factors rather than on the specific parameters of satellite links (HS or AS).

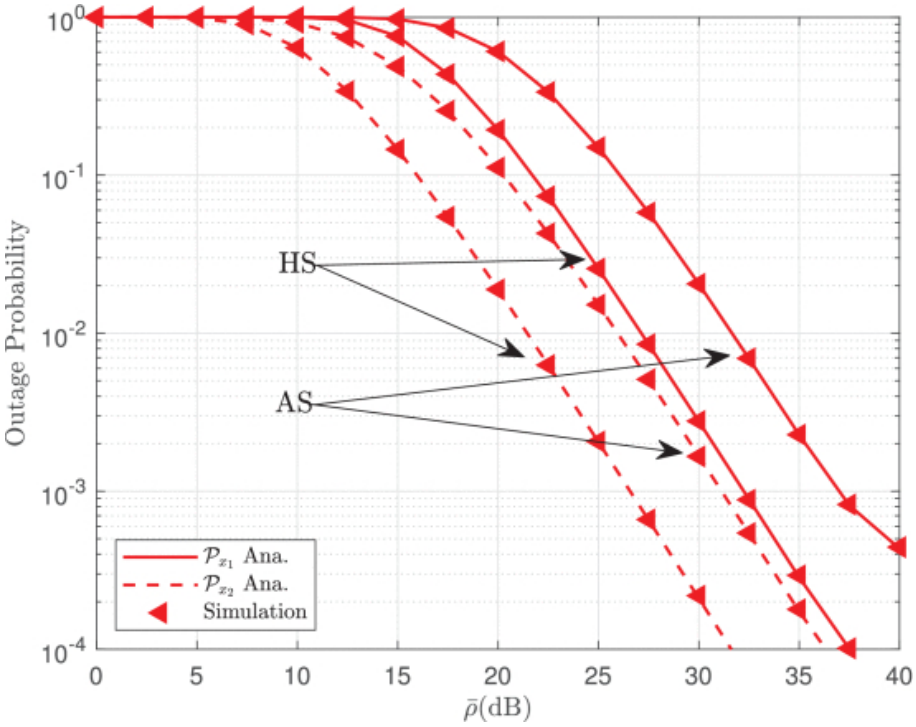

Figure 7.6: The outage probability versus $\bar{\rho}$, with different channel parameter of satellite link, where $\rho_S = 20dB$, $\rho_S = 5dB$ and $m = 2$.

Figure 7.7 continues to confirm power allocation scheme affecting the OPs of two users. It is worth noting that the OP of user SU_1 depends mainly on a_1. In particular, when we increase a_1 from 0.5 to 1, the OP performance of user SU_1 improve significantly. In the contrast, the OP performance of SU_2 is definitely better than that of SU_2 at the point of $a_1 = 0.5$, but such OP becomes worse afterward. The main reason is that a_1 plays important role in varying value of SINRs, then the corresponding OPs will be changed.

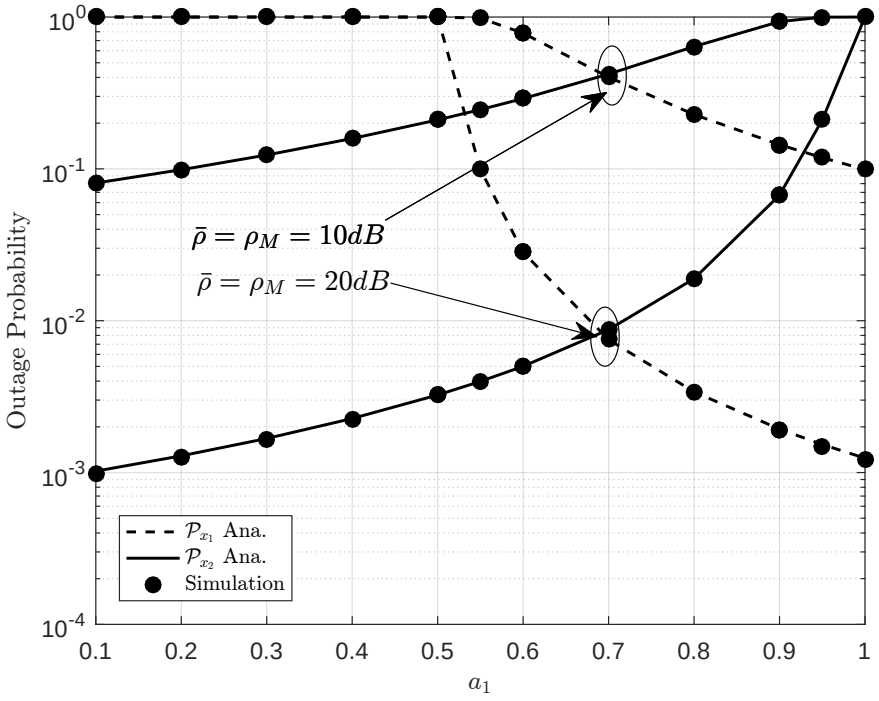

Figure 7.7: The outage probability versus a_1, with different values of $\bar{\rho} = \rho_M$, where $\rho_S = 5dB$, $m = 2$, $R_1 = R_2 = 0.5$ BPCU and the satellite link is set HS case.

Figure 7.8 further provides the curves of the total throughput versus the transmit SNR at SCB $\bar{\rho}$, i.e. throughput for case $R_1 = R_2 = 0.5$. It is clear from (7.28) that higher fixed target rates lead to high throughput. When we increase $\bar{\rho}$ from 0 to 30, the throughput changes significantly. It is reported that the case of $m = 2$ and HS indicates the best throughput performance. The reason is that the throughput is computed based on the OPs. In similar viewpoint, Figure 7.9 demonstrates how the transmit SNRs ($\rho_S = 10$, and $\rho_S = 20$ make the influence to throughput.

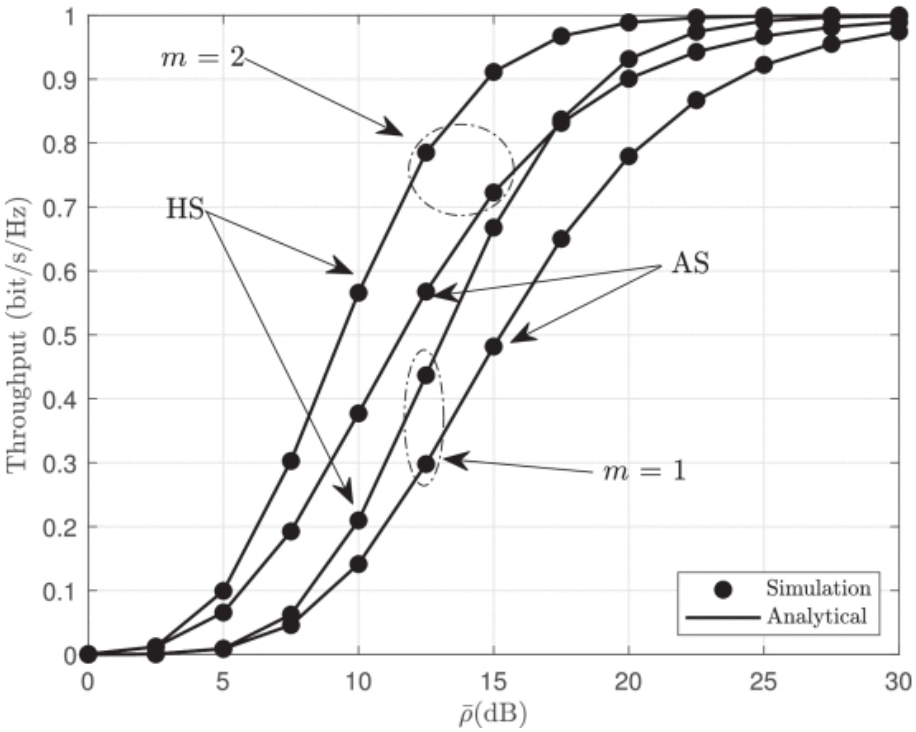

Figure 7.8: The throughput versus $\bar{\rho}$ with different channel parameter of satellite link and m, where $R_1 = R_2 = 0.5$ BPCU, $\rho_M = 20dB$ and $\rho_S = 5dB$.

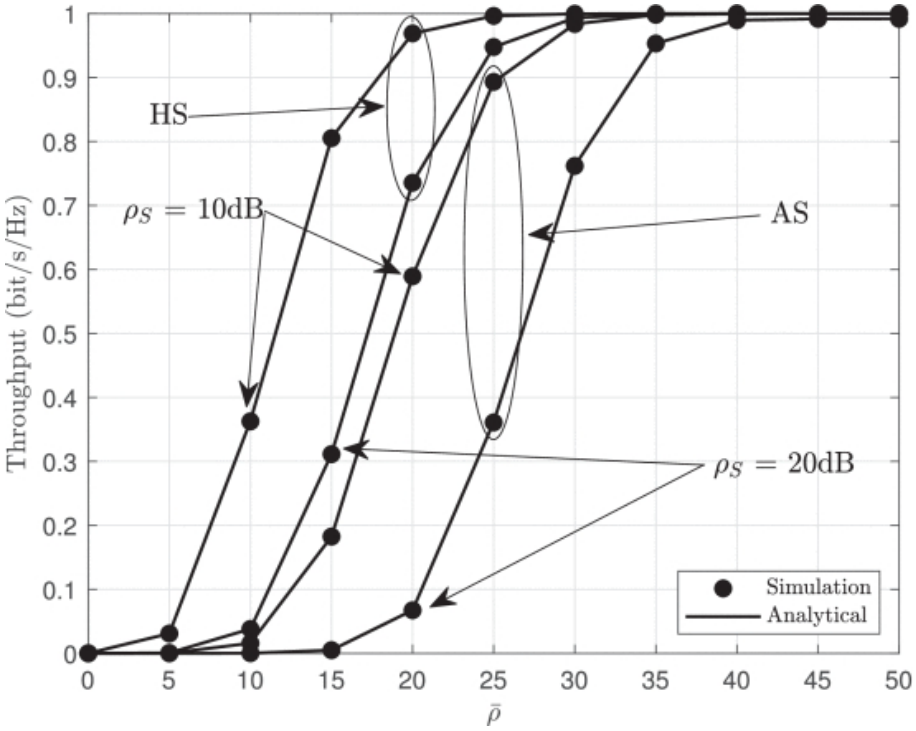

Figure 7.9: The throughput versus $\bar{\rho}$ with different channel parameter of satellite link and ρ_S , where $R_1 = R_2 = 0.5$ BPCU, $\rho_M = 20dB$ and $m = 2$.

7.4 Conclusion

In this chapter, we have studied the operation of small cell to provide reliability transmission for HSTRS. Such system includes a geostationary satellite, two terrestrial users following the principle of NOMA scheme and terrestrial relays. We considered system performance of small-cell to reduce the impact of operations related to macro-cell users. Regarding the outage performance of HSTRS, we derived closed-form and asymptotic expressions of outage probability of two small-cell users. It was shown that the outage probability of HSTRS can be improved by increasing transmit power at base station. Moreover, the outage performance of HSTRS can be enhanced by employing the NOMA scheme compared to that using OMA scheme. In future work, multiple antennas and multiple users can be deployed in such HSTRS.

7.5 Appendix

7.5.1 Appendix A

With the help (7.1) and (7.3), the first term A_1 can be written as shown follows:

$$\begin{aligned} A_1 &= \Pr\left(\frac{P_{SCB}|h_{BR}|^2 a_1}{P_{SCB}|h_{BR}|^2 a_2 + P_{MCS}|h_{MR}|^2 + N_0} > \gamma_1\right) \\ &= \underbrace{\Pr\left(\frac{\bar{\rho}_B|h_{BR}|^2 a_1}{\bar{\rho}_B|h_{BR}|^2 a_2 + \rho_S|h_{MR}|^2 + 1} > \gamma_1, \bar{\rho}_B < \frac{\rho_M}{|h_{BM}|^2}\right)}_{B_1} \\ &\quad + \underbrace{\Pr\left(\frac{\rho_M|h_{BR}|^2 a_1}{\rho_M|h_{BR}|^2 a_2 + |h_{BM}|^2\left(\rho_S|h_{MR}|^2 + 1\right)} > \gamma_1, \bar{\rho}_B > \frac{\rho_M}{|h_{BM}|^2}\right)}_{B_2}, \end{aligned} \tag{7.29}$$

where $\rho_B = \frac{P_{SCB}}{N_0}$, $\bar{\rho}_B = \frac{\bar{P}_{SCB}}{N_0}$, and $\rho_S = \frac{P_{MCS}}{N_0}$.

Then, B_1 is rewritten as follows:

$$\begin{aligned} B_1 &= \Pr\left(|h_{BR}|^2 > \frac{\theta_1\left(\rho_S|h_{MR}|^2 + 1\right)}{\bar{\rho}_B}, |h_{BM}|^2 < \frac{\rho_M}{\bar{\rho}_B}\right) \\ &= \underbrace{\Pr\left(|h_{BR}|^2 > \frac{\theta_1\left(\rho_S|h_{MR}|^2 + 1\right)}{\bar{\rho}_B}\right)}_{B_{1,1}} \underbrace{\Pr\left(|h_{BM}|^2 < \frac{\rho_M}{\bar{\rho}_B}\right)}_{B_{1,2}}, \end{aligned} \tag{7.30}$$

where $\theta_1 = \frac{\gamma_1}{a_1 - \gamma_1 a_2}$.

Moreover, $B_{1,1}$ can be calculated by

$$\begin{aligned} B_{1,1} =& \Pr\left(|h_{BR}|^2 > \frac{\theta_1\left(\rho_S |h_{MR}|^2 + 1\right)}{\bar{\rho}_B}\right) \\ =& \int_0^\infty \bar{F}_{|h_{BR}|^2}\left(\frac{\theta_1\left(\rho_S z + 1\right)}{\bar{\rho}_B}\right) f_{|h_{MR}|^2}(z)\, dz, \end{aligned} \tag{7.31}$$

where $\bar{F}_{|h|^2}(x) = 1 - F_{|h|^2}(x)$.

With the help of (7.10) and (7.13), we obtain

$$\begin{aligned} B_{1,1} =& \sum_{n_{MR}=0}^{m_{MR}-1} \zeta_{MR}(n_{MR}) \sum_{n_{BR}=0}^{m_{BR}-1} \sum_{a=0}^{n_{BR}} \binom{n_{BR}}{a} \\ &\times \frac{\alpha_{MR}\rho_S^a e^{-\frac{\theta_1}{\bar{\rho}_B\omega_{BR}}}}{\omega_{BR}^{n_{BR}} n_{BR}!} \left(\frac{\theta_1}{\bar{\rho}_B}\right)^{n_{BR}} \\ &\times \int_0^\infty z^{n_{MR}+a} e^{-\left(\frac{\theta_1\rho_S}{\bar{\rho}_B\omega_{BR}} + \Psi_{MR}\right)z} dz. \end{aligned} \tag{7.32}$$

Based on [79, Eq. (3.351.3)], the closed-form of $B_{1,1}$ is obtained as follows:

$$\begin{aligned} B_{1,1} =& \sum_{n_{MR}=0}^{m_{MR}-1} \sum_{n_{BR}=0}^{m_{BR}-1} \sum_{a=0}^{n_{BR}} \binom{n_{BR}}{a} \frac{\zeta_{MR}(n_{MR})(n_{MR}+a)!}{n_{BR}!} \\ &\times \frac{\alpha_{MR}\left(\omega_{BR}\bar{\rho}_B\right)^{n_{MR}-n_{BR}+a+1} e^{-\frac{\theta_1}{\bar{\rho}_B\omega_{BR}}}}{\rho_S^{-a}\theta_1^{-n_{BR}}\left(\theta_1\rho_S + \Psi_{MR}\bar{\rho}_B\omega_{BR}\right)^{n_{MR}+a+1}}. \end{aligned} \tag{7.33}$$

With the help of (7.13), $B_{1,2}$ is rewritten as follows:

$$\begin{aligned} B_{1,2} =& \Pr\left(|h_{BM}|^2 < \frac{\rho_M}{\bar{\rho}_B}\right) \\ =& \frac{\gamma\left(m_{BM}, \rho_M/\omega_{BM}\bar{\rho}_B\right)}{\Gamma\left(m_{BM}\right)}. \end{aligned} \tag{7.34}$$

Next, B_2 can be calculated by

$$\begin{aligned} B_2 =& \Pr\left(|h_{BR}|^2 > \frac{\theta_1 |h_{BM}|^2\left(\rho_S |h_{MR}|^2 + 1\right)}{\rho_M}, |h_{BM}|^2 > \frac{\rho_M}{\bar{\rho}_B}\right) \\ =& \int_{\frac{\rho_M}{\bar{\rho}_B}}^\infty f_{|h_{BM}|^2}(x) \int_0^\infty f_{|h_{MR}|^2}(y) \bar{F}_{|h_{BR}|^2}\left(\frac{\theta_1 x\left(\rho_S y + 1\right)}{\rho_M}\right) dy dx. \end{aligned} \tag{7.35}$$

With the help (7.10), (7.11) and (7.12), we can rewrite (7.35) as follows:

$$B_2 = \sum_{n_{MR}=0}^{m_{MR}-1} \sum_{n_{BR}=0}^{m_{BR}-1} \sum_{a=0}^{n_{BR}} \binom{n_{BR}}{a} \frac{\zeta_{MR}\left(n_{MR}\right)}{\Gamma\left(m_{BM}\right)} \times \frac{(n_{MR}+a)!\alpha_{MR}\theta_1^{n_{BR}}\left(\rho_S\right)^a}{n_{BR}!\left(\rho_M\omega_{BR}\right)^{n_{BR}}\omega_{BM}^{m_{BM}}} \times \int_0^{\infty} \frac{x^{m_{BM}+n_{BR}-1}e^{-\left(\frac{\theta_1}{\omega_{BR}\rho_M}+\frac{1}{\omega_{BM}}\right)x}\mathrm{H}\left(\frac{x\bar{\rho}_B}{\bar{\rho}_B}-1\right)}{\left(\frac{\theta_1\rho_S x}{\omega_{BR}\rho_M}+\Psi_{MR}\right)^{n_{MR}+a+1}}dx, \tag{7.36}$$

where $\mathbf{H}(.)$ denotes the Heaviside step function. Based on [83, Eq. (10)], we obtain

$$\left(1+Px\right)^{-z} = \frac{1}{\Gamma\left(z\right)}G_{1,1}^{1,1}\left[Px\left|\begin{array}{c}1-z\\0\end{array}\right.\right], \tag{7.37}$$

$$H\left(x-1\right) = G_{1,1}^{0,1}\left(x\left|\begin{array}{c}1\\0\end{array}\right.\right), \tag{7.38}$$

where $G_{p,q}^{m,n}[.]$ is the Meijer's G-function [79, Eq. (9.301)]. Then, we can rewrite B_2 as follows:

$$B_2 = \sum_{n_{MR}=0}^{m_{MR}-1} \sum_{n_{BR}=0}^{m_{BR}-1} \sum_{a=0}^{n_{BR}} \binom{n_{BR}}{a} \frac{\zeta_{MR}\left(n_{MR}\right)\left(n_{MR}+a\right)!}{n_{BR}!} \times \frac{\alpha_{MR}\theta_1^{n_{BR}}\left(\rho_S\right)^a\left(\Psi_{MR}\right)^{-n_{MR}-a-1}}{\Gamma\left(n_{PR}+a+1\right)\Gamma\left(m_{BM}\right)\left(\rho_M\omega_{BR}\right)^{n_{BR}}\omega_{BM}^{m_{BM}}} \times \int_0^{\infty} x^{m_{BM}+n_{BR}-1}e^{-\frac{\theta_1\omega_{BM}+\omega_{BR}\rho_M}{\omega_{BR}\rho_M\omega_{BM}}x}G_{1,1}^{0,1}\left[\frac{x\bar{\rho}_B}{\rho_M}\left|\begin{array}{c}1\\0\end{array}\right.\right] \times G_{1,1}^{1,1}\left[\frac{\theta_1\rho_S}{\omega_{BR}\rho_M\Psi_{MR}}x\left|\begin{array}{c}-n_{MR}-a\\0\end{array}\right.\right]dx. \tag{7.39}$$

Following results in [84, Eq. (2.6.2)], the inner integral of (7.39) is solved. Substituting (7.33) and (7.34) into (7.30) then substituting the achieved result and (7.39) into (7.29), we can achieve final result.

7.5.2 Appendix B

By using (7.1), the asymptotic of the CDF, i.e. $F_{\rho_B|h_{BR}|^2}^{\infty}\left(x\right)$ for peak interference constraint can be obtained as

$$F_{\rho_B|h_{BR}|^2}^{\infty}\left(x\right) = \int_0^{\frac{\rho_M}{\bar{\rho}_B}} F_{|h_{BR}|^2}^{\infty}\left(\frac{x}{\bar{\rho}_B}\right) f_{|h_{BM}|^2}\left(y\right)dy + \int_{\frac{\rho_M}{\bar{\rho}_B}}^{\infty} F_{|h_{BR}|^2}^{\infty}\left(\frac{xy}{\rho_M}\right) f_{|h_{BM}|^2}\left(y\right)dy.$$

With the help [79, Eq. (8.354.1)], we can write as follows:

$$\gamma\left(m_i, \frac{x}{\omega_i}\right) \overset{x\to\infty}{\approx} \frac{1}{m_i}\left(\frac{x}{\omega_i}\right)^{m_i}. \tag{7.40}$$

Then, the asymptotic of $F_{|h_{BR}|^2}$ can be written as follows:

$$F^{\infty}_{|h_BR|^2}(x) \approx \frac{1}{\Gamma(m_{BR}+1)}\left(\frac{x}{\omega_{BR}}\right)^{m_i}.$$

Next, we can obtain as follows:

$$\begin{aligned} F^{\infty}_{\rho_B|h_{BR}|^2}(x) = &\frac{\gamma\left(m_{BM}, \frac{\rho_M}{\bar{\rho}_B\omega_{BM}}\right)}{\Gamma(m_{BR}+1)\Gamma(m_{BM})}\left(\frac{x}{\omega_{BR}\bar{\rho}_B}\right)^{m_{BR}} \\ &+\frac{\Gamma\left(m_{BM}+m_R, \frac{\rho_M}{\bar{\rho}_B\omega_{BM}}\right)}{\Gamma(m_{BR}+1)\Gamma(m_{BM})}\left(\frac{\omega_{BM}x}{\omega_{BR}\rho_M}\right)^{m_{BR}}. \end{aligned} \tag{7.41}$$

Thus, $\mathrm{A}_1^{\infty}1$ can be calculated as follows:

$$\begin{aligned} \mathrm{A}_1^{\infty} =&\Pr\left(\rho_B|h_{BR}|^2 > \theta_1\left(\rho_S|h_{MR}|^2+1\right)\right) \\ =&1-\int_0^{\infty}\left(F^{\infty}_{\rho_B|h_{BR}|^2}(\theta_1(\rho_P y+1))\right)f_{|h_{MR}|^2}(y)\,dy. \end{aligned} \tag{7.42}$$

$$\begin{aligned} A_1^{\infty} = 1-&\sum_{n_{MR}=0}^{m_{MR}-1}\sum_{n_{BR}=0}^{m_{BR}}\binom{m_{BR}}{n_{BR}}\frac{\xi_{MR}n_{MR}\rho_S^{n_{BR}}\alpha_{MR}(n_{MR}+n_{BR})!}{\Gamma(m_{BR}+1)\Gamma(m_{BM})\Psi_{MR}^{n_{MR}+n_{BR}+1}}\left(\frac{\theta_1}{\omega_{BR}}\right)^{m_{BR}} \\ &\times\left(\frac{\gamma\left(m_{BM}, \frac{\rho_N}{\bar{\rho}_B\omega_{BM}}\right)}{\bar{\rho}_B^{m_{BR}}}+\Gamma\left(m_{SP}+m_R, \frac{\rho_M}{\bar{\rho}_B\omega_{BM}}\right)\left(\frac{\omega_{BM}}{\rho_M}\right)^{m_{BR}}\right). \end{aligned} \tag{7.43}$$

It is noted that the asymptotic of A_2^{∞} and A_3^{∞} can be respectively obtained as follows:

$$\begin{aligned} A_2^{\infty} = 1-&\sum_{n_{M1}=0}^{m_{M1}-1}\sum_{n_{R1}=0}^{m_{R1}}\binom{m_{R1}}{n_{B1}}\frac{\xi_{M1}n_{M1}\rho_S^{n_{R1}}\alpha_{M1}(n_{M1}+n_{R1})!}{\Gamma(m_{R1}+1)\Gamma(m_{RM})\Psi_{M1}^{n_{M1}+n_{R1}+1}}\left(\frac{\theta_1}{\omega_{R1}}\right)^{m_{R1}} \\ &\times\left(\frac{\gamma\left(m_{RM}, \frac{\rho_M}{\bar{\rho}_R\omega_{RM}}\right)}{\bar{\rho}_R^{m_R}}+\Gamma\left(m_{RM}+m_{R1}, \frac{\rho_M}{\bar{\rho}_R\omega_{RM}}\right)\left(\frac{\omega_{RM}}{\rho_M}\right)^{m_{R1}}\right), \end{aligned} \tag{7.44}$$

$$\begin{aligned} A_3^{\infty} = 1-&\sum_{n_{M2}=0}^{m_{M2}-1}\sum_{n_{R2}=0}^{m_{R2}}\binom{m_{R2}}{n_{B2}}\frac{\xi_{M2}n_{M2}\rho_S^{n_{R2}}\alpha_{M2}(n_{M2}+n_{R2})!}{\Gamma(m_{R2}+1)\Gamma(m_{RM})\Psi_{M2}^{n_{M1}+n_{R1}+1}}\left(\frac{\theta_1}{\omega_{R2}}\right)^{m_{R1}} \\ &\times\left(\frac{\gamma\left(m_{RM}, \frac{\rho_M}{\bar{\rho}_R\omega_{RM}}\right)}{\bar{\rho}_R^{m_R}}+\Gamma\left(m_{RM}+m_{R2}, \frac{\rho_M}{\bar{\rho}_R\omega_{RM}}\right)\left(\frac{\omega_{RM}}{\rho_M}\right)^{m_{R2}}\right). \end{aligned} \tag{7.45}$$

Now, using (7.43), (7.44) and (7.45), the result in (7.25) can be attained.

Part II – UAV-assisted HSTRS with Hardware Impairment and Imperfect SIC

THE dissertation investigates the outage performance of NOMA in HSTRS systems which contain hardware impairments. An UAV was implemented to forward signals from a satellite to users on the ground [NNL02]. A two-user model was applied to achieve spectral efficiency. In practical, real-life scenarios, the UAV and ground users encounter issues with imperfect hardware. The dissertation studies the performance gap between two users experiencing practical problems such as hardware impairment and imperfect SIC.

Note that the outcomes in the Chapter 7 (Part II) have been published in the paper [NNL02] entitled *"UAV Based Satellite-Terrestrial Systems with Hardware Impairment and Imperfect SIC: Performance Analysis of User Pairs"*, in **IEEE Access**,(2021), Article ID: 9521513, 9, pp.117925-117937, DOI: 10.1109/ACCESS.2021.3107253. **IF 3.367**

7.6 System Models

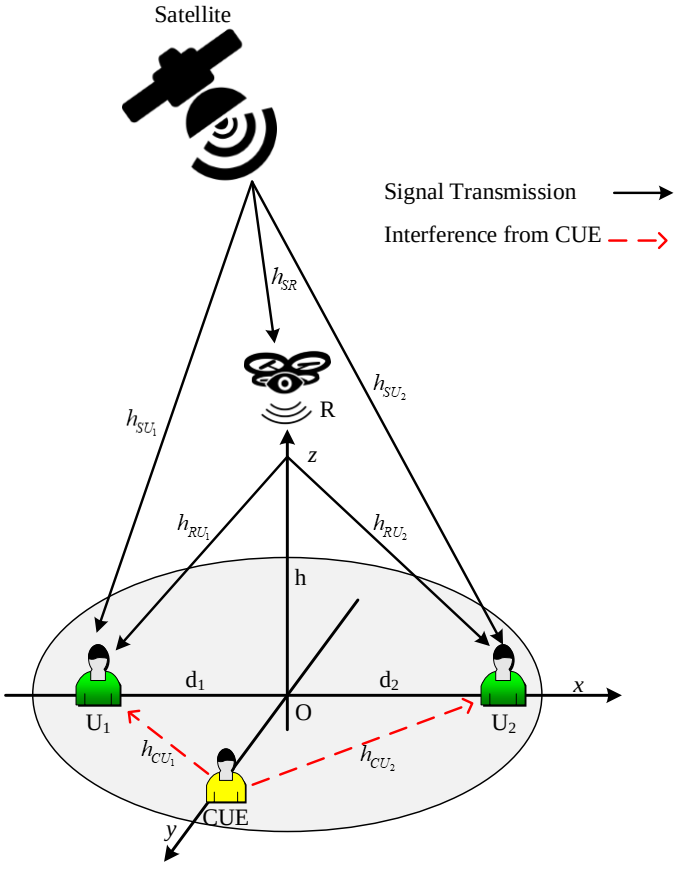

Figure 7.10: System model of small-cell HSTRS relying on NOMA.

Figure 7.10 illustrates a UAV-based satellite system which includes a satellite (S), a UAV (R), and two NOMA users $U_i, i \in \{1, 2\}$. In the coverage of the two NOMA users, we examine only

Table 7.3: Main notations of the system model.

Symbol	**Description**
x_i	Signal at U_i
a_i	Power allocation , where $a_1 < a_2$ and $a_1 + a_2 = 1$
P_S	Transmit power at S
P_R	Transmit power at R
N	Number of antenna of S
K_i	Rician factor
n_{U_i}, n_{SU_i} and n_R	Additive white Gaussian noise (AWGN), where $n_i \sim CN(0, N_0)$
$CN(\mu, \sigma^2)$	Complex normal distribution with mean μ and variance σ^2
R_i	Target rate
$\|\bullet\|_F$	Frobenius norm
$(\bullet)^\dagger$	Conjugate transpose
χ	Path loss exponent
d_{SR}	Distance from S to UAV
d_{SU_i}	Distance from S to U_i
d_{RU_i}	Distance from UAV to U_i
$\mathbf{h}_{SR}$	Channel vector from satellite to UAV relay
$\mathbf{h}_{SU_i}$	Channel vector from the satellite to the U_i
h_{RU_i}	Channel coefficient from R to U_i
h_{CU_i}	Channel coefficient from CUE to U_i
E{.}	Expectation operator
$\Gamma[.;.]$	Upper incomplete gamma function
$\gamma[.;.]$	Lower incomplete gamma function
$\Gamma[.]$	Complete gamma function
$I_i[.]$	First-kind Bessel function with order i

the worse case of interference from CUE. To improve the strength of the signal transmission, S is assumed to be equipped with N antennas while the remaining nodes R, U_i and CUE are given a simple design and equipped with a single antenna. Due to large separation and heavy shadowing, the direct link from S to the ground users U_i is also assumed unavailable [85]. The main system parameters are presented in Table 7.3.

Regarding the existence of the UAV, let us consider the three-dimensional Cartesian coordinates (x, y, z) depicted in Figure 1. The UAV relay is located at $R(0, 0, h)$ with altitude h. The locations of ground users U_1 and U_2 are given by the coordinates $U_1(-d_1, 0, 0)$ and $U_2(d_2, 0, 0)$, respectively. From analysis, we can obtain the Euclidean distance from R to U_i according to

$$d_{RU_i} = \sqrt{d_i^2 + h^2}, \tag{7.46}$$

In the first phase, S sends a signal $\sqrt{P_S}\left(\sqrt{a_1}x_1 + \sqrt{a_2}x_2\right)$ to the UAV (node R) and U_i. The signals received at the UAV and U_i are respectively given as

$$\begin{aligned} y_R &= \sqrt{L_{SR}\vartheta_S\vartheta\left(\phi_R\right)}\mathbf{h}_{SR}^{\dagger}\mathbf{h}_{SR} \\ &\times \left(\sqrt{P_S}\left(\sqrt{a_1}x_1 + \sqrt{a_2}x_2\right) + \eta_R\right) + n_R, \end{aligned} \tag{7.47}$$

$$\begin{aligned} y_{SU_i} &= \sqrt{L_{SU_i}\vartheta_S\vartheta\left(\phi_{U_i}\right)}\mathbf{h}_{SU_i}^{\dagger}\mathbf{h}_{SU_i} \\ &\times \left(\sqrt{P_S}\left(\sqrt{a_1}x_1 + \sqrt{a_2}x_2\right) + \eta_{SU_i}\right) \\ &+ P_{CUE}h_{CU_i} + n_{U_i}, \end{aligned} \tag{7.48}$$

where ϑ_S is the satellite antenna gain, η_R and η_{SU_i} are the distortion noises caused by RHI where $\eta_R \sim CN\left(0, \kappa_R^2 P_S\right)$ and $\eta_{SU_i} \sim CN\left(0, \kappa_{SU_i}^2 P_S\right)$ and κ_R and κ_{SU_i} are the levels of hardware impairment associated with the link from S to R and S to U_i, respectively [86]. We denote $\mathbf{w}_i$ as the weight vector and apply the maximum ratio transmission [87], $\mathbf{w}_{Sj} = \frac{\mathbf{h}_{SR}}{\left\|\mathbf{h}_{Sj}\right\|_F}$ for $j \in \{R, U_1, U_2\}$. In addition, $L_{SR} = \frac{1}{K_B TW}\left(\frac{c}{4\pi f_c d_{SR}}\right)^2$ and $L_{SU_i} = \frac{1}{K_B TW}\left(\frac{c}{4\pi f_c d_{SU_i}}\right)^2$ denote the instantaneous free space loss [38], where $K_B = 1.38 \times 10^{-23} J/K$ is the Boltzman constant, W and T are the carrier bandwidth and receiver noise temperature, respectively, c represents the speed of light, and f_c is the carrier frequency.

To characterize the link from S to R and S to U_i, $\vartheta\left(\phi_j\right)$ represents the beam gain and is expressed by

$$\vartheta\left(\phi_j\right) = \vartheta_j\left(\frac{I_1\left(\bar{\rho}_j\right)}{2\rho_j} + 36\frac{I_3\left(\bar{\rho}_j\right)}{\rho_j^3}\right), \tag{7.49}$$

where ϑ_R and ϑ_{U_i} are the antenna gains at the UAV and U_i, respectively, ϕ_j is the angular separation, $\bar{\rho}_j = 2.07123\frac{\sin\phi_j}{\sin\phi_{R3\text{dB}}}$, and $\phi_{R3\text{dB}}$ represents 3dB beamwidth [38].

In the first phase, the signals for the link from S to R and R to D_i are processed, and to detect the signals as expected, the signal to interference plus noise ratio (SINR) is determined.

The SINR at U_2 to detect x_2 is given by

$$\begin{aligned}\gamma_{SU_2}^{x_2} &= \frac{P_S L_{SU_2} \vartheta\left(\phi_{U_2}\right) a_2 \left\|h_{SU_2}\right\|_F^2}{P_S L_{SU_2} \vartheta\left(\phi_{U_2}\right) a_1 \left\|h_{SU_2}\right\|_F^2 + P_S L_{SU_2} \vartheta\left(\phi_{U_2}\right) \left\|h_{SR}\right\|_F^2 \kappa_{SU_2}^2 + P_{CUE} \left\|h_{CU_2}\right|^2 + N_0} \\ &= \frac{\beta_{SU_2} a_2}{\beta_{SU_2} a_1 + \beta_{SU_2} \kappa_{SU_2}^2 + \rho_{CU} \left|h_{CU_2}\right|^2 + 1}.\end{aligned} \tag{7.50}$$

Then, the SINR at U_1 to detect x_2 is given by

$$\gamma_{SU_1}^{x_2} = \frac{\beta_{SU_1} a_2}{\beta_{SU_1} a_1 + \beta_{SU_1} \kappa_{SU_1}^2 + \rho_{CU} \left|h_{CU_1}\right|^2 + 1}, \tag{7.51}$$

where $\rho_S = \frac{P_S}{N_0}$, $\rho_{CU} = \frac{P_{CUE}}{N_0}$, $\rho_{Sj} = \rho_S L_{Sj} \vartheta_S \vartheta\left(\phi_j\right)$ and $\beta_{Sj} = \rho_{Sj} \left\|\mathbf{h}_{Sj}\right\|_F^2$. Then, by performing SIC to eliminate x_2, treating signal x_2 as a noise term, x_1 is detected at the UAV. To do this, we compute the SINR from

$$\gamma_{SU_1}^{x_1} = \frac{\beta_{SU_1} a_1}{\rho_{SU_1} \left|g\right|^2 + \beta_{SU_1} \kappa_{SU_1}^2 + \rho_{CU} \left|h_{CU_1}\right|^2 + 1}. \tag{7.52}$$

Due to the effect of ipSIC, g is an interference channel modeled as a Rayleigh fading channel where $g \sim CN(0, \lambda_g)$ [88].

Similarly, the SINR at the UAV to detect x_2 is given as

$$\gamma_{SR}^{x_2} = \frac{\beta_{SR} a_2}{\beta_{SR} a_1 + \beta_{SR} \kappa_R^2 + 1}. \tag{7.53}$$

Applying SIC to detect signal x_1, the SINR is given as

$$\gamma_{SR}^{x_1} = \frac{\beta_{SR} a_1}{\rho_{SR} \left|g\right|^2 + \beta_{SR} \kappa_R^2 + 1}. \tag{7.54}$$

In the second phase, the UAV sends the signal to two NOMA users. The signal received at U_i is given as

$$\begin{aligned}y_{RU_i} = &\sqrt{\frac{P_S}{d_{RU_i}^{\chi}}} h_{RU_i} \left(\left(\sqrt{a_1} x_1 + \sqrt{a_2} x_2\right) + \eta_{U_i}\right) \\ &+ P_{CUE} h_{CU_i} + n_{RU_i},\end{aligned} \tag{7.55}$$

where η_{U_i} is the distortion noise caused by RHIs for $\eta_{U_i} \sim CN\left(0, \kappa_i^2 P_R\right)$, κ_i is the level of hardware impairments from R to U_i, h_{CU_i} is the channel from CUE following a Rayleigh fading channel with $\mathrm{E}\{h_{CU_i}\} = 1$

The SINR at U_2 to detect the signal x_2 is given as

$$\begin{aligned}\gamma_{RU_2}^{x_2} &= \frac{P_R a_2 \left|h_{RU_2}\right|^2}{P_R a_1 \left|h_{RU_2}\right|^2 + P_R \left|h_{RU_2}\right|^2 \kappa_2^2 + P_{CUE} \left|h_{CU_2}\right|^2 + N_0} \\ &= \frac{\beta_{RU_2} a_2}{\beta_{RU_2} a_1 + \beta_{RU_2} \kappa_2^2 + \rho_{CU} \left|h_{CU_2}\right|^2 + 1},\end{aligned} \tag{7.56}$$

where $\rho_R = \frac{P_R}{N_0}$, $\rho_{CU} = \frac{P_{CUE}}{N_0}$, $\rho_{RU_i} = \frac{\rho_R}{d^X_{RU_i}}$ and $\beta_{RU_i} = \rho_{RU_i} |h_{RU_i}|^2$. Then, the SINR at U_1 to detect signal x_2 is given as

$$\gamma^{x_2}_{RU_1} = \frac{\beta_{RU_1} a_2}{\beta_{RU_1} a_1 + \beta_{RU_1} \kappa_1^2 + \rho_{CU} |h_{CU_1}|^2 + 1}. \tag{7.57}$$

The SINR at U_1 to detect its the own signal x_1 is given as

$$\gamma^{x_1}_{RU_1} = \frac{\beta_{RU_1} a_1}{\rho_{RU_1} |g|^2 + \beta_{RU_1} \kappa_1^2 + \rho_{CU} |h_{CU_1}|^2 + 1}. \tag{7.58}$$

Remark 1: *These SINR expressions are crucial in evaluating other main system metrics and provide a guide to implementing a UAV-based satellite system in practical scenarios. We can observe in the SINR equations, for example* (7.56), (7.57), *and* (7.58), *the the corresponding SINRs are determined by the channel gains, the power allocation factors* a_1 *and* a_2, *and the levels of RHI. In addition, the transmit power at the satellite and the UAV play other roles in improving system performance. We consider these effects in the following section.*

7.7 System Performance Analysis

7.7.1 Channel Characterization

To further compute the system performance metric, let us assume that the channel coefficients are independent and identically distributed (i.i.d.). Then, the probability density function (PDF) of the channel coefficient $h^{(j)}_{Sj}$ from the satellite's q-th antenna to the UAV is expressed as [31]

$$f_{\left|h^{(q)}_{Sj}\right|^2}(\gamma) = e^{-\varepsilon_{SR}\gamma} \alpha_{Sj1} F_1(m_{SR}; 1; \delta_{SR}\gamma), \tag{7.59}$$

where $\varepsilon_{Sj} = \frac{1}{2b_{Sj}}$, $\alpha_{SR} = \frac{1}{2b_{Sj}} \left(\frac{2b_{Sj} m_{Sj}}{2b_{Sj} m_{Sj} + \Omega_{Sj}}\right)^{m_{Sj}}$, $\delta_{Sj} = \frac{\Omega_{Sj}}{2b_{Sj}\left(2b_{Sj} m_{Sj} + \Omega_{Sj}\right)}$, and where Ω_{Sj}, $2b_{Sj}$ and m_{Sj} are the average powers of LOS, the multipath components and the fading severity parameter, respectively. ${}_1F_1(.;.;.)$ denotes a confluent hypergeometric function of the first kind [79, Eq. (9.210)]. Then, we assume the integer values of the Shadowed-Rician fading severity parameter throughout this chapter. We can rewrite (7.59) as

$$f_{\left|h^{(q)}_{Sj}\right|^2}(\gamma) = e^{-\Delta_{SR}\gamma} \alpha_{SR} \sum_{b=0}^{m_{Sj}-1} \zeta_{Sj}(b) \gamma^b, \tag{7.60}$$

where $\Delta_{Sj} = \varepsilon_{Sj} - \delta_{Sj}$, $\zeta_{Sj}(z) = \frac{(-1)^z \left(1 - m_{Sj}\right)_z \left(\delta_{Sj}\right)^z}{(z!)^2}$, and $(.)_x$ is the Pochhammer symbol [79, p.xliii]. Applying the result from [89], the PDF of $\|\mathbf{h}_{Sj}\|^2_F$ under i.i.d. Shadowed-Rician fading can be formulated as

$$f_{\|\mathbf{h}_{Sj}\|^2_F}(x) = \sum_{b_1=0}^{m_{Sj}-1} \cdots \sum_{b_N=0}^{m_{Sj}-1} \Xi(Sj) \gamma^{\Lambda-1} e^{-\Delta_{Sj}\gamma}, \tag{7.61}$$

where

$$\Xi\left(Sj\right)=\alpha_{Sj}^{N}\prod_{u=1}^{N}\zeta_{Sj}\left(b_{u}\right)\prod_{v=1}^{N-1}B\left(\sum_{l=1}^{v}b_{l}+v,b_{v+1}+1\right), \tag{7.62}$$

$$\Lambda=\sum_{u=1}^{N}b_{u}+N. \tag{7.63}$$

and $B(.,.)$ is the Beta function [79, Eq. (8.384.1)]. From the above analysis, the PDF of β_{Sj} is expressed as

$$f_{\beta_{Sj}}\left(\gamma\right)=\sum_{b_{1}=0}^{m_{Sj}-1}\cdots\sum_{b_{N}=0}^{m_{Sj}-1}\frac{\Xi\left(Sj\right)}{\left(\rho_{Sj}\right)^{\Lambda}}\gamma^{\Lambda-1}e^{-\frac{\Delta_{Sj}}{\rho_{Sj}}\gamma}. \tag{7.64}$$

Using [79, Eq. (3.351.1)], we obtain the CDF of β_{Sj} as

$$F_{\beta_{Sj}}\left(\gamma\right)=\sum_{b_{1}=0}^{m_{Sj}-1}\cdots\sum_{b_{N}=0}^{m_{Sj}-1}\frac{\Xi\left(Sj\right)}{\left(\Delta_{Sj}\right)^{\Lambda}}\gamma\left(\Lambda,\frac{\Delta_{Sj}}{\rho_{Sj}}\gamma\right). \tag{7.65}$$

Then, the PDF of the links from R to U_i can be expressed as [41]

$$f_{\left|h_{RU_{i}}\right|^{2}}\left(\gamma\right)=\varpi_{i}e^{-K_{i}}e^{-\varpi_{i}\gamma}I_{0}\left(2\sqrt{\varpi_{i}K_{i}\gamma}\right), \tag{7.66}$$

where $\varpi_i=\frac{(1+K_i)}{\Omega_i}$, and K_i and Ω_i are the Rician factor and average fading power, respectively. Then, the PDF of β_{RU_i} can be expressed as

$$f_{\beta_{RU_{i}}}\left(\gamma\right)=\frac{\varpi_{i}e^{-K_{i}}}{\rho_{RU_{i}}}e^{-\frac{\varpi_{i}}{\Omega_{i}}\gamma}I_{0}\left(2\sqrt{\frac{K_{i}\varpi_{i}}{\rho_{RU_{i}}}\gamma}\right). \tag{7.67}$$

Based on [79, Eq. (8447.1)], we can then rewrite

$$f_{\beta_{RU_{i}}}\left(\gamma\right)=\sum_{b=0}^{\infty}\frac{\left(K_{i}\right)^{b}e^{-K_{i}}}{\left(b!\right)^{2}}\left(\frac{\varpi_{i}}{\rho_{RU_{i}}}\right)^{b+1}\gamma^{b}e^{-\frac{\varpi_{i}}{\rho_{RU_{i}}}\gamma}. \tag{7.68}$$

Similarly, the CDF of β_{RU_i} can be expressed as

$$F_{\beta_{RU_{i}}}\left(\gamma\right)=\sum_{b=0}^{\infty}\frac{\left(K_{i}\right)^{b}e^{-K_{i}}}{\left(b!\right)^{2}}\gamma\left(b+1,\frac{\varpi_{i}}{\rho_{RU_{i}}}\gamma\right). \tag{7.69}$$

7.7.2 Outage Probability of U_1

The OP defines that the probability of the instantaneous SINR γ_k falls below a predefined threshold φ_{th}, i.e.,

$$P_{out}=\Pr\left(\gamma_{k}<\varphi_{th}\right), \tag{7.70}$$

where Pr(.) is the probability function.

Based on the selection combining technique, the OP of U_1 can be determined by maximizing the SINR of the link from S to U_i and the link from S to R. The OP of U_1 can then be expressed

as [90]

$$P_{out,1} = \Psi_1 \times \Psi_2, \tag{7.71}$$

where

$$\Psi_1 = 1 - \Pr\left(\gamma_{SU_1}^{x_2} > \varphi_2, \gamma_{SU_1}^{x_1} > \varphi_1\right), \tag{7.72}$$

$$\begin{aligned}\Psi_2 = 1 &- \Pr\left(\gamma_{SR}^{x_2} > \varphi_2, \gamma_{SR}^{x_1} > \varphi_1\right) \\ &\times \Pr\left(\gamma_{SR}^{x_2} > \varphi_2, \gamma_{SR}^{x_1} > \varphi_1\right),\end{aligned} \tag{7.73}$$

and where $\varphi_i = 2^{R_i} - 1$, R_i are the target rates.

Lemma 1: The term Ψ_1 is given as

$$\Psi_1 = 1 - I_1 + I_2, \tag{7.74}$$

where I_1 and I_2 are expressed by

$$\begin{aligned}I_1 = &\sum_{b_1=0}^{m_{SU_1}-1} \cdots \sum_{b_N=0}^{m_{SU_1}-1} \sum_{a=0}^{\Lambda-1} \frac{\Xi\left(SU_1\right)\Gamma\left(\Lambda\right) e^{-\frac{\Delta_{SU_1}\upsilon_{\max}}{\rho_{SU_1}}}}{a!\lambda_{CU_1}\left(\Delta_{SU_1}\right)^{\Lambda-a}} \\ &\times \left(\frac{\upsilon_{\max}}{\rho_{CU}\rho_{SU_1}}\right)^a \left(\frac{1}{\lambda_{CU_1}} + \frac{\Delta_{SU_1}\upsilon_{\max}\rho_{CU}}{\rho_{SU_1}}\right)^{-a-1} \\ &\times e^{\frac{1}{\lambda_{CU_1}\rho_{CU}} + \frac{\Delta_{SU_1}\upsilon_{\max}}{\rho_{SU_1}}} \Gamma\left(a+1, \frac{1}{\lambda_{CU_1}\rho_{CU}} + \frac{\Delta_{SU_1}\upsilon_{\max}}{\rho_{SU_1}}\right),\end{aligned} \tag{7.75}$$

and

$$\begin{aligned}I_2 = &\sum_{b_1=0}^{m_{SU_1}-1} \cdots \sum_{b_N=0}^{m_{SU_1}-1} \Xi\left(SU_1\right) \sum_{a=0}^{\Lambda-1} \frac{(\Lambda-1)!\left(\upsilon_{\max}\right)^a e^{-\Theta_2}}{\lambda_{CU_1} a!\left(\Theta_1\right)^{a+1}} \\ &\times \left(\Delta_{SU_1} + \frac{1}{\upsilon_1\lambda_g}\right)^{-\Lambda+a} \left(\frac{\rho_{CU}}{\rho_{SU_1}}\right)^a e^{\frac{\Theta_1}{\rho_{CU}}} \Gamma\left(a+1, \frac{\Theta_1}{\rho_{CU}}\right).\end{aligned} \tag{7.76}$$

Proof: See Appendix 7.9.1 (pp. 91).

Lemma 2: The closed-form expression to compute Ψ_2 can be expressed as

$$\Psi_2 = 1 - A_1 \times A_2. \tag{7.77}$$

Because the computations of A_1 and A_2 are complicated, we present these details in the appendix.

Proof: See Appendix 7.9.2 (pp. 92).

7.7.3 Outage Probability of U_2

Similarly, the OP of U_2 is given as [90]

$$P_{out,2} = \bar{\Psi}_1 \times \bar{\Psi}_2, \tag{7.78}$$

where

$$\bar{\Psi}_1 = 1 - \Pr\left(\gamma_{SU_2}^{x_2} > \varphi_2\right) \tag{7.79}$$

and

$$\bar{\Psi}_2 = 1 - \Pr\left(\gamma_{SR}^{x_2} > \varphi_2, \gamma_{SR}^{x_1} > \varphi_1\right) \Pr\left(\gamma_{RU_2}^{x_2} > \varphi_2\right). \tag{7.80}$$

Lemma 3: The closed-form expression of the outage probability, denoted by $\bar{\Psi}_1$, is given as

$$\begin{aligned}\bar{\Psi}_1 = 1 - &\sum_{b_1=0}^{m_{SU_2}-1} \cdots \sum_{b_N=0}^{m_{SU_2}-1} \frac{\Xi\left(SU_2\right)\left(\rho_{CU}\upsilon_2\right)^a e^{-\frac{\Delta_{SU_2}\upsilon_2}{\rho_{SU_2}}}}{\left(\rho_{SU_2}\right)^a \lambda_{CU_2}\left(\Delta_{SU_2}\right)^{\Lambda-a}} \\ &\times \sum_{a=0}^{\Lambda-1} \frac{(\Lambda-1)!}{a!}\Gamma\left(a+1, \frac{1}{\lambda_{CU_2}\rho_{CU}} + \frac{\Delta_{SU_2}\rho_{CU}\upsilon_2}{\rho_{SU_2}\rho_{CU}}\right) \\ &\times \left(\frac{1}{\lambda_{CU_2}} + \frac{\Delta_{SU_2}\rho_{CU}\upsilon_2}{\rho_{SU_2}}\right)^{-a-1} e^{\frac{1}{\lambda_{CU_2}\rho_{CU}} + \frac{\Delta_{SU_2}\rho_{CU}\upsilon_2}{\rho_{SU_2}\rho_{CU}}}.\end{aligned} \tag{7.81}$$

Proof: From the result from (7.50), we can rewrite (7.81) as

$$\begin{aligned}\bar{\Psi}_1 &= 1 - \Pr\left(\beta_{SU_2} > \upsilon_2\left(\rho_{CU}\left|h_{CU_2}\right|^2 + 1\right)\right) \\ &= 1 - \int_0^{\infty} f_{\left|h_{CU_2}\right|^2}(y) \int_{\upsilon_2(\rho_{CU}y+1)}^{\infty} f_{\beta_{SU_2}}(x)dxdy.\end{aligned} \tag{7.82}$$

Then, we calculate

$$\begin{aligned}\bar{\Psi}_1 = 1 - &\sum_{b_1=0}^{m_{SU_2}-1} \cdots \sum_{b_N=0}^{m_{SU_2}-1} \frac{\Xi\left(SU_2\right)}{\left(\rho_{SU_2}\right)^{\Lambda}\lambda_{CU_2}} \\ &\int_0^{\infty} e^{-\frac{y}{\lambda_{CU_2}}} \int_{\upsilon_2(\rho_{CU}y+1)}^{\infty} x^{\Lambda-1} e^{-\frac{\Delta_{SU_2}}{\rho_{SU_2}}x}.dxdy.\end{aligned} \tag{7.83}$$

$\bar{\Psi}_1$ can then be expressed as

$$\begin{aligned}\bar{\Psi}_1 = 1 - &\sum_{b_1=0}^{m_{SU_2}-1} \cdots \sum_{b_N=0}^{m_{SU_2}-1} \frac{\Xi\left(SU_2\right) e^{-\frac{\Delta_{SU_2}\upsilon_2}{\rho_{SU_2}}}}{\left(\rho_{SU_2}\right)^a \lambda_{CU_2}} \\ &\times \sum_{a=0}^{\Lambda-1} \frac{(\Lambda-1)!\left(\rho_{CU}\upsilon_2\right)^a}{a!\left(\Delta_{SU_2}\right)^{\Lambda-a}} \\ &\times \int_0^{\infty} \left(y + \frac{1}{\rho_{CU}}\right)^a e^{-\left(\frac{1}{\lambda_{CU_2}} + \frac{\Delta_{SU_2}\rho_{CU}\upsilon_2}{\rho_{SU_2}}\right)y} dy.\end{aligned} \tag{7.84}$$

We thus similarly obtain $\bar{\Psi}_1$. This ends the proof.

Lemma 4: The term $A_3 = \Pr\left(\gamma_{RU_2}^{x_2} > \varphi_2\right)$ can be expressed as

$$\begin{aligned} A_3 = & \sum_{b=0}^{\infty}\sum_{c=0}^{b} \frac{(K_2)^b \rho_{RU_2} e^{-K_2} \left(\tilde{\theta}_2 \varpi_2 \rho_{CU} \lambda_{CU_2}\right)^c}{b!c! \left(\tilde{\theta}_2 \varpi_2 \lambda_{CU_2} \rho_{CU} + \rho_{RU_2}\right)^{c+1}} \\ & \times e^{-\frac{\tilde{\theta}_2 \varpi_2}{\rho_{RU_2}} + \frac{\tilde{\theta}_2 \varpi_2 \lambda_{CU_2} \rho_{CU} + \rho_{RU_2}}{\lambda_{CU_2} \rho_{CU} \rho_{RU_2}}} \\ & \times \Gamma\left(c+1, \frac{\tilde{\theta}_2 \varpi_2 \lambda_{CU_2} \rho_{CU} + \rho_{RU_2}}{\lambda_{CU_2} \rho_{CU} \rho_{RU_2}}\right). \end{aligned} \tag{7.85}$$

Proof: Applying (7.56), A_3 can be expressed as

$$\begin{aligned} A_3 &= \Pr\left(\beta_{RU_2} > \tilde{\theta}_2 \left(\rho_{CU} \left|h_{CU_2}\right|^2 + 1\right)\right) \\ &= \int_0^{\infty} \int_{\tilde{\theta}_2(\rho_{CU} x + 1)}^{\infty} f_{\left|h_{CU_2}\right|^2}(x) f_{\beta_{RU_2}}(y) dy dx. \end{aligned} \tag{7.86}$$

Simplified, (7.86) can be expressed as

$$\begin{aligned} A_3 = & \sum_{b=0}^{\infty}\sum_{c=0}^{b} \frac{(K_2)^b e^{-K_2}}{b!c! \lambda_{CU_2}} e^{-\frac{\varpi_1 \tilde{\theta}_2}{\rho_{RU_1}}} \left(\frac{\tilde{\theta}_2 \rho_{CU} \varpi_2}{\rho_{RU_2}}\right)^c \\ & \times \int_0^{\infty} \left(x + \frac{1}{\rho_{CU}}\right)^c e^{-\frac{\varpi_2 \tilde{\theta}_2 \rho_{CU}}{\rho_{RU_2}} x - \frac{x}{\lambda_{CU_2}}} dy dx. \end{aligned} \tag{7.87}$$

We thus obtain (7.59) similarly to (7.105). This ends the proof.

Finally, by combining (7.74) and (7.85), the closed-form expression of the OP, i.e., $\bar{\Psi}_2$, is expressed by

$$\bar{\Psi}_2 = 1 - A_1 \times A_3. \tag{7.88}$$

Remark 2: *The expressions for OP depend on various system parameters determined from the constraints encountered in practical scenarios. We can observe in the relevant OP equations, for example* (7.72) *and* (7.78)*, the effects due to the number of transmit antennas at the satellite, the satellite link configuration, the satellite transmit power, the power allocation factors* a_1 *and* a_2*, and the levels of RHI. Applying numerical simulations, we verify these effects in the system performance metrics.*

7.7.4 Diversity order

To provide more insight, we need to derive an asymptotic expression of the OP at a high SNR $\rho = \rho_S = \rho_R \to \infty$. The diversity order of the terrestrial user can be given by [72]

$$d = -\lim_{\rho \to \infty} \frac{\log\left(P_{out}^{\infty}(\rho)\right)}{\log \rho}, \tag{7.89}$$

where P_{out}^{∞} denotes the asymptotic OP.

Then, by applying a Maclaurin series, we have $e^{-x} \simeq (1-x)$. We can also write (7.71) in the case of a high SNR as

$$P_{out,1}^{\infty} = \Psi_1^{\infty} \times \Psi_2^{\infty}, \tag{7.90}$$

where Ψ_1^{∞} is expressed as

$$\begin{aligned}
\Psi_1^{\infty} = 1 - & \sum_{b_1=0}^{m_{SU_1}-1} \cdots \sum_{b_N=0}^{m_{SU_1}-1} \sum_{a=0}^{\Lambda-1} \sum_{b=0}^{a} \frac{\Xi\left(SU_1\right)\Gamma\left(\Lambda\right)}{b!\lambda_{CU_1}\left(\Delta_{SU_1}\right)^{\Lambda-a}} \\
& \times \left(1 - \frac{\Delta_{SU_1}\theta_{\max}}{\rho_{SU_1}}\right)\left(\frac{1}{\lambda_{CU_1}} + \frac{\Delta_{SU_1}\theta_{\max}\rho_{CU}}{\rho_{SU_1}}\right)^{-a-1} \\
& \times \left(\frac{\theta_{\max}}{\rho_{CU}\rho_{SU_1}}\right)^{a}\left(\frac{1}{\lambda_{CU_1}\rho_{CU}} + \frac{\Delta_{SU_1}\theta_{\max}}{\rho_{SU_1}}\right)^{b} \\
& + \sum_{b_1=0}^{m_{SU_1}-1} \cdots \sum_{b_N=0}^{m_{SU_1}-1} \sum_{a=0}^{\Lambda-1} \sum_{b=0}^{a} \frac{\Xi\left(SU_1\right)\Gamma\left(\Lambda\right)\left(1-\Theta_2\right)}{\lambda_{CU_1} b!\left(\Theta_1\right)^{a+1}} \\
& \times \left(\frac{\upsilon_{\max}\rho_{CU}}{\rho_{SU_1}}\right)^{a}\left(\frac{\Theta_1}{\rho_{CU}}\right)^{b}\left(\Delta_{SU_1} + \frac{1}{\upsilon_1\lambda_g}\right)^{-\Lambda+a}.
\end{aligned} \tag{7.91}$$

Then, Ψ_1^{∞} is given by

$$\Psi_1^{\infty} = 1 - A_1^{\infty} \times A_2^{\infty}, \tag{7.92}$$

where

$$\begin{aligned}
A_1^{\infty} = & \sum_{b_1=0}^{m_{SR}-1} \cdots \sum_{b_N=0}^{m_{SR}-1} \Xi\left(SR\right) \sum_{n=0}^{\Lambda-1} \frac{(\Lambda-1)!}{n!\left(\Delta_{SR}\right)^{\Lambda}} \\
& \times \left(1 - \frac{\Delta_{SR}\theta_{\max}}{\rho_{SR}}\right)\left(\frac{\Delta_{SR}\theta_{\max}}{\rho_{SR}}\right)^{n} \\
& - \sum_{b_1=0}^{m_{SR}-1} \cdots \sum_{b_N=0}^{m_{SR}-1} \Xi\left(SR\right) \sum_{n=0}^{\Lambda-1} \frac{(\Lambda-1)!}{n!} \\
& \times \left(\frac{\theta_1\lambda_g}{\Delta_{SR}\lambda_g\theta_1 + 1}\right)^{\Lambda-n}\left(\frac{\theta_{\max}}{\rho_{SR}}\right)^{n} \\
& \times \left(1 - \frac{\left(\Delta_{SR}\lambda_g\theta_1 + 1\right)\theta_{\max}}{\theta_1\rho_{SR}\lambda_g} + \frac{1}{\rho_{SR}\lambda_g}\right),
\end{aligned} \tag{7.93}$$

and

$$
\begin{aligned}
A_2^{\infty} = & \sum_{b=0}^{\infty}\sum_{c=0}^{b}\sum_{d=0}^{c}\frac{\left(K_1\right)^b e^{-K_1}\rho_{RU_1}}{d!b!\lambda_{CU_1}} \\
& \times \frac{\left(\varpi_1\tilde{\theta}_{\max}\rho_{CU}\lambda_{CU_1}\right)^c}{\left(\varpi_1\tilde{\theta}_{\max}\rho_{CU}\lambda_{CU_1}+\rho_{RU_1}\right)^{c+1}} \\
& \times \left(\frac{\varpi_1\tilde{\theta}_{\max}\rho_{CU}\lambda_{CU_1}+\rho_{RU_1}}{\rho_{RU_1}\rho_{CU}\lambda_{CU_1}}\right)^d \left(1-\frac{\varpi_1\tilde{\theta}_{\max}}{\rho_{RU_1}}\right) \\
& - \sum_{b=0}^{\infty}\sum_{c=0}^{b}\sum_{d=0}^{c}\frac{\left(K_1\right)^b\left(\varpi_1\right)^{b+1}e^{-K_1}}{d!c!\lambda_{CU_1}\xi^{c+1}} \\
& \times \left(\frac{\lambda_g\tilde{\theta}_1}{\varpi_1\lambda_g\tilde{\theta}_1+1}\right)^{b-c+1}\left(\frac{\rho_{CU}\tilde{\theta}_{\max}}{\rho_{RU_1}}\right)^c\left(\frac{\xi}{\rho_{CU}}\right)^d \\
& \times \left(1-\frac{\left(\varpi_1\lambda_g\tilde{\theta}_1+1\right)\tilde{\theta}_{\max}}{\lambda_g\tilde{\theta}_1\rho_{RU_1}}+\frac{1}{\lambda_g\rho_{RU_1}}\right).
\end{aligned}
\tag{7.94}
$$

The asymptotic OP for U_2 is thus similarly obtained as

$$
P_{out,2}^{\infty} = \bar{\Psi}_1 \times \bar{\Psi}_2, \tag{7.95}
$$

where $\bar{\Psi}_1$ is given by

$$
\begin{aligned}
\bar{\Psi}_1^{\infty} = & 1 - \sum_{b_1=0}^{m_{SU_2}-1}\cdots\sum_{b_N=0}^{m_{SU_2}-1}\frac{\Xi\left(SU_2\right)\left(\rho_{CU}\upsilon_2\right)^a}{\left(\rho_{SU_2}\right)^a\left(\Delta_{SU_2}\right)^{\Lambda-a}} \\
& \times \sum_{a=0}^{\Lambda-1}\sum_{b=0}^{a}\frac{(\Lambda-1)!}{b!\lambda_{CU_2}}\left(\frac{1}{\lambda_{CU_2}}+\frac{\Delta_{SU_2}\rho_{CU}\upsilon_2}{\rho_{SU_2}}\right)^{-a-1} \\
& \times \left(\frac{1}{\lambda_{CU_2}\rho_{CU}}+\frac{\Delta_{SU_2}\rho_{CU}\upsilon_2}{\rho_{SU_2}\rho_{CU}}\right)^a \\
& \times \left(1+\frac{1}{\lambda_{CU_2}\rho_{CU}}+\frac{\Delta_{SU_2}\rho_{CU}\upsilon_2}{\rho_{SU_2}\rho_{CU}}\right) \\
& \times \left(1-\frac{1}{\lambda_{CU_2}\rho_{CU}}-\frac{\Delta_{SU_2}\rho_{CU}\upsilon_2}{\rho_{SU_2}\rho_{CU}}-\frac{\Delta_{SU_2}\upsilon_2}{\rho_{SU_2}}\right).
\end{aligned}
\tag{7.96}
$$

Then, $\bar{\Psi}_2$ is given by

$$
\bar{\Psi}_2 = 1 - A_1^{\infty} \times A_3^{\infty}, \tag{7.97}
$$

where

$$
\begin{aligned}
A_3^{\infty} = & \sum_{b=0}^{\infty}\sum_{c=0}^{b}\sum_{d=0}^{c}\frac{\left(K_2\right)^b\rho_{RU_2}e^{-K_2}\left(\tilde{\theta}_2\varpi_2\rho_{CU}\lambda_{CU_2}\right)^c}{b!d!\left(\tilde{\theta}_2\varpi_2\lambda_{CU_2}\rho_{CU}+\rho_{RU_2}\right)^{c+1}} \\
& \times \left(1-\frac{\tilde{\theta}_2\varpi_2}{\rho_{RU_2}}\right)\left(\frac{\tilde{\theta}_2\varpi_2\lambda_{CU_2}\rho_{CU}+\rho_{RU_2}}{\lambda_{CU_2}\rho_{CU}\rho_{RU_2}}\right)^d.
\end{aligned}
\tag{7.98}
$$

We may straight forwardly conclude that the diversity orders of users U_1 and U_2 both equal zero.

Table 7.4: Table of Satellite Channel Parameters [81]

Shadowing	b	m	Ω
Average shadowing (AS)	0.251	5	0.279
Heavy shadowing (HS)	0.063	1	0.0007

Table 7.5: Table of Main Simulated Parameters

Monte Carlo simulations	10^6 iterations
Satellite type	GEO
Carrier frequency	$f_c = 2GHz$
Carrier bandwidth	$W = 15Mhz$
Distance from satellite to UAV and satellite to U_i	$d_{SR} = d_{SU_1} = d_{SU_2} = 35786Km$
Receiver noise temperature	$T = 500^oK$
Speed of light	$c = 3{\times}10^8 m/s$
Antenna gain at satellite	$\vartheta_S = 4$dBi
Antenna gain at UAV and U_i	$\vartheta_R = \vartheta_{U_i} = 48$dB
Angular separation	$\phi_R = 0.8^o$
3dB beamwidth	$\phi_{R3dB} = 0.3^o$
Power allocation	$a_1 = 0.25$ and $a_2 = 0.75$
Path loss exponent	$\chi = 2$
Level of hardware impairment	$\kappa^2 = \kappa^2_{SU_i} = \kappa^2_R = \kappa^2_i = 0.01$
Altitude	$h = 10$m
Target rate	$R_1 = 0.2$ (BPCU) and $R_2 = 0.4$ (BPCU)
Rician factor	$K_1 = K_2 = 5$
Average fading power	$\Omega_1 = \Omega_2 = 1$
Distance	$d_1 = 5$m and $d_2 = 10$m

In this section, we present numerical simulations to verify the derived expressions. The Shadowed-Rician fading parameters are listed in Table 7.4, and the parameters for the numerical results are summarized in Table 7.5, where BPCU refers to *bit per channel use*. We also set $\rho = \rho_S = \rho_R$, with the exception of the specific case mentioned later.

Figure 7.11 depicts the outage performance of the UAV-based satellite system against the transmit SNR at the satellite ρ. From the illustration, we can see that the OP decreases for two users as the value of ρ increases. A clear observation is that the performance gap between two users is just as large at the middle range of the SNR, i.e., ρ varies from 40 to 50 (dB). This is significant because we can see that the Monte-Carlo and analytical simulations match very closely, confirming the corrections in the related expressions for OP. The asymptotic curves match with exact curves in the high SNR region, verifying the validity of the corresponding expressions. The advantage of the proposed system is clear in a comparison of its performance with an OMA-assisted HSTRS system. By adjusting the PA factors (a_1, and a_2), the system can also produce different performance for two users, however, in the high SNR region, the system performance does not depend on a_1 and a_2. The configuration of AS mode is superior to that of HS, and outage performance for both users therefore improves when the satellite links are subject to AS rather than HS.

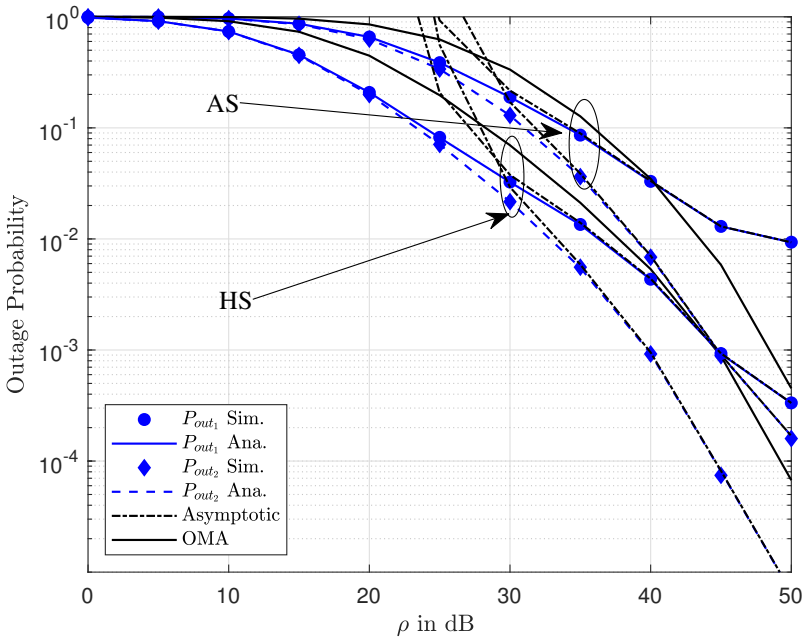

Figure 7.11: Outage probability versus ρ for different values of the satellite link, where $N = 1$, $\rho_{CU} = 15$dB, and $\lambda_g = 0.01$.

Figure 7.12 shows the improvement of outage performance at high SNR. When we increase ρ, the corresponding outage performance of two users improves significantly, especially if we raise the number of transmit antennas at the satellite from $N = 1$ to $N = 2$ or $N = 3$. For $N = 3$, we obtained better results. A greater number of antennas equipped at the satellite improves the

channel gain, which results in better performance, especially in the performance gap between two users, similar to the results shown in Figure 7.12. However, examining the entire range of ρ in the cases $N = 1$ and $N = 2$, saturation is attained much more quickly than with $N = 3$, the reason being that a greater number of antennas significantly improves the outage performance.

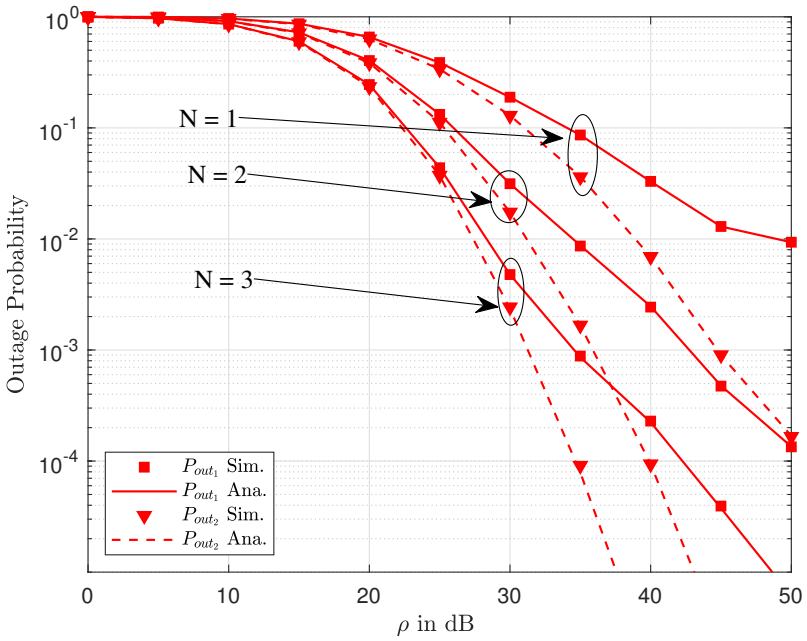

Figure 7.12: Outage probability versus ρ for different values of N, where $\rho_{CU} = 15$dB, $\lambda_g = 0.01$, and the satellite link is set to HS.

Figure 7.13 reveals similar results to the simulations in Figures 7.11 and 7.12 and indicates the trends of outage behavior for two users under perfect SIC and ipSIC schemes. When we raise ρ from 40 to 60 dB, the outage performance for perfect SIC is superior to ipSIC, the main reason being that interference from ipSIC limits the SINR, and the corresponding system performance of secondary users is thus reduced. Two levels of the ipSIC case confirm that $\lambda_g = 0.01$ is superior to $\lambda_g = 0.1$.

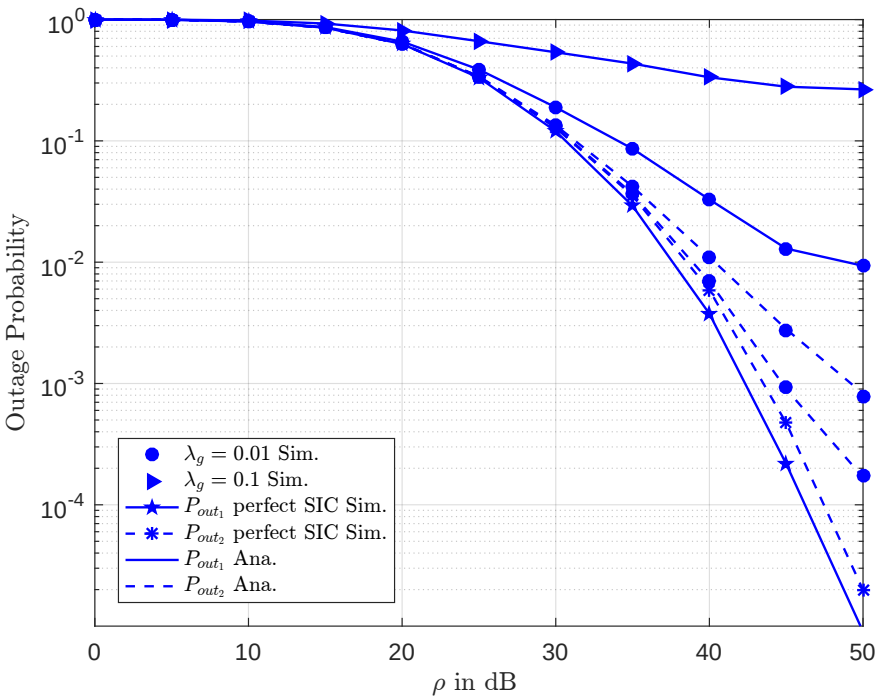

Figure 7.13: Outage probability versus ρ for different values of λ_g, where $N = 1$, $\rho_{CU} = 15$dB, and the satellite link is set to HS.

As with the effect caused by ipSIC, the interference channel of the CUE has an effect on the outage performance of two users (Figure 7.14). Here, $\rho_{CU} = 1$ dB produces the corresponding OP as the best result of the three considered cases.

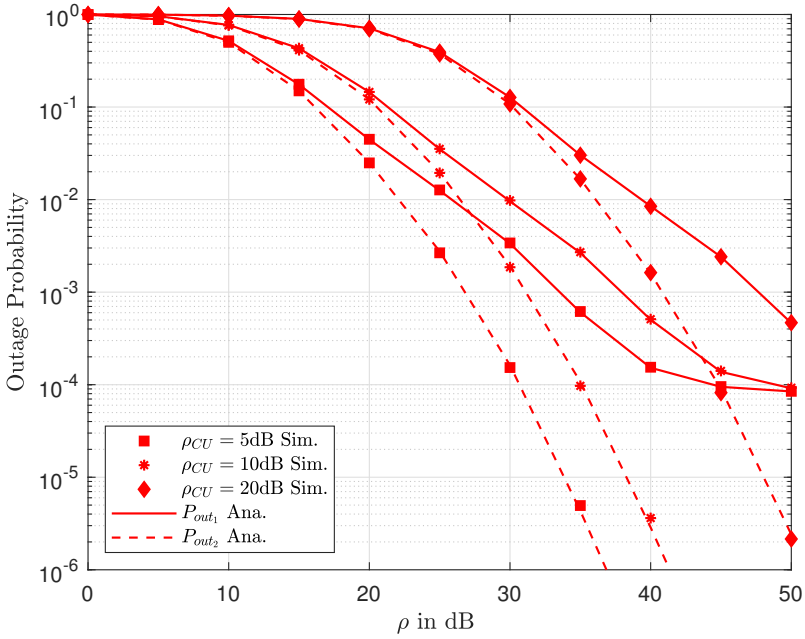

Figure 7.14: Outage probability versus ρ for different values of ρ_{CU}, where $N = 2$, $\lambda_g = 0.01$, and the satellite link is set to HS.

Figure 7.15 shows that when the UAV flies at a greater height, it leads to worse quality in the ground links and consequently worse OP for the two users. This can be explained by the distances between the UAV and ground users computed from (7.46), which depends on the height h. This demonstrates the advantage of the UAV in determining expected system performance. We can achieve the desired performance simply by controlling the height of the UAV.

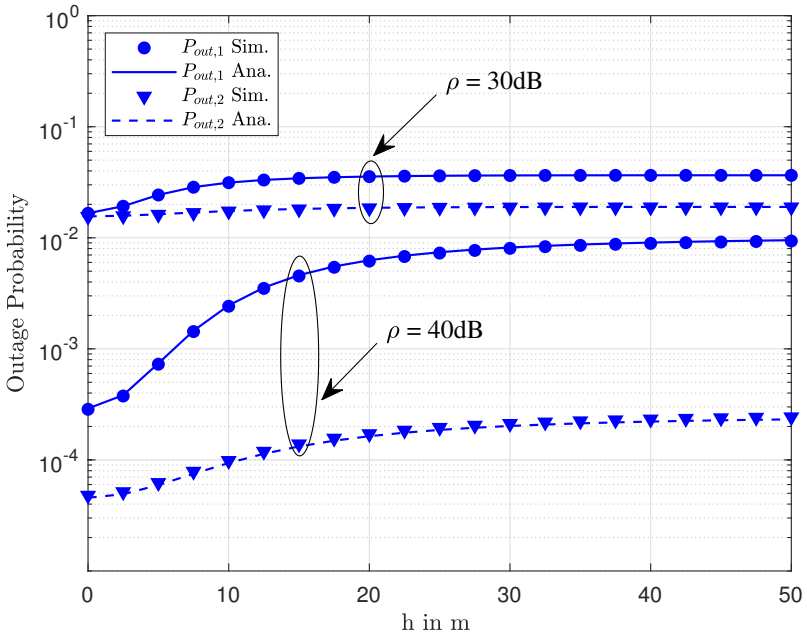

Figure 7.15: Outage probability versus h for different values of ρ, where $N = 2$, $\rho_{CU} = 15$dB, $\lambda_g = 0.01$, and the satellite link is set to HS.

Figure 7.16 shows that the outage performance can be enhanced significantly under Rician channel conditions. The configuration $K_1 = K_2 = 10$ indicates the best case associated with the considered values of the links from the UAV to the ground users, the reason being that the OP in (7.86), (7.88) contains values of $K_1 = K_2$. The quality of the ground channels plays an important role in altering the OP values.

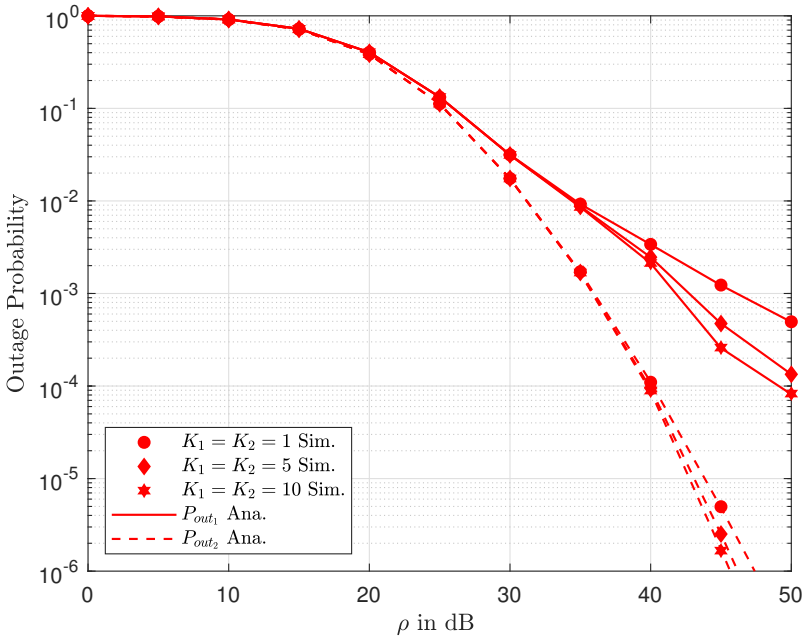

Figure 7.16: Outage probability versus ρ for different values of $K_1 = K_2$, where $N = 2$, $\rho_{CU} =$ 15dB, $\lambda_g = 0.01$, and the satellite link is set to HS.

Figure 7.17 shows the effect of hardware impairment level κ^2 with respect to the OP for two users. It is easy to conclude that the lower level of hardware impairment exhibits the best outage performance for two users in the considered system. We note that $\kappa^2 = 0.5$ is a serious degradation in terms of outage for two users. Therefore, a high requirement in perfect hardware design is crucial for maintaining system performance at a desired acceptable quality.

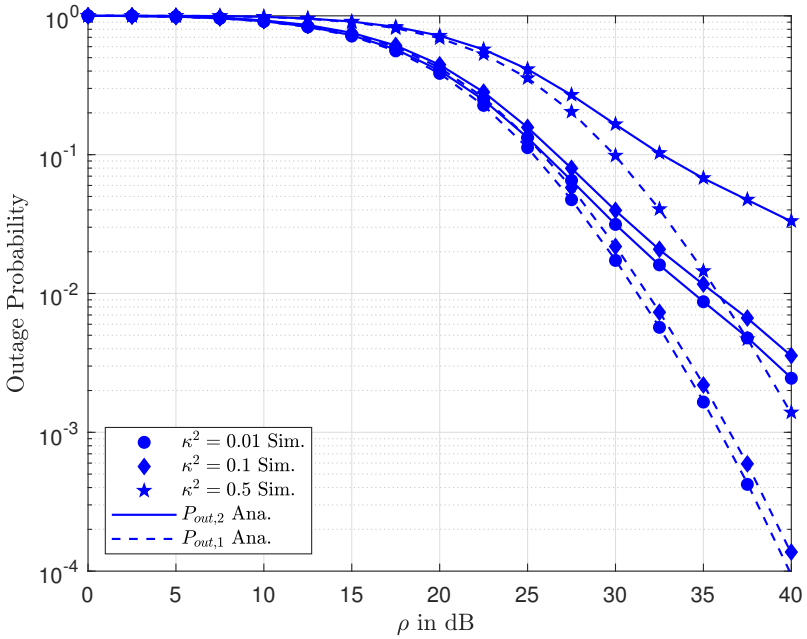

Figure 7.17: Outage probability versus ρ for different values of κ^2, where $N = 2$, $\rho_{CU} = 15$dB, $\lambda_g = 0.01$, and the satellite link is set to HS.

7.8 Conclusion

We investigated the OP performance of a UAV-assisted HSTRS with a multi-antenna satellite and NOMA scheme containing hardware impairments and imperfect SIC. To demonstrate the main system performance metric, we derived novel and closed-form expressions of the OP. The results showed that the detrimental effects of interference from a non-NOMA user and the deterioration of the OP due to imperfect SIC could be mitigated by increasing the number of antennas at the satellite and thus improve system performance. The numerical simulations demonstrated the effect of various key system/channel parameters on the OP and provided a guide for the joint deployment of a UAV and multi-antenna satellite in such systems. In future work, it would be interesting to consider multiple antennas at the UAV or even the ground users, providing a more general scenario for study.

7.9 Appendix

7.9.1 Appendix A

By substituting (7.54) and (7.55), we write the term Ψ_1 as

$$\begin{aligned}
\Psi_1 &= 1 - \Pr\left(\frac{\beta_{SU_1} a_2}{\beta_{SU_1} a_1 + \beta_{SU_1}\kappa_{SU_1}^2 + \rho_{CU}\left|h_{CU_1}\right|^2 + 1} > \varphi_2,\right. \\
&\left.\frac{\beta_{SU_1} a_2}{\beta_{SU_1} a_1 + \beta_{SU_1}\kappa_{SU_1}^2 + \rho_{CU}\left|h_{CU_1}\right|^2 + 1} > \varphi_1\right) \\
&= 1 - \Pr\left(\beta_{SU_1} > \theta_{\max}\left(\rho_{CU}\left|h_{CU_1}\right|^2 + 1\right), |g|^2 < \frac{\beta_{SU_1}}{\theta_1 \rho_{SU_1}} - \frac{\rho_{CU}\left|h_{CU_1}\right|^2 + 1}{\rho_{SU_1}}\right) \\
&= 1 - \underbrace{\int_0^{\infty} f_{|h_{CU_1}|^2}(x) \int_{\theta_{\max}(\rho_{CU}x+1)}^{\infty} f_{\beta_{SU_1}}(y) dy dx}_{I_1} \\
&+ \underbrace{\int_0^{\infty} f_{|h_{CU_1}|^2}(x) \int_{\upsilon_{\max}(\rho_{CU}x+1)}^{\infty} f_{\beta_{SU_1}}(y) \int_{\frac{y}{\upsilon_1\rho_{SU_1}} - \frac{\rho_{CU}x+1}{\rho_{SU_1}}}^{\infty} f_{|g|^2}(z) dz dy dx}_{I_2}.
\end{aligned} \tag{7.99}$$

where $\upsilon_1 = \frac{\varphi_1}{a_1 + \varphi_1\kappa_{SU_1}^2}$, $\upsilon_2 = \frac{\varphi_2}{a_2 - \varphi_2\left(a_1 + \kappa_{SU_i}^2\right)}$ and $\upsilon_{\max} = \max(\upsilon_1, \upsilon_2)$.

Based on (7.64), the term I_1 in (7.99) can be expressed as

$$\begin{aligned}
I_1 = &\sum_{b_1=0}^{m_{SU_1}-1} \cdots \sum_{b_N=0}^{m_{SU_1}-1} \frac{\Xi(SU_1)}{(\rho_{SU_1})^{\Lambda}\lambda_{CU_1}} \\
&\times \int_0^{\infty} e^{-\frac{x}{\lambda_{CU_1}}} \int_{\upsilon_{\max}(\rho_{CU}x+1)}^{\infty} y^{\Lambda-1} e^{-\frac{\Delta_{SU_1}}{\rho_{SU_1}}y} dy dx.
\end{aligned} \tag{7.100}$$

Using [79, Eq. (3.351.2)], we can express I_1 as

$$\begin{aligned}
I_1 = &\sum_{b_1=0}^{m_{SU_1}-1} \cdots \sum_{b_N=0}^{m_{SU_1}-1} \frac{\Xi(SU_1) e^{-\frac{\Delta_{SU_1}\upsilon_{\max}}{\rho_{SU_1}}}}{\lambda_{CU_1}(\Delta_{SU_1})^{\Lambda-a}} \\
&\times \sum_{a=0}^{\Lambda-1} \frac{(\Lambda-1)!}{a!}\left(\frac{\upsilon_{\max}\rho_{CU}}{\rho_{SU_1}}\right)^a \\
&\times \int_0^{\infty}\left(x + \frac{1}{\rho_{CU}}\right)^a e^{-\left(\frac{1}{\lambda_{CU_1}} + \frac{\Delta_{SU_1}\upsilon_{\max}\rho_{CU}}{\rho_{SU_1}}\right)x} dx.
\end{aligned} \tag{7.101}$$

Then, using [79, Eq. (3.382. 4)] we rewrite I_1, as expected.

The term I_2 is thus expressed as

$$\begin{aligned} I_2 &= \sum_{b_1=0}^{m_{SU_1}-1} \cdots \sum_{b_N=0}^{m_{SU_1}-1} \frac{\Xi\left(SU_1\right) e^{\frac{1}{\rho_{SU_1}\lambda_g}}}{\left(\rho_{SU_1}\right)^{\Lambda}\lambda_{CU_1}} \int_0^{\infty} e^{-\frac{x}{\lambda_{CU_1}}+\frac{\rho_{CU}}{\rho_{SU_1}\lambda_g}x} \\ &\times \int_{\upsilon_{\max}(\rho_{CU}x+1)}^{\infty} y^{\Lambda-1} e^{-\frac{\Delta_{SU_1}}{\rho_{SU_1}}y} e^{-\frac{y}{\upsilon_1\rho_{SU_1}\lambda_g}} dydx \\ &= \sum_{b_1=0}^{m_{SU_1}-1} \cdots \sum_{b_N=0}^{m_{SU_1}-1} \Xi\left(SU_1\right) \sum_{a=0}^{\Lambda-1} \frac{(\Lambda-1)!\left(\upsilon_{\max}\right)^a e^{-\Theta_2}}{\lambda_{CU_1} a!\left(\rho_{SU_1}\right)^a} \\ &\times \left(\Delta_{SU_1}+\frac{1}{\upsilon_1\lambda_g}\right)^{-\Lambda+a} \int_0^{\infty} \left(\rho_{CU}x+1\right)^a e^{-\Theta_1 x} dx, \end{aligned} \tag{7.102}$$

where $\Theta_1 = \frac{1}{\lambda_{CU_1}} - \frac{\rho_{CU}}{\rho_{SU_1}\lambda_g} + \frac{\Delta_{SU_1}\upsilon_{\max}\rho_{CU}}{\rho_{SU_1}} + \frac{\upsilon_{\max}\rho_{CU}}{\upsilon_1\rho_{SU_1}\lambda_g}$ and $\Theta_2 = \frac{\Delta_{SU_1}\upsilon_{\max}}{\rho_{SU_1}} + \frac{\upsilon_{\max}}{\upsilon_1\rho_{SU_1}\lambda_g} - \frac{1}{\rho_{SU_1}\lambda_g}$.

Based on [79, Eq. (3.382.4)], we obtain I_2 as (7.76).

Substituting (7.100) and (7.76) into (7.99), we obtain the final result.

7.9.2 Appendix B

First, we denote $A_1 = \Pr\left(\gamma_{SR}^{x_2} > \varphi_2, \gamma_{SR}^{x_1} > \varphi_1\right)$ and $A_2 = \Pr\left(\gamma_{SR}^{x_2} > \varphi_2, \gamma_{SR}^{x_1} > \varphi_1\right)$. Substituting (7.53) and (7.54) into A_1, we have

$$\begin{aligned} A_1 &= \Pr\left(\frac{\beta_{SR}a_2}{\beta_{SR}a_1+\beta_{SR}\kappa_R^2+1} > \varphi_2, \frac{\beta_{SR}a_1}{\rho_{SR}\left|g\right|^2+\beta_{SR}\kappa_R^2+1} > \varphi_1\right) \\ &= \Pr\left(\beta_{SR} > \theta_{\max}, \left|g\right|^2 < \frac{\beta_{SR}-\theta_1}{\theta_1\rho_{SR}}\right) \\ &= \underbrace{\int_{\theta_{\max}}^{\infty} f_{\beta_{SR}}(x)dx}_{A_{1,1}} - \underbrace{\frac{1}{\lambda_g}\int_{\theta_{\max}}^{\infty} f_{\beta_{SR}}(x)e^{-\frac{x-\theta_1}{\theta_1\rho_{SR}}}dx}_{A_{1,2}}, \end{aligned} \tag{7.103}$$

where $\theta_1 = \frac{\varphi_1}{a_1-\varphi_1\kappa_R^2}$, $\theta_2 = \frac{\varphi_2}{a_2-\varphi_2\left(a_1+\kappa_R^2\right)}$, $\theta_{\max} = \max\left(\theta_1, \theta_2\right)$.

Based on (7.64) and [79, Eq. (3.351.2)], we obtain the term $A_{1,1}$ from

$$A_{1,1} = \sum_{b_1=0}^{m_{SR}-1} \cdots \sum_{b_N=0}^{m_{SR}-1} \frac{\Xi\left(SR\right)}{\left(\Delta_{SR}\right)^{\Lambda}} \Gamma\left(\Lambda, \frac{\Delta_{SR}\theta_{\max}}{\rho_{SR}}\right). \tag{7.104}$$

Applying (7.64), we can express $A_{1,2}$ as

$$\begin{aligned} A_{1,2} &= \sum_{b_1=0}^{m_{SR}-1} \cdots \sum_{b_N=0}^{m_{SR}-1} \frac{\Xi\left(SR\right)}{\left(\rho_{SR}\right)^{\Lambda}} e^{\frac{1}{\rho_{SR}\lambda_g}} \\ &\times \int_{\theta_{\max}}^{\infty} x^{\Lambda-1} e^{-\left(\frac{\Delta_{SR}}{\rho_{SR}}+\frac{1}{\theta_1\rho_{SR}\lambda_g}\right)x} dx. \end{aligned} \tag{7.105}$$

Similarly, we obtain $A_{1,2}$ from

$$\begin{aligned} A_{1,2} = & \sum_{b_1=0}^{m_{SR}-1} \cdots \sum_{b_N=0}^{m_{SR}-1} \Xi\left(SR\right) \left(\frac{\theta_1 \lambda_g}{\Delta_{SR} \lambda_g \theta_1 + 1}\right)^{\Lambda} \\ & \times e^{\frac{1}{\rho_{SR} \lambda_g}} \Gamma\left(\Lambda, \frac{\left(\Delta_{SR} \lambda_g \theta_1 + 1\right) \theta_{\max}}{\theta_1 \rho_{SR} \lambda_g}\right). \end{aligned} \tag{7.106}$$

Applying (7.57) and (7.58), A_2 can be calculated as

$$\begin{aligned} A_2 = & \Pr\left\{\beta_{RU_1} > \tilde{\theta}_{\max}\left(\rho_{CU}\left|h_{CU_1}\right|^2 + 1\right), |g|^2 < \frac{\beta_{RU_1}}{\tilde{\theta}_1 \rho_{RU_1}} - \frac{\left(\rho_{CU}\left|h_{CU_1}\right|^2 + 1\right)}{\rho_{RU_1}}\right\} \\ = & \underbrace{\int_0^{\infty} f_{\left|h_{CU_1}\right|^2}(x) \int_{\tilde{\theta}_{\max}(\rho_{CU} x + 1)}^{\infty} f_{\beta_{RU_1}}(y) dy dx}_{A_{2,1}} \\ & - \underbrace{\int_0^{\infty} f_{\left|h_{CU_1}\right|^2}(x) \int_{\tilde{\theta}_{\max}(\rho_{CU} x + 1)}^{\infty} f_{\beta_{RU_1}}(y) \int_{\frac{y}{\tilde{\theta}_1 \rho_{RU_1}} - \frac{(\rho_{CU} x + 1)}{\rho_{RU_1}}}^{\infty} f_g(z) dz dy dx}_{A_{2,2}}. \end{aligned} \tag{7.107}$$

Based on (7.68), $A_{2,1}$ is rewritten as

$$\begin{aligned} A_{2,1} = & \sum_{b=0}^{\infty} \sum_{c=0}^{b} \frac{\left(K_1\right)^b e^{-K_1}}{b! c! \lambda_{CU_1}} \left(\frac{\tilde{\theta}_{\max} \rho_{CU} \varpi_1}{\rho_{RU_1}}\right)^c e^{-\frac{\varpi_1 \tilde{\theta}_{\max}}{\rho_{RU_1}}} \\ & \times \int_0^{\infty} \left(x + \frac{1}{\rho_{CU}}\right)^c e^{-\frac{\varpi_1 \tilde{\theta}_{\max} \rho_{CU} \lambda_{CU_1} + \rho_{RU_1}}{\rho_{RU_1} \lambda_{CU_1}} x} dx. \end{aligned} \tag{7.108}$$

Based on [79, Eq. (3.382.4)], we obtain $A_{2,1}$ from

$$\begin{aligned} A_{2,1} = & \sum_{b=0}^{\infty} \sum_{c=0}^{b} \frac{\left(K_1\right)^b e^{-K_1} \rho_{RU_1} \left(\varpi_1 \tilde{\theta}_{\max} \rho_{CU} \lambda_{CU_1}\right)^c}{c! b! \lambda_{CU_1}} \\ & \times \frac{e^{-\frac{\varpi_1 \tilde{\theta}_{\max}}{\rho_{RU_1}} + \frac{\varpi_1 \tilde{\theta}_{\max} \rho_{CU} \lambda_{CU_1} + \rho_{RU_1}}{\rho_{RU_1} \rho_{CU} \lambda_{CU_1}}}}{\left(\varpi_1 \tilde{\theta}_{\max} \rho_{CU} \lambda_{CU_1} + \rho_{RU_1}\right)^{c+1}} \\ & \times \Gamma\left(c + 1, \frac{\varpi_1 \tilde{\theta}_{\max} \rho_{CU} \lambda_{CU_1} + \rho_{RU_1}}{\rho_{RU_1} \rho_{CU} \lambda_{CU_1}}\right). \end{aligned} \tag{7.109}$$

We then obtain $A_{2,2}$ from

$$\begin{aligned} A_{2,2} &= \sum_{b=0}^{\infty} \frac{(K_1)^b e^{-K_1}}{(b!)^2 \lambda_{CU_1}} \left(\frac{\varpi_1}{\rho_{RU_1}}\right)^{b+1} e^{\frac{1}{\lambda_g \rho_{RU_1}}} \\ &\times \int_0^{\infty} e^{-\left(\frac{1}{\lambda_{CU_1}} - \frac{\rho_{CU}}{\lambda_g \tilde{\theta}_1 \rho_{RU_1}}\right)x} \\ &\times \int_{\tilde{\theta}_{\max}(\rho_{CU}x+1)}^{\infty} y^b e^{-\left(\frac{\varpi_1}{\rho_{RU_1}} + \frac{1}{\lambda_g \tilde{\theta}_1 \rho_{RU_1}}\right)y} dy dx. \end{aligned} \tag{7.110}$$

We apply a computation similar to (7.109) and express $A_{2,2}$ as

$$\begin{aligned} A_{2,2} &= \sum_{b=0}^{\infty} \sum_{c=0}^{b} \frac{(K_1)^b (\varpi_1)^{b+1} e^{-K_1}}{b! c! \lambda_{CU_1} \xi^{c+1}} \\ &\times \left(\frac{\rho_{CU}\tilde{\theta}_{\max}}{\rho_{RU_1}}\right)^c \left(\frac{\lambda_g \tilde{\theta}_1}{\varpi_1 \lambda_g \tilde{\theta}_1 + 1}\right)^{b-c+1} \\ &\times e^{\frac{\xi}{\rho_{CU}} + \frac{1}{\lambda_g \rho_{RU_1}} - \frac{(\varpi_1 \lambda_g \tilde{\theta}_1 + 1)\tilde{\theta}_{\max}}{\lambda_g \tilde{\theta}_1 \rho_{RU_1}}} \Gamma\left(c+1, \frac{\xi}{\rho_{CU}}\right). \end{aligned} \tag{7.111}$$

Based on (7.104), (7.106), (7.109) and (7.111), we obtain Ψ_2 .

Chapter 8:

Summary

THE proposed three main aims achieved the results as following.
In the first aim (Chapter 5 - Part I), I examined a next generation cellular wireless network adopted emerging NOMA technique and investigated the efficiency of multiple antennae equipped at the BS to serve and enhance the OP of multiple NOMA end-users. We introduced a power distribution model to NOMA users who joined direct connection and relay connection to improve QoS. We determined the SNR to discover separate signals for each user and derived the novel exact OP expressions. We also compared the proposed system's performance with a similar system which used the OMA technique. Further, I extended the previous model (Chapter 5 - Part II), where the AP was equipped with multi antennas and the relay could EH from a power beacon. System improvement could be achieved. The performance gap between two users was evaluated over a Rayleigh fading channels model. Then, I compared NOMA scheme to the traditional scheme, i.e., the OMA technique. The achieved results plotted that the proposed model adopted NOMA technique could significantly achieve better performance comparing to the previous models adopted OMA technique.

In the second aim, we investigated the performance of the PLS for next generation cellular wireless networks which integrated emerging techniques such as FD, NOMA, multiple antennas, and RS techniques. I examined two novel PLS schemes:

- In the first model, the SOP performance of the CR network, which adopted NOMA in the down-link scenario, will be derived. The MISO architecture with TAS strategy will also be given special consideration in this model. Further, we exploited the optimal PA factor to optimize SOP.

- In the second model, we designed a NOMA based FD-DF relay network and evaluated the SOP performance in the presence of a passive eavesdropper. The novel closed-form expressions for the end-to-end SINR in the legitimate connection and the wiretap connection were derived over a Rayleigh fading channel. The achieved results confirmed the proposed model adopted NOMA technique provided better SOP performance than OMA technique.

In the final aim, we proposed an integrated satellite model to enhance QoS in future cellular networks to provide a large number of connections and wide band access for mobile users. We studied an HSTRS which assisted small-cell. The HSTRS model could be significant enhanced by using the NOMA technique to optimal spectral efficiency. Besides, I derived the novel exact expressions for OP and throughput of the considered HSTRS model over Shadowed-Rician fading channels for satellite links and Nakagami-m fading channels for terrestrial links. The OP performances of the two users, which belonged to PA factors, were investigated. The achieved

results in Chapter 7 provided potential deep insight for the design of future HSTRS for small-cell communications.

For future works, although the achieved results in the dissertation have demonstrated the potential and effective implementations of UAVs for future cellular networks. However, it still opens up some challenges that need to be effectively addressed such as:

- Firstly, the UAV has a disadvantage since on-board power limitation due to the small size of craft. In this case, simultaneous wireless information and power transfer (SWIPT) could be adopted to prolong UAV's lifetime.
- The last but not at least, UAV's real position could be tracked. Based on UAV's position, we could allocate at the suitable position for UAV where could provide the best QoS for the users.

References

[1] S. R. Islam, N. Avazov, O. A. Dobre, and K.-S. Kwak, "Power-domain non-orthogonal multiple access (noma) in 5g systems: Potentials and challenges," *IEEE Communications Surveys & Tutorials*, vol. 19, no. 2, pp. 721–742, 2016, DOI: 10.1109/COMST.2016.2621116.

[2] D.-T. Do, M.-S. Van Nguyen, T.-A. Hoang, and M. Voznak, "Noma-assisted multiple access scheme for iot deployment: Relay selection model and secrecy performance improvement," *Sensors*, vol. 19, no. 3, p. 736, 2019, DOI: 10.3390/s19030736.

[3] T.-L. Nguyen and D.-T. Do, "Exploiting impacts of intercell interference on swipt-assisted non-orthogonal multiple access," *Wireless Communications and Mobile Computing*, vol. 2018, 2018, DOI: 10.1155/2018/2525492.

[4] D.-T. Do and C.-B. Le, "Application of noma in wireless system with wireless power transfer scheme: Outage and ergodic capacity performance analysis," *Sensors*, vol. 18, no. 10, p. 3501, 2018, DOI: 10.3390/s18103501.

[5] T.-L. Nguyen and D.-T. Do, "Power allocation schemes for wireless powered noma systems with imperfect csi: An application in multiple antenna–based relay," *International Journal of Communication Systems*, vol. 31, no. 15, p. e3789, 2018, DOI: 10.1002/dac.3789.

[6] X. Liu, X. Wang, and Y. Liu, "Power allocation and performance analysis of the collaborative noma assisted relaying systems in 5g," *China Communications*, vol. 14, no. 1, pp. 50–60, 2017, DOI: 10.1109/CC.2017.7839757.

[7] D.-T. Do and M.-S. Van Nguyen, "Device-to-device transmission modes in noma network with and without wireless power transfer," *Computer Communications*, vol. 139, pp. 67–77, 2019, DOI: 10.1016/j.comcom.2019.04.003.

[8] X. Lu, P. Wang, D. Niyato, D. I. Kim, and Z. Han, "Wireless networks with rf energy harvesting: A contemporary survey," *IEEE Communications Surveys & Tutorials*, vol. 17, no. 2, pp. 757–789, 2014, DOI: 10.1109/COMST.2014.2368999.

[9] D.-T. Do, "Energy-aware two-way relaying networks under imperfect hardware: Optimal throughput design and analysis," *Telecommunication Systems*, vol. 62, no. 2, pp. 449–459, 2016, DOI: 10.1007/s11235-015-0085-7.

[10] M. Wakaiki, K. Suto, K. Koiwa, K.-Z. Liu, and T. Zanma, "A control-theoretic approach for cell zooming of energy harvesting small cell networks," *IEEE Transactions on Green Communications and Networking*, vol. 3, no. 2, pp. 329–342, 2018, DOI: 10.1109/TGCN.2018.2889897.

[11] H. Wang, J. Wang, G. Ding, L. Wang, T. A. Tsiftsis, and P. K. Sharma, "Resource allocation for energy harvesting-powered d2d communication underlaying uav-assisted networks,"

IEEE Transactions on Green Communications and Networking, vol. 2, no. 1, pp. 14–24, 2017, DOI: 10.1109/TGCN.2017.2767203.

[12] M. Pratibha, K. H. Li, and K. C. Teh, "Channel selection in multichannel cognitive radio systems employing rf energy harvesting," *IEEE Transactions on Vehicular Technology*, vol. 65, no. 1, pp. 457–462, 2015, DOI: 10.1109/TVT.2015.2392770.

[13] J. Ren, J. Hu, D. Zhang, H. Guo, Y. Zhang, and X. Shen, "Rf energy harvesting and transfer in cognitive radio sensor networks: Opportunities and challenges," *IEEE Communications Magazine*, vol. 56, no. 1, pp. 104–110, 2018, DOI: 10.1109/MCOM.2018.1700519.

[14] S. Arzykulov, T. A. Tsiftsis, G. Nauryzbayev, and M. Abdallah, "Outage performance of cooperative underlay cr-noma with imperfect csi," *IEEE Communications Letters*, vol. 23, no. 1, pp. 176–179, 2018, DOI: 10.1109/LCOMM.2018.2878730.

[15] H. A. David and H. N. Nagaraja, *Order Statistics*. Wiley, 2003.

[16] Y. Saito, A. Benjebbour, Y. Kishiyama, and T. Nakamura, "System-level performance of downlink non-orthogonal multiple access (noma) under various environments," in *2015 IEEE 81st vehicular technology conference (VTC Spring)*, pp. 1–5, IEEE, 2015, DOI: 10.1109/VTCSpring.2015.7146120.

[17] Z. Ding, P. Fan, and H. V. Poor, "Impact of user pairing on 5g nonorthogonal multiple-access downlink transmissions," *IEEE Transactions on Vehicular Technology*, vol. 65, no. 8, pp. 6010–6023, 2015, DOI: 10.1109/TVT.2015.2480766.

[18] T. M. Cover and J. A. Thomas, *Elements of Information Theory*. Wiley, 2012.

[19] L. Lv, J. Chen, Q. Ni, Z. Ding, and H. Jiang, "Cognitive non-orthogonal multiple access with cooperative relaying: A new wireless frontier for 5g spectrum sharing," *IEEE Communications Magazine*, vol. 56, no. 4, pp. 188–195, 2018, DOI: 10.1109/MCOM.2018.1700687.

[20] Z. Ding, F. Adachi, and H. V. Poor, "The application of mimo to non-orthogonal multiple access," *IEEE Transactions on Wireless Communications*, vol. 15, no. 1, pp. 537–552, 2015, DOI: 10.1109/TWC.2015.2475746.

[21] Y. Liu, G. Pan, H. Zhang, and M. Song, "On the capacity comparison between mimo-noma and mimo-oma," *IEEE Access*, vol. 4, pp. 2123–2129, 2016, DOI: 10.1109/ACCESS.2016.2563462.

[22] W. Han, J. Ge, and J. Men, "Performance analysis for noma energy harvesting relaying networks with transmit antenna selection and maximal-ratio combining over nakagami-m fading," *IET Communications*, vol. 10, no. 18, pp. 2687–2693, 2016.

[23] X. Liu and X. Wang, "Efficient antenna selection and user scheduling in 5g massive mimo-noma system," in *2016 IEEE 83rd Vehicular Technology Conference (VTC Spring)*, pp. 1–5, IEEE, 2016, DOI: 10.1109/VTCSpring.2016.7504208.

[24] J. Men and J. Ge, "Non-orthogonal multiple access for multiple-antenna relaying networks," *IEEE Communications Letters*, vol. 19, no. 10, pp. 1686–1689, 2015, DOI: 10.1109/LCOMM.2015.2472006.

[25] D.-T. Do and A.-T. Le, "Noma based cognitive relaying: Transceiver hardware impairments, relay selection policies and outage performance comparison," *Computer Communications*, vol. 146, pp. 144–154, 2019, DOI: 10.1016/j.comcom.2019.07.023.

[26] D. Do, M. Vaezi, and T. Nguyen, "Wireless powered cooperative relaying using noma with imperfect csi," in *2018 IEEE Globecom Workshops (GC Wkshps)*, pp. 1–6, 2018, DOI: 10.1109/GLOCOMW.2018.8644154.

[27] D. Do, A. Le, and B. M. Lee, "Noma in cooperative underlay cognitive radio networks under imperfect sic," *IEEE Access*, vol. 8, pp. 86180–86195, 2020, DOI: 10.1109/ACCESS.2020.2992660.

[28] B. Evans, M. Werner, E. Lutz, M. Bousquet, G. E. Corazza, G. Maral, and R. Rumeau, "Integration of satellite and terrestrial systems in future multimedia communications," *IEEE Wireless Communications*, vol. 12, no. 5, pp. 72–80, 2005, DOI: 10.1109/MWC.2005.1522108.

[29] G. Zheng, S. Chatzinotas, and B. Ottersten, "Generic optimization of linear precoding in multibeam satellite systems," *IEEE Transactions on Wireless Communications*, vol. 11, no. 6, pp. 2308–2320, 2012, DOI: 10.1109/TWC.2012.040412.111629.

[30] A. Vanelli-Corali, G. E. Corazza, G. Karagiannidis, P. Mathiopoulos, D. Michalopoulos, C. Mosquera, S. Papaharalabos, and S. Scalise, "Satellite communications: Research trends and open issues," in *2007 international workshop on satellite and space communications*, pp. 71–75, IEEE, 2007, DOI: 10.1109/IWSSC.2007.4409393.

[31] M. R. Bhatnagar and M. Arti, "Performance analysis of af based hybrid satellite-terrestrial cooperative network over generalized fading channels," *IEEE Communications Letters*, vol. 17, no. 10, pp. 1912–1915, 2013, DOI: 10.1109/LCOMM.2013.090313.131079.

[32] V. K. Sakarellos, C. Kourogiorgas, and A. D. Panagopoulos, "Cooperative hybrid land mobile satellite–terrestrial broadcasting systems: Outage probability evaluation and accurate simulation," *Wireless personal communications*, vol. 79, no. 2, pp. 1471–1481, 2014, DOI: 10.1007/s11277-014-1941-6.

[33] M. Arti and V. Jain, "Relay selection-based hybrid satellite-terrestrial communication systems," *Iet Communications*, vol. 11, no. 17, pp. 2566–2574, 2017.

[34] S. Sreng, B. Escrig, and M.-L. Boucheret, "Exact outage probability of a hybrid satellite terrestrial cooperative system with best relay selection," in *2013 IEEE International Conference on Communications (ICC)*, pp. 4520–4524, IEEE, 2013, DOI: 10.1109/ICC.2013.6655280.

[35] K. An, M. Lin, J. Ouyang, Y. Huang, and G. Zheng, "Symbol error analysis of hybrid satellite–terrestrial cooperative networks with cochannel interference," *IEEE Communications Letters*, vol. 18, no. 11, pp. 1947–1950, 2014, DOI: 10.1109/LCOMM.2014.2361517.

[36] H. Wu, Y. Zou, W. Cao, Z. Chen, T. A. Tsiftsis, M. R. Bhatnagar, and R. C. De Lamare, "Impact of hardware impairments on outage performance of hybrid satellite-terrestrial relay systems," *IEEE Access*, vol. 7, pp. 35103–35112, 2019, DOI: 10.1109/ACCESS.2019.2905129.

[37] R. Wang, F. Zhou, J. Bian, K. An, and K. Guo, "Performance evaluation of harq-assisted hybrid satellite-terrestrial relay networks," *IEEE Communications Letters*, vol. 24, no. 2, pp. 423–427, 2019, DOI: 10.1109/LCOMM.2019.2962800.

[38] P. K. Sharma, D. Deepthi, and D. I. Kim, "Outage probability of 3-d mobile uav relaying for hybrid satellite-terrestrial networks," *IEEE Communications Letters*, vol. 24, no. 2, pp. 418–422, 2019, DOI: 10.1109/LCOMM.2019.2956526.

[39] Y. Zou, J. Zhu, X. Wang, and L. Hanzo, "A survey on wireless security: Technical challenges, recent advances, and future trends," *Proceedings of the IEEE*, vol. 104, no. 9, pp. 1727–1765, 2016, DOI: 10.1109/JPROC.2016.2558521.

[40] X. Li, M. Zhao, Y. Liu, L. Li, Z. Ding, and A. Nallanathan, "Secrecy analysis of ambient backscatter noma systems under i/q imbalance," *IEEE Transactions on Vehicular Technology*, vol. 69, no. 10, pp. 12286–12290, 2020, DOI: 10.1109/TVT.2020.3006478.

[41] X. Li, Q. Wang, H. Peng, H. Zhang, D.-T. Do, K. M. Rabie, R. Kharel, and C. C. Cavalcante, "A unified framework for hs-uav noma networks: Performance analysis and location optimization," *IEEE Access*, vol. 8, pp. 13329–13340, 2020, DOI: 10.1109/ACCESS.2020.2964730.

[42] X. Li, Q. Wang, Y. Liu, T. A. Tsiftsis, Z. Ding, and A. Nallanathan, "Uav-aided multiway noma networks with residual hardware impairments," *IEEE Wireless Communications Letters*, vol. 9, no. 9, pp. 1538–1542, 2020, DOI: 10.1109/LWC.2020.2996782.

[43] X. Yan, H. Xiao, C.-X. Wang, and K. An, "Outage performance of noma-based hybrid satellite-terrestrial relay networks," *IEEE Wireless Communications Letters*, vol. 7, no. 4, pp. 538–541, 2018, DOI: 10.1109/LWC.2018.2793916.

[44] X. Yan, H. Xiao, K. An, G. Zheng, and W. Tao, "Hybrid satellite terrestrial relay networks with cooperative non-orthogonal multiple access," *IEEE Communications Letters*, vol. 22, no. 5, pp. 978–981, 2018, DOI: 10.1109/LCOMM.2018.2815610.

[45] X. Yan, H. Xiao, C.-X. Wang, and K. An, "On the ergodic capacity of noma-based cognitive hybrid satellite terrestrial networks," in *2017 IEEE/CIC International Conference on Communications in China (ICCC)*, pp. 1–5, IEEE, 2017, DOI: 10.1109/ICCChina.2017.8330454.

[46] X. Yan, K. An, T. Liang, G. Zheng, and Z. Feng, "Effect of imperfect channel estimation on the performance of cognitive satellite terrestrial networks," *IEEE Access*, vol. 7, pp. 126293–126304, 2019, DOI: 10.1109/ACCESS.2019.2939165.

[47] V. Singh, V. Bankey, and P. K. Upadhyay, "Underlay cognitive hybrid satellite-terrestrial networks with cooperative-noma," in *2020 IEEE Wireless Communications and Networking Conference (WCNC)*, pp. 1–6, IEEE, 2020, DOI= 10.1109/WCNC45663.2020.9120607.

[48] R. Madan, J. Borran, A. Sampath, N. Bhushan, A. Khandekar, and T. Ji, "Cell association and interference coordination in heterogeneous lte-a cellular networks," *IEEE Journal on selected areas in communications*, vol. 28, no. 9, pp. 1479–1489, 2010, DOI: 10.1109/JSAC.2010.101209.

[49] S. Singh and J. G. Andrews, "Joint resource partitioning and offloading in heterogeneous cellular networks," *IEEE Transactions on Wireless Communications*, vol. 13, no. 2, pp. 888–901, 2013, DOI: 10.1109/TWC.2013.120713.130548.

[50] J. G. Andrews, "Seven ways that hetnets are a cellular paradigm shift," *IEEE communications magazine*, vol. 51, no. 3, pp. 136–144, 2013, DOI: 10.1109/MCOM.2013.6476878.

[51] Z. Tan, X. Li, F. R. Yu, H. Ji, and V. C. Leung, "Joint resource allocation in cache-enabled small cell networks with massive mimo and full duplex," in *GLOBECOM 2017-2017 IEEE Global Communications Conference*, pp. 1–6, IEEE, 2017, DOI: 10.1109/GLOCOM.2017.8254680.

[52] D.-T. Do, C.-B. Le, and F. Afghah, "Enabling full-duplex and energy harvesting in uplink and downlink of small-cell network relying on power domain based multiple access," *IEEE Access*, vol. 8, pp. 142772–142784, 2020, DOI: 10.1109/ACCESS.2020.3013912.

[53] T.-N. Tran, *Study of IoT Networks Inspired by the Emerging NOMA Technique: Analysis, Simulations and Improvements*. PhD thesis, VSB - Technical University of Ostrava, 2021.

[54] Y. Endo, Y. Kishiyama, and K. Higuchi, "Uplink non-orthogonal access with mmse-sic in the presence of inter-cell interference," in *2012 international symposium on wireless communication systems (ISWCS)*, pp. 261–265, IEEE, 2012, DOI: 10.1109/ISWCS.2012.6328370.

[55] B. Kim, W. Chung, S. Lim, S. Suh, J. Kwun, S. Choi, and D. Hong, "Uplink noma with multi-antenna," in *2015 IEEE 81st Vehicular Technology Conference (VTC Spring)*, pp. 1–5, 2015, DOI: 10.1109/VTCSpring.2015.7146149.

[56] G. Maral, M. Bousquet, and Z. Sun, *Satellite communications systems: systems, techniques and technology*. John Wiley & Sons, 2020.

[57] X. Chen, Z. Zhang, C. Zhong, and D. W. K. Ng, "Exploiting multiple-antenna techniques for non-orthogonal multiple access," *IEEE Journal on Selected Areas in Communications*, vol. 35, no. 10, pp. 2207–2220, 2017, DOI: 10.1109/JSAC.2017.2724420.

[58] Z. Ding, R. Schober, and H. V. Poor, "A general mimo framework for noma downlink and uplink transmission based on signal alignment," *IEEE Transactions on Wireless Communications*, vol. 15, no. 6, pp. 4438–4454, 2016, DOI: 10.1109/TWC.2016.2542066.

[59] J. Cui, Z. Ding, and P. Fan, "Outage probability constrained mimo-noma designs under imperfect csi," *IEEE Transactions on Wireless Communications*, vol. 17, no. 12, pp. 8239–8255, 2018, DOI: 10.1109/TWC.2018.2875490.

[60] M. Zeng, A. Yadav, O. A. Dobre, G. I. Tsiropoulos, and H. V. Poor, "On the sum rate of mimo-noma and mimo-oma systems," *IEEE Wireless Communications Letters*, vol. 6, no. 4, pp. 534–537, 2017, DOI: 10.1109/LWC.2017.2712149.

[61] L. Dai, B. Wang, Z. Ding, Z. Wang, S. Chen, and L. Hanzo, "A survey of non-orthogonal multiple access for 5g," *IEEE communications surveys & tutorials*, vol. 20, no. 3, pp. 2294–2323, 2018, DOI: 10.1109/COMST.2018.2835558.

[62] D.-T. Do, M.-S. Van Nguyen, T. N. Nguyen, X. Li, and K. Choi, "Enabling multiple power beacons for uplink of noma-enabled mobile edge computing in wirelessly powered iot," *IEEE Access*, vol. 8, pp. 148892–148905, 2020, DOI: 10.1109/ACCESS.2020.3015741.

[63] J. Men, J. Ge, and C. Zhang, "Performance analysis of nonorthogonal multiple access for relaying networks over nakagami-m fading channels," *IEEE Transactions on Vehicular Technology*, vol. 66, no. 2, pp. 1200–1208, 2016, DOI: 10.1109/TVT.2016.2555399.

[64] Z. Zhang, Z. Ma, M. Xiao, Z. Ding, and P. Fan, "Full-duplex device-to-device-aided cooperative nonorthogonal multiple access," *IEEE Transactions on Vehicular Technology*, vol. 66, no. 5, pp. 4467–4471, 2016, DOI: 10.1109/TVT.2016.2600102.

[65] Y. Liu, Z. Ding, M. Elkashlan, and J. Yuan, "Nonorthogonal multiple access in large-scale underlay cognitive radio networks," *IEEE Transactions on Vehicular Technology*, vol. 65, no. 12, pp. 10152–10157, 2016, DOI: 10.1109/TVT.2016.2524694.

[66] F. Lu, M. Xu, L. Cheng, J. Wang, J. Zhang, and G. Chang, "Non-orthogonal multiple access with successive interference cancellation in millimeter-wave radio-over-fiber systems," *Journal of Lightwave Technology*, vol. 34, no. 17, pp. 4179–4186, 2016, DOI: 10.1109/JLT.2016.2593665.

[67] H. Marshoud, V. M. Kapinas, G. K. Karagiannidis, and S. Muhaidat, "Non-orthogonal multiple access for visible light communications," *IEEE Photonics Technology Letters*, vol. 28, no. 1, pp. 51–54, 2016, DOI: 10.1109/LPT.2015.2479600.

[68] M. Bloch, J. Barros, M. R. D. Rodrigues, and S. W. McLaughlin, "Wireless information-theoretic security," *IEEE Transactions on Information Theory*, vol. 54, no. 6, pp. 2515–2534, 2008, DOI: 10.1109/TIT.2008.921908.

[69] Y. Zhang, H. Wang, Q. Yang, and Z. Ding, "Secrecy sum rate maximization in non-orthogonal multiple access," *IEEE Communications Letters*, vol. 20, no. 5, pp. 930–933, 2016, DOI: 10.1109/LCOMM.2016.2539162.

[70] Z. Qin, Y. Liu, Z. Ding, Y. Gao, and M. Elkashlan, "Physical layer security for 5g non-orthogonal multiple access in large-scale networks," in *2016 IEEE International Conference on Communications (ICC)*, pp. 1–6, 2016, DOI: 10.1109/ICC.2016.7510755.

[71] Y. Liu, Z. Qin, M. Elkashlan, Y. Gao, and L. Hanzo, "Enhancing the physical layer security of non-orthogonal multiple access in large-scale networks," *IEEE Transactions on Wireless Communications*, vol. 16, no. 3, pp. 1656–1672, 2017, DOI: 10.1109/TWC.2017.2650987.

[72] Z. Ding, Z. Yang, P. Fan, and H. V. Poor, "On the performance of non-orthogonal multiple access in 5g systems with randomly deployed users," *IEEE signal processing letters*, vol. 21, no. 12, pp. 1501–1505, 2014, DOI: 10.1109/LSP.2014.2343971.

[73] B. V. Nguyen and K. Kim, "Secrecy outage probability of optimal relay selection for secure anf cooperative networks," *IEEE Communications Letters*, vol. 19, no. 12, pp. 2086–2089, 2015, DOI: 10.1109/LCOMM.2015.2486768.

[74] B. Van Nguyen and K. Kim, "Single relay selection for secure communication in a cooperative system with multiple full-duplex decode-and-forward relays," in *2015 IEEE International Workshop on Information Forensics and Security (WIFS)*, pp. 1–6, IEEE, 2015, DOI: 10.1109/WIFS.2015.7368590.

[75] H. Liu and K. S. Kwak, "Opportunistic relaying for cooperative small-cell systems with unreliable wireless backhauls," in *2018 IEEE Wireless Communications and Networking Conference (WCNC)*, pp. 1–6, IEEE, 2018, DOI: 10.1109/WCNC.2018.8377016.

[76] B. Yafis, K.-T. Feng, and C.-M. Yu, "Renewable energy-based resource allocation for full-duplex small cell networks," *IEEE Access*, vol. 6, pp. 24746–24756, 2018, DOI: 10.1109/ACCESS.2018.2831706.

[77] H. Zhang, Y. Wang, H. Ji, and X. Li, "A sleeping mechanism for cache-enabled small cell networks with energy harvesting function," *IEEE Transactions on Green Communications and Networking*, vol. 4, no. 2, pp. 497–505, 2020, DOI: 10.1109/TGCN.2020.2988276.

[78] X. Yue, Y. Liu, S. Kang, A. Nallanathan, and Z. Ding, "Exploiting full/half-duplex user relaying in noma systems," *IEEE Transactions on Communications*, vol. 66, no. 2, pp. 560–575, 2017, DOI: 10.1109/TCOMM.2017.2749400.

[79] I. S. Gradshteyn and I. M. Ryzhik, *Table of integrals, series, and products*. Academic press, 2014.

[80] A. Haider and S.-H. Hwang, "Maximum transmit power for ue in an lte small cell uplink," *Electronics*, vol. 8, no. 7, p. 796, 2019, DOI: 10.3390/electronics8070796.

[81] N. I. Miridakis, D. D. Vergados, and A. Michalas, "Dual-hop communication over a satellite relay and shadowed rician channels," *IEEE Transactions on Vehicular Technology*, vol. 64, no. 9, pp. 4031–4040, 2014, DOI: 10.1109/TVT.2014.2361832.

[82] A. Abdi, W. C. Lau, M.-S. Alouini, and M. Kaveh, "A new simple model for land mobile satellite channels: First-and second-order statistics," *IEEE Transactions on Wireless Communications*, vol. 2, no. 3, pp. 519–528, 2003, DOI: 10.1109/TWC.2003.811182.

[83] V. Adamchik and O. Marichev, "The algorithm for calculating integrals of hypergeometric type functions and its realization in reduce system," in *Proceedings of the international symposium on Symbolic and algebraic computation*, pp. 212–224, 1990, DOI: 10.1145/96877.96930.

[84] A. M. Mathai and R. K. Saxena, "The h function with applications in statistics and other disciplines," 1978.

[85] V. Bankey, P. K. Upadhyay, D. B. Da Costa, P. S. Bithas, A. G. Kanatas, and U. S. Dias, "Performance analysis of multi-antenna multiuser hybrid satellite-terrestrial relay systems for mobile services delivery," *IEEE Access*, vol. 6, pp. 24729–24745, 2018, DOI: 10.1109/ACCESS.2018.2830801.

[86] K. Guo, K. An, B. Zhang, Y. Huang, and G. Zheng, "Outage analysis of cognitive hybrid satellite-terrestrial networks with hardware impairments and multi-primary users," *IEEE Wireless Communications Letters*, vol. 7, no. 5, pp. 816–819, 2018, DOI: 10.1109/LWC.2018.2827067.

[87] M. K. Simon and M.-S. Alouini, *Digital communication over fading channels*, vol. 95. John Wiley & Sons, 2005.

[88] X. Yue, Y. Liu, Y. Yao, T. Li, X. Li, R. Liu, and A. Nallanathan, "Outage behaviors of noma-based satellite network over shadowed-rician fading channels," *IEEE Transactions on Vehicular Technology*, vol. 69, no. 6, pp. 6818–6821, 2020, DOI: 10.1109/TVT.2020.2988026.

[89] P. K. Upadhyay and P. K. Sharma, "Max-max user-relay selection scheme in multiuser and multirelay hybrid satellite-terrestrial relay systems," *IEEE Communications Letters*, vol. 20, no. 2, pp. 268–271, 2015, DOI: 10.1109/LCOMM.2015.2502599.

[90] S. Lee, D. B. Da Costa, Q.-T. Vien, T. Q. Duong, and R. T. de Sousa, "Non-orthogonal multiple access schemes with partial relay selection," *IET Communications*, vol. 11, no. 6, pp. 846–854, 2017, DOI: 10.1049/iet-com.2016.0836.

Candidate's Results Cited in the Dissertation

The list of results indexed in WoS/Scopus during my Ph.D. studies, where individual ideas of the dissertation are published.

[NNL01] **Nguyen, N.-L.**, Nguyen, H.-N., and Nguyen, N.-T. et al. *On Performance Analysis of NOMA-Aided Hybrid Satellite Terrestrial Relay With Application in Small-Cell Network.* IEEE Access, (2020), Article ID: 9229415, 8, pp. 188526–188537, DOI: 10.1109/ACCESS.2021.3069247. **IF 3.367** (2020).

[NNL02] **Nguyen, N.-L.** et al. *UAV Based Satellite-Terrestrial Systems with Hardware Impairment and Imperfect SIC: Performance Analysis of User Pairs.* IEEE Access, (2021), Article ID: 9521513, 9, pp.117925-117937, DOI: 10.1109/ACCESS.2021.310725. **IF 3.367** (2021).

[NNL03] **Nguyen, N.-L.**, Nguyen, H.-N., and Do, D.-T. et al. *On Secure Cognitive Radio Networks with NOMA: Design of Multiple-Antenna and Performance Analysis.* (2020), In Proc. MTTW 2020, Riga, pp. 1-6. DOI: 10.1109/MTTW51045.2020.9245070.

[NNL04] **Nguyen, N.-L.**, Hong, N.-N., and Loan, N. T.-P. et al. *A performance analysis in AF full duplex relay selection network.* (2018), AIP Conf. Proc., vol. 1954, No. 1, Article ID 040013. DOI: 10.1063/1.5033413.

[NNL05] Dao, T.T.-T., **Nguyen, N.L.**, and Nguyen, H.-N. et al. *Exploiting Secure Performance of Full-Duplex Decode and Forward in Optimal Relay Selection Networks.* (2018), Elektronika Ir Elektrotechnika, vol. 24, No. 4, pp. 72-76, **IF 0.707**.

[NNL06] Le, S.-P., Van Nguyen, M.-S., Do, D.-T., and Nguyen, H.-N., **Nguyen, N.-L.** et al. *Enabling wireless power transfer and multiple antennas selection to IoT network relying on NOMA.* (2020), Elektronika ir Elektrotechnika, 26(5), 59-65, DOI:10.5755/j01.eie.26.5.27889. **IF 0.707**.

[NNL07] Le, S.-P., Le, C.-B., Nguyen, H.-N., and **Nguyen, N.-L.** et al. *Exploitting Performance Of Miso Based Non-Orthogonal Multiple Access.* 42nd International Conference on Telecommunications and Signal Processing - TSP 2019. Budapest, Hungary, pp 454-458, DOI: 10.1109/TSP.2019.8768834.

[NNL08] Nguyen, H.-N., **Nguyen, N.-L.**, and Nguyen, N.-T. et al. *Reliable and Secure Transmission in Multiple Antennas Hybrid Satellite-Terrestrial Cognitive Networks Relying on NOMA.* IEEE Access, (2020), Article ID: 9274311, 8, pp. 215044-215056, DOI: 10.1109/ACCESS.2020.3041680. **IF 3.367** (2020).

[NNL09] Nguyen, N.-T., Nguyen, H.-N., and **Nguyen, N.-L.** et al. *Enhancing Spectrum Efficiency and Fairness for Multiple Users in Hybrid Satellite-Terrestrial Networks.*, IEEE Access, (2021), Article ID: 9388646, 9, pp. 50291-50300, DOI: 10.1109/ACCESS.2021.3069247. **IF 3.367**(2021).

[NNL10] Nguyen, H.-N., Le, S.-P., Le, C.-B., and **Nguyen, N.-L.** et al. *Cognitive Radio Assisted Non−Orthogonal Multiple Access: Outage Performance.* International Conference on Telecommunications and Signal Processing - TSP 2019. Budapest, Hungary, pp 449-453, DOI: 10.1109/TSP.2019.8768873.

[NNL11] Le, S.-P., Nguyen, H.-N., and **Nguyen, N.-L.** et al. *Device-to-Device Network with MISO Scheme for Wireless Power Transfer: Outage Performance Analysis.* 41st International Conference on Telecommunications and Signal Processing - TSP 2018. Athens, Greece, pp. 1-4, DOI: 10.1109/TSP.2018.8441401.

[NNL12] Nguyen, H.-N., **Nguyen N.-L.**, and Nguyen N.-T. et al. *Outage Probability of CR-NOMA Schemes with Multiple Antennas Selection and Power Transfer Approach.* Advances in Networked-Based Information Systems (NBiS), (2021), Springer, vol 313, pp 131-142, DOI: 10.1007/978-3-030-84913-9_12

[NNL13] Do, D.-T., Le, C.-B., Nguyen, H.-N., Tam, N.-K., and **Nguyen N.-L.** et al. *Wireless power transfer enabled NOMA relay systems: two SIC modes and performance evaluation.* Telkomnika (Telecommunication Computing Electronics and Control), (2019), 17(6), pp. 2697–2703, DOI: 10.12928/Telkomnika.v17i6.12218.

About the Candidate

Research Activities

I provide the following list of indexed results in relevant scientific databases as documentary evidence of my research activities during the period of my doctoral studies:

ORCID: 0000-0002-3365-8648
Scopus Author ID: 57203356901
Web of Science ResearcherID: AAX-2450-2021
Articles in journals indexed in WoS/Scopus: 6.
Conference papers indexed in WoS/Scopus: 7.
Citations: 25 in Scopus and 11 in Web of Science.

Participation in Research Project

The research leading to the results shown in the dissertation received funding from:

- Proj. reg. no. SP2018/59 - Networks and Communications Technologies for Smart Cities I., Student Grant Competition of VSB-TUO (2018).
- Proj. reg. no. SP2019/41 - Networks and Communications Technologies for Smart Cities II., Student Grant Competition of VSB-TUO (2019).
- Proj. reg. no. SP2020/65 - Networks and Communications Technologies for Smart Cities III., Student Grant Competition of VSB-TUO (2020).
- Proj. reg. no. SP2021/25 - Networks and Communications Technologies for Smart Cities IV., Student Grant Competition of VSB-TUO.(2021)